University of Zurich[UZH]

Department of Informatics

Efficient and Comprehensive Haptic Information for Grasp Control in Upper-Limb Prosthetics

A dissertation submitted to the Faculty of Economics, Business Administration and Information Technology of the University of Zurich

for the degree of
Doctor of Science (Ph.D.)

by
Dana Damian
from Romania

Accepted on the recommendation of
Prof. Dr. Rolf Pfeifer
Prof. Dr. Roger Gassert

2012

University of Zurich[UZH]

The Faculty of Economics, Business Administration and Information Technology of the University of Zurich herewith permits the publication of the aforementioned dissertation without expressing any opinion on the views contained therein.

Zurich, September, 2012*

Head of the Ph.D. committee for informatics: Prof. Abraham Bernstein, Ph.D.

* Graduation date

Abstract

Defining the Self is a long-standing quest, which has been addressed by psychologists, mathematicians and philosophers. Prosthetics has become an exciting branch of robotics that carries the potential of answering this question, using a synthetic or robotic framework, due to the controllability of the relation between the prosthetic device and the human wearer in the interaction with the environment. The incorporation of the robotic prosthesis as part of the wearer's body has been found to be a sensorimotor artificial transformation subjected to complex technological challenges due to the unstructured environments in which humans operate. This thesis addresses the technological and information-related challenges of haptic interfaces -both haptic sensing and displays- for upper-limb prostheses. It introduces the notion of efficient feedback in prosthetics, a concept through which, technologically, morphology in the design of tactile sensors and haptic displays enhances the relayed information using minimal resources (e.g., electronical, computational and physical). Within the same concept, extended to the information dimension of sensing, this thesis proposes the nature of haptic information which needs to be provided to the prosthesis wearer for a comprehensive environmental representation and an efficient grasp.

We show that a quantitative feedback description of proprioceptive sensing, e.g., grip force strength, and exteroceptive sensing, e.g., object slip speed, for prosthetic hands, endows prosthesis users with a robust guidance towards stable grasp, i.e., grip force within safe margins against slip. Additionally, we show the distinct role of grip force and slip speed feedback in regulating the artificial grasp. Following up on these ideas, we developed a haptic device that displays both force and slip in a quantitative way and reveals efficient design principles for prosthetics.

We also look at efficient design principles of tactile sensing systems for extracting enhanced haptic information. Ridged patterns on an artificial skin are inspected for their potential to encode haptic stimuli in their morphology during static and dynamic events. We developed a ridged artificial skin that detects stimulus force, slip occurrence, speed and location, by using a single force sensor. Based on evolutionary algorithms, we provide insights into the trade-off between tactile sensing resolution and sensitivity, as an expression of the number and spatial distribution of ridges, respectively.

The thesis deepens the understanding of artificial sensorimotor transformations in prosthetic systems and shows the potential of exploiting morphology for efficient sensory feedback schemes in prosthetics.

Acknowledgments

I am deeply grateful to my supervisor, Rolf Pfeifer, for providing me a truly unique environment, the Artificial Intelligence Laboratory, to enjoy research in many possible ways. It has been a great pleasure to be part of this lab that he has built. I wish to thank Alejandro Hernandez Arieta for being present during all my years of research, especially for his advice and support in the first years of my PhD. Special thanks go to Allison Okamura, for the interesting discussions and great supervision I benefited from during my stay at Johns Hopkins University and Stanford University. I would also like to thank and express my appreciation to Roger Gassert, for his kind willingness to offer me advice and comments on this thesis. The members of AILab are great colleagues and friends, always offering help, support and motivation. It was a privilege to be among them and I thank them truly. I also thank my colleagues and friends I met in the USA; I learned many things from them and I will always be endowed to them. I thank Shuhei Miyashita, for always keeping up and high my research thinking and motivation. Our research discussions were a source of energy during all these years. Finally, I thank my family in Romania, for providing me with the best environment to develop my dreams, and for their sustained strength and love.

- **Chapter 2** is based on [42]. I thank all the co-authors, Alejandro Hernandez Arieta, Harold Martinez and Rolf Pfeifer for their contributions. I would like to thank Dr. Max Lungarella, PD Dr. Daniel Kiper and Dr. rer. nat. Bertolt Meyer for their input to this contribution. This work is supported by the Swiss National Science Foundation within the project # CR23I2_132702/1.

- **Chapter 3** is based on [44], and I thank Marco Fisher, Costas Dermitzakis and Rolf Pfeifer. Also special thanks to Alejandro Hernandez Arieta for his assistance. We thank Marvin Ludersdorfer for helping with the mechanical construction. This work is supported by the SNF fellowship grant PBZHP2-135917.

- **Chapter 4** is based on [46], and I thank Harold Martinez, Konstantinos Dermitzakis, Alejandro Hernandez-Arieta and Rolf Pfeifer for their valuable contributions. This work is supported by the Swiss National Science Foundation within the project # CR23I2_132702/1.

- **Chapter 5** is based on [47], and I thank Taylor Newton, Rolf Pfeifer and Allison M. Okamura for the contributions. This work is supported by the Swiss National Science Foundation Fellowship PBZHP2-135917 and Stanford University.

- **Chapter 6** is based on [93] and I thank Marvin Ludersdorfer, Alejandro Hernandez Arieta, Rolf Pfeifer and Allison M. Okamura for their contributions. This work is supported by the SNF fellowship grant PBZHP2-135917.

- **Chapter 7** is based on [43] made possible with the contributions of Alejandro Hernandez Arieta and Allison M. Okamura. This work is supported by the SNF fellowship grant PBZHP2-135917 and the Johns Hopkins Brain Science Institute.

- **Chapter 8** is based on [45]; I am grateful to Marvin Ludersdorfer, Yeongmi Kim, Alejandro Hernandez Arieta, Rolf Pfeifer and Allison M. Okamura for their contributions. The authors would like to thank Konstantinos Dermitzakis for technical assistance. The work is supported by the Swiss National Science Foundation Fellowship PBZHP2-135917 and the Johns Hopkins Brain Science Institute.

This research has been supported by the Swiss National Science Foundation projects CR23I2 132702/1 and PBZHP2-135917, the Johns Hopkins Brain Institute and Stanford University. I am extremely thankful for this support.

Contents

List of Figures

List of Tables

Chapter 1

Introduction

Who am I? - This is an eternal question that has fascinated many philosophers, from Aristotle to Descartes and to minds of the present. It has taken on various answers under the concepts of "substance", "soul", "thoughts", etc. Science, in general, and robotics, in particular, have been an outstanding source of enlightenment for many questions of humanity, grounding our existence in sensible and concise theories. A bottom-up approach to living systems by means of robotics has been proving its potential in explaining and synthesizing complex notions and behaviors that emerge as a consequence of an embodied interaction among bodies and environments through various scales [122]. Robotic self-assembly has revealed interesting properties through the embodied dynamical interactions of small-scale robots, possibly related to the emergence of life [104]. Sophisticated locomotion has been shown to rely on passive mechanisms [37] or soft material designs [144] in interaction with the environment. Soft manipulators [24] [8] have demystified the intriguing phenomenon of grasping, once viewed as a highly demanding computational process and now seen as a compliant physical interaction between the hand's micro- and macro-structures and the manipulated objects. Prosthetics, as a robotic field within the human-robot-environment interaction discipline, has brought significant contributions to restoring the integrity of physically challenged people. At the same time, it sheds more light on the meaning of the Self by using robotic devices as parts of humans.

This thesis explores the requirements and design principles that may contribute to the incorporation of robotic devices into the human body, with respect to haptic interfaces (haptic sensors and displays). The context in which this thesis is situated is upper-limb prosthetics. By building robotic devices and synthesizing artificial interfaces between the human and the prosthetic hand, we introduce a means to restore complete embodied interactions between the prosthesis wearer and the environment, and shed light on principles that may contribute to the bodily incorporation of robotic devices.

1.1 Subject-object division for prosthetics

Prosthetics is an instance of the expression of the subject-object division, in which the subject is the amputee and the object is his prosthesis. The grand challenge in prosthetics has been the realization of a transparent amputee-

prosthesis interface insofar as the prosthesis is no longer an object or tool, but a part of the subject. Although the notion of Self has remained abstract [48], it is a useful reference concept in characterizing prosthetics or rehabilitation processes that have arisen the field of robotics and neuroscience.

Philipona et al. [124] define the self of a linked body, in opposition to the environment, as a correlated flow of sensory stimulation, under displacement (or movement) conditions performed by the linked body. This congruency between the sensory and motor flow is a powerful theoretical indicator that sensory feedback is critical for resolving the subject-object division present in prosthetic applications. Partly, this hypothesis has been supported by experimental work [25] [111] [155].

1.1.1 Grasp stability

Taking into account a common characteristic appearing in the studies dedicated to defining self or tool incorporation, it becomes obvious that a major prerequisite for self awareness is body movement. Through the dynamics of the body, sensory-motor correlations are acquired and body models are built. For the case of hand prostheses, grasp, as the interaction between the human, prosthesis and environment, represents the method to enable sensorymotor transformations that may lead to the integration of the prosthesis into the amputee's body scheme. To this aim, grasp stability and, ultimately, dexterity, are critical to maintain a stable interaction with the environment and implicitly the motor and sensory flow [39] [34]. Stability in grasping is attributed to a sensorimotor system that is able to transform information about grasp forces in the human hand in order to ensure adequate safety margins against slip. As an object is grasped, grip forces must be regulated in such a way that slip or excessive forces are avoided. Otherwise, the object is damaged, because it is dropped or crushed, respectively. Based on experimental work, Johansson and Cole [72] advocate that grasp stability relies on both predictive models in the central nervous system (CNS) and on discrete events sensory-driven control. The former control scheme characterizes predictable grasp attributes, e.g., object weight, frictional coefficients, whereas the latter characterizes unanticipated events that threaten the stability of the grasp, e.g. passive slip. Howard and Kumar [66] present a kinematic perspective of grasp stability and define it as an equilibrium that implicitly entails that the sum of all forces and moments acting on a body equals zero. In a frictionless system, they show that grasp stability depends on the local curvature of the held object and the magnitude and distribution of the contact forces. Jenmalm et al. [71] show, through experimental work, that the safety margin against frictional slips used by subjects of the study was influenced by the object curvature, in that it was higher for curved objects than for flat-surfaced objects.

Grasp stability in the human hand has been resolved by means of an intricate network of mechanoreceptors integrating numerous cues about mechanical events, through an ontogenetic grasp practice. Prosthetic hands introduce an engineered sensorimotor interface that hinders the natural reliance on neural predictive models and is prone to generating significant perturbations in the grasping process. In such scenarios, stable grasp control becomes a sensorimotor transformation that is highly dependent on incoming sensory information. This transformation is aimed at regulating grip force and removing perturba-

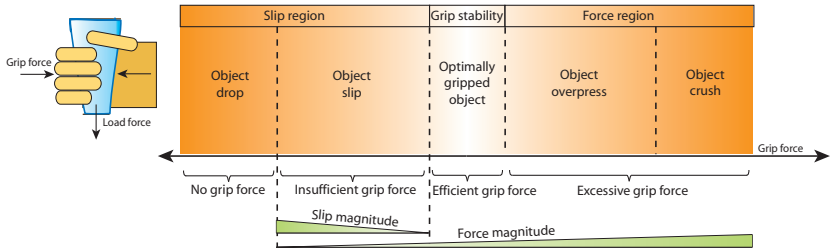

Figure 1.1: Grasp stability chart. A. Load and grip forces in grasping. B. Regions of stability and instability.

tions such as slip and excessive force, which can damage the held object or cause unnecessary energy use. This thesis strongly relies on this hypothesis. Based on this kind of characterization of the grasp using prostheses, this thesis provides a novel approach to grasp, by largely taking into account perturbations and exploiting them in order to achieve a stable and sustainable grasp.

1.1.2 "Human-in-the-loop" grasp

There exist two main approaches to grasp stability in upper-limb prostheses that differ in the type of grasp control. Automatic grasp control is an approach in which the grip is performed by internal mechanism of the robotic hand triggered by grasp events detected by tactile sensors, with no human intervention. It relies on various transduction methods for slip and force detection to automatically adjust the grip force of a robot hand, e.g., [135] [85] [162]. This type of technology has also been implemented into commercially available prosthetic hands, e.g., those manufactured by Otto Bock [65] and RSL Steeper [149]. Automatic grasping relies heavily on elaborating the complex deterministic algorithms necessary for grasp planning with robot hands, based on actuator's encoders or touch/tactile sensors. In many cases, such algorithms assume that a number of geometric and material properties related to the held object or hand are *a priori* available. While this analytic approach provides a fundamental understanding of grasp, it also requires prior knowledge that is generally lacking in unstructured environments. The analytical formulation considers grasp as a set of contacts between the object and the robot hand, and further takes into account the normal force, the tangential force, and the torsional moment around the normal at each point of contact. Using this terminology, the static equilibrium of the object can be defined, and the interaction forces of the grasp can be determined through various optimization methods. Nonetheless, this solution does not guarantee stability unless grasp is considered as a dynamical system. The complexity of the algorithms increases with the complexity of the object model and the kinematics of the fingers. A detailed review on this topic can be found in [17]. Recent work in hand neurophysiology [136] suggests that postural hand synergies are involved in tool grasping, of which two account for more than 80% of grasp variance. These findings have inspired automatic grasp strategies that reduce the dimensionality of the parameters, e.g., degrees of freedom (DOFs), used for planning robotic grasps [34]. Gabiccini et al. [58] show through theoretical work that optimal contact forces strongly depend on the selection of postural synergies and that the first two synergies, generated by

the dimensionality reduction algorithm, are sufficient to establish a safe grip. Nonetheless, prior environmental information is still needed. Industrial manipulation or, restrictively, humanoid manipulation, may profit from the research findings related to robotic grasping. One of the notable features of this technology is an apparently fast automatic grasp response time (e.g. approx. 750 ms as reported in [162]). In prosthetics, however, this approach has some undesirable limitations. Firstly, the environment in which prosthesis wearers operate extends considerably beyond the space of conditions that the proposed analytical solutions cover. In daily activities, there is little *a priori* information available, because objects have a large variety of properties, especially when the prosthetic hand is structurally and functionally different than the biological hand. Secondly, the automatic grasp approach removes the sensory input awareness of the user, which has been regarded as a critical element for a sustainable use of the prosthetic hand and its incorporation into the wearer's body. An alternative feedback modality to vision for manipulative actions is one of the most highly demanded design features among amputees, as reported in [9]. The absence of sensory feedback is frequently held accountable for amputees rejecting their prosthesis, e.g., [95] [19]. Concurrently, research seems to corroborate the theory that intermodal sensory feedback correlations enforce the self-attribution of an artificial limb, e.g., [22] [101]. These arguments have led to the adoption of the second type of control strategy - "human-in-the-loop" grasp - according to which sensory feedback about grasp is artificially relayed to the users to provide them with the command over the prosthesis. The two lines of research are equally significant, as studies on shared control [35] suggest that grip control may be a combination of these two approaches in order to grant best performances.

Although there has been an increasing body of work on enriching the artificial tactile sense of robotic/prosthetic hands for automatic grasp (a recent overview is found in [41]), enriching the haptic interface has received limited consideration. The feedback information relayed to the prosthesis user can be formulated in similar terms, as discussed in the automatic grasp control framework. Normal and tangential forces are relevant in describing the grip force and load force (or object slip), respectively. In this regard, Figure 1.1 illustrates a grasp stability chart with respect to the ratio between load forces and grip forces. An optimal balance between these two forces guarantee a grasp within the safety margins against slip, that is the ratio between the tangential force and the normal force should be less than or equal to the static friction coefficient μ, according to Coulomb's law). In contrary cases, slip occurs. Another type of perturbation is exerting excessive force (large normal or grip force) that can also damage the held object or involve unnecessary energy use. A mathematical description of grasp force and slip, limited to the object-robot hand system is found in [18]. These characteristics of grasp, within the "human-in-the-loop" approach, entail the development of adequate tactile sensors for the prosthetic hand as well as haptic feedback modalities and devices to relay them to the prosthesis wearer (see Fig. 1.2).

Sensing for prosthetic hands. To date, the acquisition of normal force is implemented using a large set of sensor technologies, e.g. resistive, capacitive, optical, magnetic, piezoelectric, quantum tunnel composites (QTC) [41]. The force sensors based on these technologies measure the grip force applied to the grasped object by the robotic hand. These sensing technologies extend to arrays of sensors that acquire forces from various sites, or to combinations of

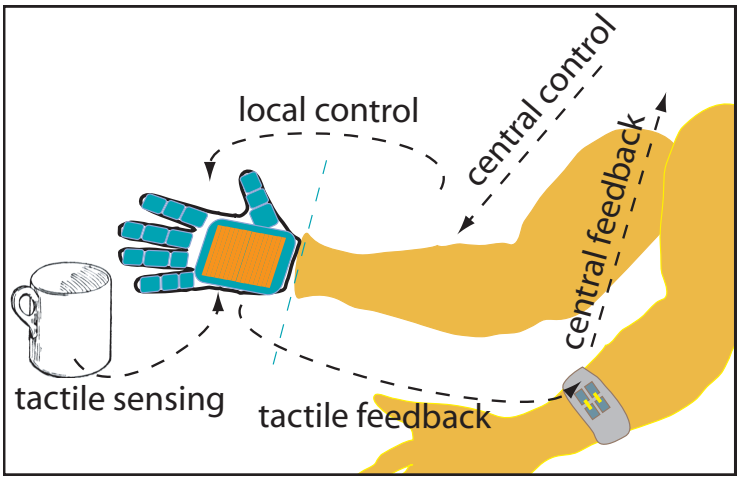

Figure 1.2: Feedback loop comprising of tactile sensors (orange area) for a prosthetic hand and the haptic device mounted on the prosthesis wearer's arm.

the relative topologies of such sensors in order to also detect shear force or slip. Details and examples of sensor technologies are presented in following sections. Obviously, without prior knowledge of the static coefficient of friction, even if both normal and tangential forces can be computed, differentiating between slip, safe grasp and crush is extremely difficult - if not impossible - for both robots and humans. Explicit slip detection has been popularly implemented by interpreting vibrations in force sensing data.

Haptics for prosthesis wearer. Regarding the haptic display of grasp events, focus has been largely dedicated to relaying force to prosthesis users, yet slip feedback has been rather neglected (details are provided in the following sections). In general, results of experiments with human users performing grasp with force feedback show that the human users can manage a safe grasp. However, the success of these experiments are limited to controlled environments in which a reduced set of objects is used and the appropriate grip force is relayed based on the known friction coefficient of the tested objects. As can be seen from the chart in Figure 1.1, low forces characterize object slip and high forces characterize object crush. Therefore, relaying only force feedback represents insufficient guidance towards stopping slip or avoiding object crush, and thus removing grasp perturbations. Physiological studies have shown that slip is a pivotal determinant in grip control [72] [10]. Slip, artificially generated by changing the load force on an object held in the human hand, was found to trigger an upgrade in the agility of the grip response that depended on the load force rate. This result is a prime indicator that the rate of slip may influence the grip response. The paradigm of displaying quantified grip perturbations, rather than grip force only, holds promise for restoring grasp stability and removing grasp dependency on vision for prosthesis users which is a fundamental step towards improving the quality of their lives.

1.2 Requirements in prosthetics

Engineering the tactile sensing in prostheses as well as the fusion between the prosthetic hand and its user imposes high demands on the design of the sensory interface. The challenge can be categorized from two perspectives. Scientifically, making the boundary between the subject (the amputee) and the object (the robot hand) less perceivable carries deep questions about the type and amount of sensory information necessary to incorporate the object in the subject. Technologically, it is highly non-trivial to find an engineering solution that is competitive in richness and sensitivity to the lost sensory interface. The road to tapping into the Self, and in particular, to achieving the incorporation of the robot hand into the wearer's body, require high demands in order for the prosthetic hand to be more than a mere robotic tool. On the other hand, scientific limitations and technological constraints are erecting barriers to reaching these requirements. We will discuss both the demands and limitations in prosthetics in the following sections. The glabrous skin of the human hand is endowed with about 17000 mechanoreceptors [74] and an immense computational capability to acquire and process them. It is, thus, a truly ambitious engineering task to replicate a model of the human hand with prosthetics. Endeavors in developing prosthetic hands still face considerable difficulties in being accepted by the end users.

As a result of various surveys, a list of requirements for the design of prosthetic hands is compiled in what follows.

Sensory feedback. A priority demand among prosthesis wearers is the sensory feedback in manipulative tasks [9] [27] [118]. The survey findings has been also confirmed by neuroscience studies with amputees according to which visual, tactile and sensorimotor systems all contribute to phantom limb awareness [67]. The absence of sensory feedback hinders the natural response of the prosthesis in accordance with the environmental stimuli [70]. Experiments conducted in the study of [109] suggest that grip force control requires at least intermittent sensory feedback in order to update internal models of grasping. Previous studies have shown that haptic displays enhanced manipulative task performance in terms of the interaction with virtual objects by about 50% and reduced the learning time by 50% [127]. A comparison of grip force regulation using tactile display and sensory substitution (both auditory and visual) indicates that tactile display is more successful than sensory substitution. This is most likely because the tactile display mimicks the natural tactile sensation and is thus more intuitive. Additionally, the redundancy offered by combining feedback modalities increases performance in grip force regulation and dexterous manipulation [128]. Although vision alone is able to provide sufficient information for maintaining objects in the grip, evidence indicates that it entails higher grip forces than necessary [70]. Additionally, monitoring the prosthesis using vision alone limits the tasks that can be performed simultaneously and increases the cognitive effort required of prosthesis wearers [9] [128]. Restoring able-bodied quality proprioception and somatosensation is one of the pivotal factors in the sustainable use of prosthetic devices and their seamless integration into the body [60].

Energy-efficiency. Unsatisfactory power schemes for prostheses have been cited as a perennial issue [9]. One of the most frequent repairs or maintenance procedures that prosthesis wearers undergo is the replacement of the prosthetic battery [86]. A more efficient power/energy scheme would provide a longer life

for the prosthesis and would endow amputees with the ability to increase the usage of their prosthesis. One argument is that the high-energy batteries available for portable computers are not sufficient for prosthetic devices [33]. While this argument remains sensible, the issue of energy consumption by prosthetic devices may find a solution through a change in the approach to prosthesis design. Rather than building prosthetic devices by combining energy-consuming components and increasing computational load, a careful consideration of the mechanical design that outsources the functional and computational load to the morphology of the prosthesis may be the key to overcoming the energy issue.

Control abilities. As a result of surveys among prosthesis wearers, achieving able-bodied levels of performance across tasks and across environments has been classified as a priority [9] [27] [60] [118]. One statistical study suggests that about $30 - 50\%$ of amputees wearing myoelectrically-controlled prostheses do not use them regularly or do not use them at all due to low functional capabilities [146]. Prosthetic systems that enable stable and dexterous grasp have been a major research focus, yet this issue was mainly tackled from a pure robot control approach. Many prosthetic hands feature a high-number of actuated joints, yet for amputees it is extremely difficult and counterintuitive to control the many degrees of freedom of these dexterous prosthetic hands. As a consequence, Otto Bock prosthetic hands provide one or two degrees of freedom. This issue can be approached by outsourcing the computation pertaining to robotic control to the morphology of the hand. Evidence for the potential of this approach exists in the work of Dollar et al. [50] and Dermitzakis et al. [49]. Gilja et al. [60] emphasize that an additional focus for future advancements must be robustness, implying that the prosthetic devices of the future should operate over long periods of time and maintain their functionality across multiple decades.

Appearance. The appearance of the prosthetic hand seems to be among the highest-ranked concerns of amputees [153] [86]. The prosthesis must preserve, at least to some extent, the mechanical properties of the biologic hand, such as mass, center of mass, such that it does not generate unbalance or excessive energy in its use.

1.3 Tactile sensors

Technological advancements in multi-DOF robotic hands must be complemented by sensory capabilities in order to attain dexterous control. Providing that the human hand is one of the most sensitive areas of the body, the ability to sense force, slip, vibration, contact, temperature, etc., represents a considerable challenge for the engineering of tactile sensors for robotics or prosthetics. Figure 1.3 provides a selection of the tactile sensors developed to date with respect to two dimensions: (1) the number of sensing elements and (2) the type of information extracted from the tactile sensor, e.g., force, slip, temperature, etc. From the point of view of composition, tactile sensors usually contain an active element, i.e., energy consuming element, e.g., force sensor, slip sensor, etc., and a passive element, e.g., a polymer to cover the active elements.

Presently, there is an apparent tendency towards developing distributed tactile sensor arrays, which are matrices of active elements that acquire local information from a large number of channels. Typically, these sensors are built

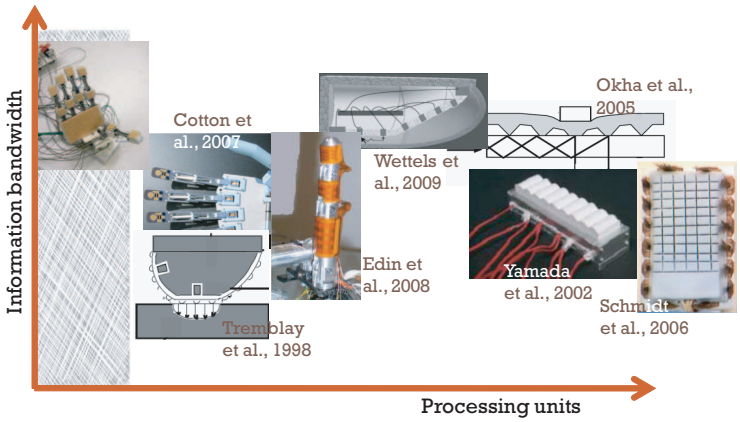

Figure 1.3: Tactile sensor trend with respect to sensing units (number of sensors), as a denominator for used resources, and information bandwidth (type of information that can be extracted). The sensors are presented in the work of Cotton et al. [38], Tremblay et al. [151], Edin et al. [14], Wettels et al. [163], Yamada et al. [167], Okha et al. [112] and Schmidt et al. [140]. These sensors are also briefly described in [46]. An efficient tactile sensing for prosthetics would reside in the leftmost (shaded) area, characterized by rich information using minimal resources.

in such a way as to acquire normal or shear force information. In grasp scenarios, this information notifies about grip forces or slip events. The vast number of sensors also introduces an additional challenge related to the processing of individual sensors and signal integration. The sensitivity and accuracy of the sensor units depend on the materials used, the fabrication process and the arrangement of electronics. The passive element, or cover, is usually used for protection against damage and for interpolating the forces to neighboring sensor units. To date, the distributed tactile sensing technique has been highly parameterized. It contains a network of heterogeneous or homogeneous types of sensors, of various geometrical arrangements, scale, spatial resolutions and physical flexibilities. However, the actual potential of tactile sensors arrays has not been tested in prosthetic applications and has been scarcely assessed on robotic hands.

Force sensors. In [141], a distributed modular skin based on capacitive technology is reported. Interconnected triangular shapes cover the non-flat surfaces of robots such as ICub, Nao, and Kaspar. Local chips integrate groups of sensor inputs to reduce the number of wires and to compensate for the hysteresis and sensor drifts. A force sensor for fingertips is proposed in [26]. This sensor consists of a matrix structure (24.36×34.9 mm) with 64 sensitive sites based on FSR technology. The maximum resolution is about 1 mm and the minimum resolution is about 5 mm. Evaluated on a glove, the force sensor provides good repeatability and sensitivity, although further research is needed to address sensor linearity and hysteresis.

Inspired by the variety of multi-modal sensory capabilities of human skin mechanoreceptors, distributed heterogeneous tactile sensors have been developed. Takamuku et al. [150] developed an artificial skin that embeds two types of sensors (strain gauges and polyvinylidene fluoride (PVDF)) between two sil-

icone layers. This skin has been proven to discriminate between a number of textures during squeezing and tapping. An alternative design for tactile sensors is presented in [163]. The artificial skin features a rigid core equipped with an array of electrodes surrounded by a weak conductive fluid. The volumetric flow path can be differentially measured by each electrode to acquire information about force magnitude, direction or object shape.

As a major stride toward increasing the spatial resolution of sensors' sensitivity, steps have been taken towards the miniaturization of tactile sensors. Oddo et al. [110] showed that a 2×2 array of a 3-D MEMS-based tactile sensor array, providing 16 sensitive elements to external mechanical stimuli in an area of about 20 mm^2, can discriminate roughness by estimation of signal frequency and knowledge of slip velocity. A MEMS-based capacitive tactile sensor array for surface texture discrimination fabricated using using a bonded and etched-back silicon-on-insulator (BESOI) wafer as a substrate and featuring a single crystal silicon diaphragm is presented in [107]. Individual sensors have a size of 500 μm $\times$400 μm, being separated by 150 μm.

An additional requirement related to accommodating such sensors on challenging curve sites has been further tackled by introducing stretchable circuits. The method of fabricating such sensors is presented in [81]. This sensor is a high-performance, single-crystalline silicon complementary metal-oxide semiconductor (Si-CMOS) integrated circuit (IC) that is reversibly foldable and stretchable. The sensor mainly consists of arrays of silicone nanoribbons and ultrathin elastomeric substrates. Similar properties of sensors are obtained by [92] through the use of these conductive elastic films of single-walled carbon nanotubes. On this scale, contact force was determined by a flexible capacitive three-axis tactile sensor made of polydimethylsiloxane (PDMS) [88]. One sensor unit includes four capacitors. Nubs in the upper layer spatially distribute the force to the four units in order to determine normal and shear force. The evaluated sensor consists of eight such units, each able to detect forces in the range of $0 - 20$ mN. A similar sensor can also be found in the work of [32]. Also, a μm-scale sensor array, sensitive to millinewton forces was fabricated by [62], although high hysteresis remains an issue.

Slip sensors. Slip detection is a primary requirement for stable grasp, yet building sensors for accurate slip detection has not received sufficient attention. A 18×18 mm sensor for detecting slip is presented in [103]. Four force sensitive resistors (FSR) [69] placed in different regions of this surface acquire the position of the force and its activation in time through rubber cylinders that cover them and transduce the external force. Cotton et al. [38] developed a sensor based on thick-film piezoelectric material shown to detect incipient slip for a friction coefficient of 0.3. However, this sensor is prone to noise, and therefore its accuracy in detecting incipient slip in real world scenarios has yet to be determined. In [15], a miniature silicon sensor (1.5 mm $\times$1.5 mm μm) is composed of four integrated piezoresistors that are used independently to acquire the three components of an external applied force. This sensor was shown to detect slip with a delay from a minimum of 24.5 ms to a maximum of 44 ms in the majority of experiments. Figure 1.4 depicts some of the discussed tactile sensor arrays.

Although there are obvious advantages related to distributed tactile sensing systems, such as spatial sensitivity, there are many challenges that have to be addressed in order for this approach to become suitable for implementation in prosthetic applications. While the literature offers a plethora of designs

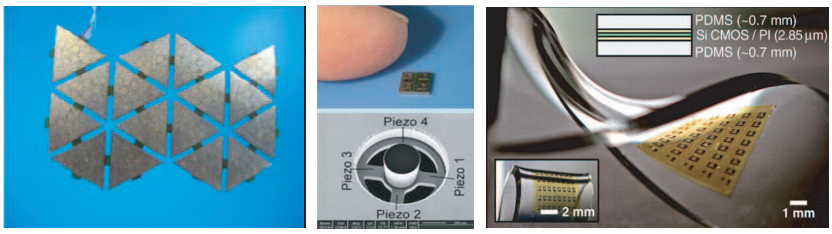

Figure 1.4: Tactile sensor arrays: Tactile sensing system based on capacitive technology for robotic grasp control [141](left), tactile sensor based on 3D MEMS for texture discrimination [110] (middle), highly stretchable tactile sensor based on nanotechnology (right).

and mechanisms for tactile sensors, few studies discuss the impact of numerous factors, such as the space and number of embedded electronics, distributed computing, networking, integration of sensory data, wiring, crosstalk, robustness, power consumption, ease of manufacturing, cost, and maintainability, on the usability and feasibility of the proposed artificial sensing solution. In particular, the spatial arrangement and the transduction method used in the development of tactile arrays are factors of high concern in a dual quest of high spatial resolution and high sensitivity. The amount of wired interconnections associated with tactile arrays represents an impediment to dexterity due to the increased amount of time required to scan and transmit the readings from the array's taxels. Indeed, processing a large amount of data has been considered a major challenge in the field of sensor fusion. Although work has been done in the local pre-processing of the data (compensation of temperature and drifts, data preselection, etc.) by affixing local microcontrollers, the technological limitations of data buses hinder the number of taxels that can be used in tactile arrays or efficient computations on the acquired data. The sensory transmission time imposes another limit on the number of taxels, as the speed of transmission depends on the time needed to scan and multiplex the sensor elements of the array. Power consumption is also a major concern because the prosthetic hand is expected to function consistently and for long durations. Clearly, there is a positive correlation between the number of taxels and the power consumption of the artificial sensory system. A large number of taxels intrinsically affects the robustness of the system due to the interconnections between the taxels. Redundancy could be the positive flip side of this issue.

1.4 Haptic displays

Haptics is the technology that provides an agent, e.g. human user, robot, with the sense of touch, in order to extend the current senses or to substitute or restore missing senses. The concept of haptics has been presented by [59], who advocates that the skin carries the potential of a message transducer as a complement to vision and audition. Haptic feedback has been shown to be beneficial in a plethora of research studies related to tele-operation, virtual environments, surgery, prosthetics and more. Users can carry out operations remotely in space [1], experience virtual environments with realistic tactile feedback [83] [105], are able to perform minimally-invasive surgical in-

terventions [137] and feel tissue forces [16]. Reviews on haptic feedback and displays is found in [64] [98]. Haptic feedback has been evaluated largely in virtual environments, mostly due to the simplicity of the stimulus and control schemes corresponding to virtual environments. In tele-operation or surgery, haptic feedback provides more dexterity in the usage of tools that operate in remote sites. In prosthetics, the demands of the haptic feedback are considerably high. The performance of the haptic feedback is ultimately evaluated by whether the prosthesis was accepted or not by the users who wear the robotic system everyday and who are challenged to participate in unstructured and complex activities. Saunders et al. [138] show that haptic feedback becomes pivotal under feed-forward uncertainties. The result of their study indicates that the use of a prosthesis - as a new body part that is no longer fully compatible with the predictive motor models in the brain - strongly calls for efficient haptic feedback. Concurrently, research seems to corroborate the theory that intermodal sensory feedback correlations enforce the bodily integration of an artificial limb [22] [101]. For reviews on natural human haptics, the reader is encouraged to read the ample studies on skin sensitivity [145], perception [78] and location sense [36]. Although humans experience a wide range of sensations, sensory psychophysics was found to be described by four main attributes: location, timing, intensity and modality [80]. Haptic devices and interfaces are basically tailored to display these attributes or a mixture of them, within the sensing capabilities of the human users, which include: force feedback, contact location, slip and shear, object shape, temperature, etc.

Haptics in prosthetics has emerged as a natural solution to the requirements of prosthesis users to remove vision as the main feedback modality for the control of their prosthetic hand. The substitution of the lost tactile senses to support the complex daily activities carried out by prosthesis users, entails several demands: (1) interface compatibility with the functions and spatial distribution of human skin mechanoreceptors; (2) stimuli coverage necessary to describe the environmental interaction events; (3) intuitiveness of the artificial stimuli; and (4) light, small, and affordable haptic displays.

Research on sensory substitution has given substantial attention to the development of tactile force displays. Popular technologies include push (or pressure) mechanisms and vibrations. A design pattern often encountered in haptics is to convert the tactile display to an array or matrix of actuated stimulators whenever more information has to be transmitted. Although enhanced feedback is desired to construct an environmental representation of satisfactory resolution with respect to the spatial and temporal acuity of the human sense, consideration must be given to energy-consumption. Relaying tactile stimulation to the fingertips, an area of high density of mechanoreceptors, has been a preferred choice in many general haptic applications [115]. While for tasks such as video games, special tool manipulation, virtual environments, haptic feedback to the fingertips is appropriate, in prosthetics stimulation the fingertip of the healthy hand implies obstructing fine control and complex manipulation. Alternative stimulation sites for various haptic applications represent foot toes [114], lumbar area [143], tongue [166], forearm [165], etc.

Force displays. Meek et al. [102] presented a force feedback system that proportionally maps the exteroceptive force to the prosthesis users. In their study, a force was applied by a motor-driven pusher on the biceps of the users. Their results showed an improvement mainly in object manipulation and grip

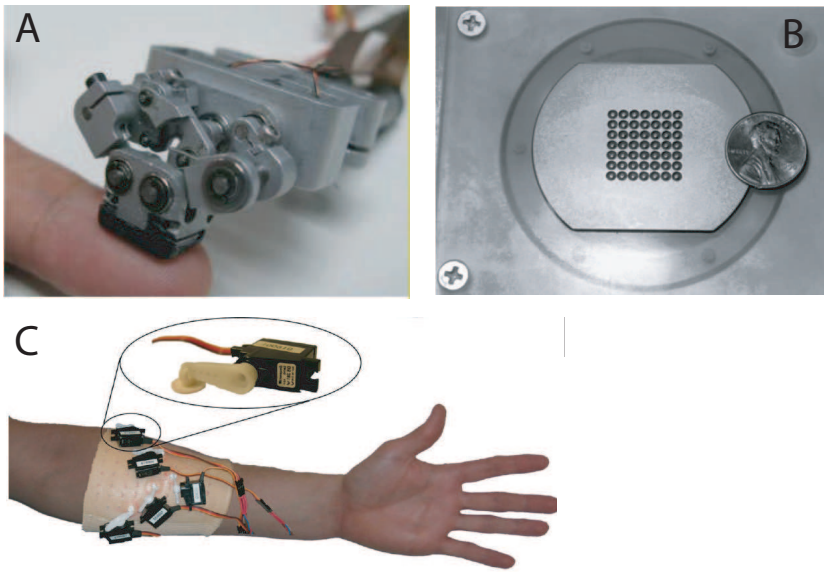

Figure 1.5: Tactile stimulation arrays. A. Multi-function haptic device for displaying touch, pressure, vibration, shear force and temperature for patients that undergone reinnervation(TR) surgery [82]. B. A 49 electrode array for tongue stimulation and pattern display [166]. C. An array of motors to display forces for each hand finger by a push mechanism [4].

control for users provided with direct force as feedback, as opposed to a low success rate for users engaged in open-loop manipulation tasks. Similarly, Patterson et al. [116] translated grip pressure from an object to hydraulic pressure in a cuff around the upper arm of the user. The authors compared various feedback modalities such as vibration, pressure, vision, vibration and vision, and pressure and vision. Combined pressure and vision feedback resulted in the smallest error in gripping a block, while pressure feedback alone performed better than vibration feedback alone in relaying grip pressure. Although both studies successfully argue that high performance in manipulation is sustained by one-to-one physiologically compatible stimulation, the feedback signals are less likely to stabilize the grip without the assistance of vision. In more recent work by Li et al. [89], force was mapped into vibration for multiple sclerosis patients in an effort to help them manipulate objects more efficiently. Depending on the level of patient impairment, the methodology consisted of relaying amplitude-based feedback proportional to the grip force, or event-cue vibration feedback, which alerted users when their grip force strayed from a safe-grasp force range. Under these conditions, patients could grasp and lift objects more successfully than they could without any feedback. The approach is viable for rehabilitation training in which the manipulation of a limited set of objects with known coefficients of friction is sufficient. Panarese et al. [114] provided grip force feedback to the toes and showed that participants in the study grasped a test object by appropriately regulating the grip force applied by a robot hand. Force feedback is relevant for characterizing the applied grip force of prosthesis wearers.

Eliciting physiological tactile sensations through cutaneous electromechanical vibration and electrical stimulation pioneered with [12] and were thoroughly investigated by [79]. Bach-y-Rita et al. evaluated a 16×16 matrix of electrodes placed on the tongue to provide body position information to visually impaired people who have vestibular problems [166]. The technique was further implemented in surgery [131]. Electrical and vibtotactile stimulation showed potential for prosthetic application for representing skin contact with held objects [142] or for grip force adjustments [31], respectively. Vibrotactile stimulation in conjunction with vision was also implemented in [35] for the display of grip force in upper-limb prostheses. Figure 1.5 shows a selection of tactile stimulation arrays that were mentioned above.

Slip displays Slip or motion cues feedback in prosthetic applications has not received much attention, although it's role in grasp stability is pivotal. Tsagarakis et al. [152] developed a device that embeds two miniature motors in a "V" configuration to generate sensations of relative lateral motion at the fingertip. Kim et al. [82] developed a number of multifunctional tactile feedback devices that can be used to provide feedback on contact, pressure, shear force, vibration, and temperature for users that have undergone targeted reinnervation surgery. For tele-manipulation, Edin et al. [14] devised a mechanism in which a user holding an instrumented object receives frictional information through solenoids mounted on the object to elicit physiological responses that resemble the responses observed during slips. These studies, however, do not examine the possible benefits of slip feedback for prosthesis or tele-manipulation users. Webster et al. [160] developed a tactile slip display for virtual reality applications. The device reproduces the sensations of sliding contact and incipient slip through the rotation of a ball positioned under the user's fingertip. According to the authors' findings, slip and force feedback represent a better solution than force feedback alone for assisting participants in the manipulation of a virtual object with lower forces.

Considering the requirements attributed to haptic technology, this thesis subscribes to taking an economical approach to the feedback interface. According to this approach, haptic mechanisms should be designed with minimal resources and relay a maximum amount of information.

1.5 The economical view on the feedback loop

Nature is not wasteful with respect to the resources it uses. A plethora of examples confirm this statement. To name a few, the black ghost knife fish of the Amazon, only needs about 4 milliwatts of power to swim (a thousand times less than an iPhone uses). With this tiny amount of power it sustains not only its body and brain, but also its "electric headlamp", an organ that continually emits a weak electric field so it can sense things in the dark when it hunts [97]. Some spiders prefer to move in an upside-down position, using gravity to allow less muscle power usage to propel themselves forward [108]. The flight of the albatross, during its dynamic soaring, is aided by a shoulder lock tendon which locks its wing into the fully extended position, enabling it to maintain this posture while using little muscle expenditure [130] [2]. One example relevant for human sensing resides in the skin morphology at the fingertips. The ridges on the human fingertips may act as high frequency filters, thus facilitating

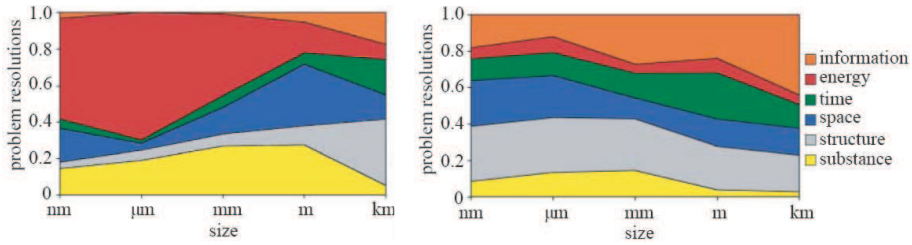

Figure 1.6: Difference between biology (left) and technology (right) with respect to scale and various resources used for solutions to problems [157].

the excitation of Pacinian corpuscles for sensing fine texture [139]. Although energy-efficient mechanisms can be found throughout nature, in engineering, increasing the behavioral complexity is usually equated with increasing the energy. Vincent et al. [157] advocates that engineering techniques primarily make use of energy, whereas biological systems primarily exploit structure, space and information (see Fig. 1.6). For prosthetic hands (and for robotics at large) it would highly be desired to implement the latter approach to fulfill the afore mentioned constraints: providing rich tactile information, while reducing the complexity and increasing the energy-efficiency of the prosthetic interface, and improving its robustness in meaningful tasks such as grasping.

This thesis introduces an economical view on the feedback loop, promoting comprehensive yet efficient sensory information. The thesis investigates the upper-limb prosthesis-related requirements and design for tactile sensing and haptic display systems. We define *economical tactile sensing* as the ability of the tactile sensing system to make use of reduced resources, e.g. electrical components, computation, wiring, etc., to produce an increased amount of information. In this thesis, this attribute is enabled in dynamical events such as object slippage. The economical sensing is achieved through the intrinsic morphology of the artificial skin. In the following chapters, we introduce a silicone-based artificial skin featuring surface ridges. Using a single force transducer, this artificial skin encodes force, slip detection and slip speed when the ridges are uniformly distributed on the skin. Additionally, arranging the ridges on the skin in a non-uniform manner (and thus breaking the symmetry of the distribution of ridges) enhances the sensing capability by adding location information content. By exploiting morphological cues such as shapes, shape arrangements, and materials used in the design of the artificial skin, the circuitry, wiring and amount of energy are reduced. This approach is opposite to that of distributed tactile sensing, wherein a large network of sensors acquires environmental cues, pre-processes the data with local microcontrollers, and multiplexes and transmits the data for subsequent processing and interpretation. The advantages of distributed tactile sensing clearly reside in such features as data redundancy. Some characteristics of the economical and distributed tactile sensing systems are summarized in the Table 1.1. Our approach does not refute the advantages of distributed tactile sensing, but aims to introduce the perspective of morphology exploitation as a powerful design with the potential to advance efficient tactile sensing systems. In our work, the skin morphology intrinsically encodes rich environmental information and introduces the means for an economical design

	Economical tactile sensing	Distributed tactile sensing
Number of sensors	Low	Large
Numbers of wires	Low	Large
Robustness	Yes	Yes
Circuitry complexity	No	Yes
Information redundancy	No	Yes
Crosstalk probability	Low	High
Distributed computing	No	Yes
Cost	Low	High

Table 1.1: Economical tactile sensing and distributed tactile sensing.

	Economical haptic display	Distributed haptic display
Number of actuators	Low	Large
Numbers of wires	Low	Large
Robustness	Yes	Yes
Circuitry complexity	No	Yes
Information gain	Yes	No
Cost	Low	High

Table 1.2: Economical haptic display and distributed haptic display.

for tactile sensing systems. The significance of the economical tactile sensing systems becomes pivotal in upper-limb prosthetics for which the information amount, energy-consumption, device's weight, robustness and affordability are essential features, as described above in section 1.2. Our novel approach has an impact on the simplicity of tactile sensors, while at the same time meeting the demanding requirements of prosthetic applications.

We define *economical haptic display* as the ability of the haptic system to make use of reduced resources, e.g. actuators, energy, computation, etc., to produce enhanced haptic stimuli via tactors. We apply this approach to the design of a haptic display in order to relay force and slip information to human users. The haptic display is actuated by a single conventional electromagnetic motor. By exploiting the two directions of rotation of this motor, passive local mechanisms and soft materials, two silicone belts are driven in a mutual-exclusive way to relay a normal or tangential force on the skin and create a realistic haptic representation of the grasp. These two stimulations designate the grip force and the slip speed of an object during manipulation. The selection of the type of stimulation is achieved by combining the global control provided by the rotation direction of the motor, and local control provided by a passive mechanisms that decouples the two silicone belts. Realistic sensations of normal pressure and slip speed are created through the careful choice of material, stiffness variation,and texture of the tactors that come in contact with the skin. Contrary to this approach, multi-modal haptic devices tend to use a large number of actuators in order to control each individual tactors or each information channel [158] [154]. Table 1.2 summarizes some of the characteristics of the two approaches for haptic displays.

1.6 Overview of the thesis

The remaining content of this thesis is organized in seven chapters, as described in Fig. 1.7. Chapters 2 and 3 investigate the requirements pertaining a comprehensive representation of grasp for efficient grasp stability in upper-limb prostheses. Chapter 2 focuses on the role of the slip speed feedback in grasp stability. We explore the advantages of quantitative slip feedback, as a complement to existing approaches on force feedback for haptic interfaces.

Chapter 3 studies the individual and combined benefit of force and slip speed feedback for grasp stability. In this study, we integrate an artificial skin for force and slip sensing with a graphical display of grip force and slip speed.

Chapters 4 and 5 introduce a ridged artificial skin, whose morphology enables an efficient haptic sensing in prostheses. Chapter 4 presents the artificial skin featuring linearly-distributed ridges for the detection of grip force, slip occurrence and speed of a held object. In Chapter 5, the capabilities of the artificial skin are extended to location detection, by distributing the ridges on the skin in a non-uniform manner.

Chapters 6, 7 and 8 investigate efficient techniques for relaying rich haptic information to the prosthesis wearer through the design of haptic devices. Chapter 6 presents a haptic apparatus used to study potential information transmitted by moving or by making/breaking contacts to an (artificial) skin. Chapter 7 focuses on the influence of the shapes of soft tactors to generate grip force by periodically making/breaking the contact with a surface. Chapter 8 presents the development and the evaluation of an efficient wearable haptic device that is able to relay grip force and slip speed information.

Finally, this thesis is wrapped up with discussions and a conclusion in Chapter 9.

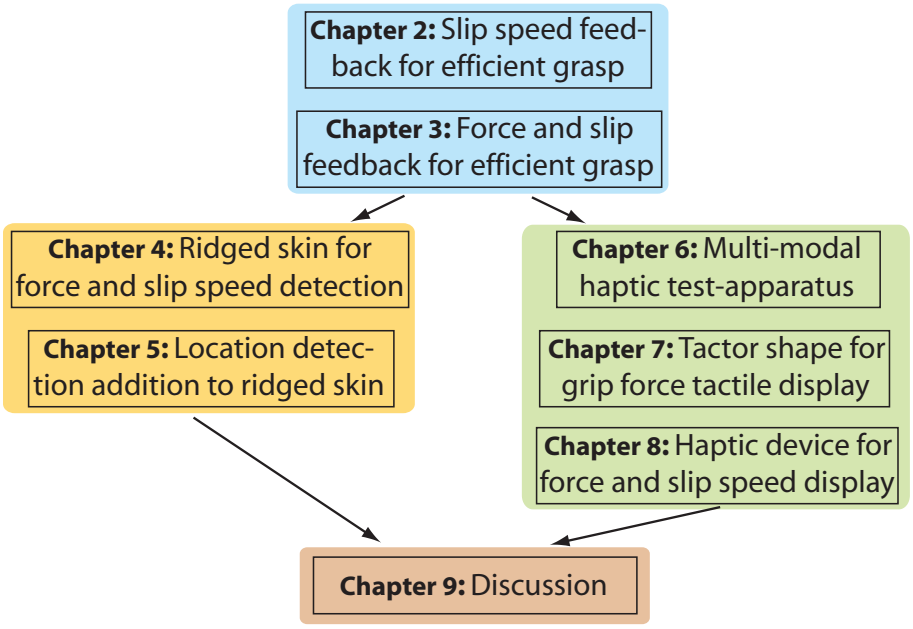

Figure 1.7: The structure of the core of the thesis. The first two chapters investigate requirements for efficient grasp in upper-limb prostheses. Chapters 4 and 5 focus on efficient tactile sensing. The potential of a ridged artificial skin is investigated for force, slip occurrence, slip speed and location detection. Chapters 6, 7 and 8 investigate an efficient tactile display to relay force and slip. Chapter 9 discusses the overall results of the thesis and future research avenues.

Chapter 2

Slip Speed Feedback for Prosthetic Applications

Role of slip speed feedback for grasp stability

Chapter 2 describes a set of experiments whose results motivated further investigation of slip speed feedback for efficient grasp stability.

Grasp stability in the human hand has been resolved by means of an intricate network of mechanoreceptors integrating numerous cues about mechanical events, through an ontogenetic grasp practice. An engineered prosthetic interface introduces considerable perturbation risks in grasping, e.g. object instability, calling for feedback modalities that address the underlying slip phenomenon. In the present study, we propose an enhanced slip feedback modality, with potential for myoelectric-based prosthetic applications, that relays information regarding slip events, particularly slip occurrence and slip speed. The proposed feedback modality, implemented using electrotactile stimulation, was evaluated in psychophysical studies of slip control in a simplified setup. The obtained results were compared with vision and a binary slip feedback that transmits on-off information about slip detection. The slip control efficiency of the slip speed display is comparable to that obtained with vision feedback, and it clearly outperforms the efficiency of the on-off slip modality in such tasks. These results suggest that the proposed tactile feedback is a promising sensory method for the restoration of stable grasp in prosthetic applications.

[1]Parts of the material in this chapter previously appeared in: Dana D. Damian, Alejandro Hernandez Arieta, Harold Roberto Martinez Salazar and Rolf Pfeifer (2012) "Slip Speed Feedback for Prosthetic Applications", *IEEE Transactions on Biomedical Engineering*, (in press).

2.1 Introduction

Stability in grasping is attributed to a sensorimotor system that is able to transform information about grasp forces in the human hand in order to ensure adequate safety margins against slip. Stable grasp with the human hand requires both anticipatory parameter control, based on a predictive model in the central nervous system (CNS), and discrete-event sensory-driven control [72]. The latter type of control is specifically related to involuntary slip scenarios and is based on sensory information to regulate the ratio between grip and load forces [63] [10]. With prior knowledge about the grasped object, proprioceptive cues, and incoming exteroceptive signals, such as force, pressure, motion and vibration, the CNS is able to integrate sensory information in order to ensure a grip force within safe margins. Prosthetic hands introduce an engineered sensorimotor interface that hinders the natural reliance on predictive models and is prone to generating significant perturbations in the grasping process. In such scenarios, stable grasp control becomes a sensorimotor transformation highly dependent on incoming sensory information. This transformation is aimed to regulate the grip force and remove perturbations such as slip and excessive force, which can damage the held object or involve unnecessary energy use.

Currently, there are two main approaches to grasp stability that differ in the type of grasp control. Automatic grasp control relies on various transduction methods for slip and force detection to automatically adjust the grip force of a robot hand, e.g., [135] [85] [162]. This type of technology has also been implemented in commercially available prosthetic hands, e.g., Otto Bock [65] and RSL Steeper [149]. One of the notable features of this technology is a fast automatic grasp response time (e.g., approx. 750 ms as reported in [162]). The limitation of this approach is that it commonly removes the sensory input awareness of the user, which is a critical element for a sustainable use of the prosthetic hand and its incorporation into the wearer's body. An alternative feedback modality to vision for manipulative actions is a design priority among amputees wearing myoelectric-based prostheses, as reported in [9]. The absence of sensory feedback is a frequent cause for amputees' rejection of their prosthesis, e.g., [19]. Concurrently, research seems to corroborate the theory that intermodal sensory feedback correlations enforce the self-attribution of an artificial limb, e.g., [22] [101]. These arguments have led to the adoption of the second type of control strategy. Within this approach, sensory feedback about grasp is artificially relayed to the users to provide them with command over the prosthesis. The two lines of research are equally significant, as studies on shared control [35] suggest that the best performance in grip control might result from a combination of these two approaches. Although there is an increasing body of work on enriching the artificial tactile sense of robotic/prosthetic hands for automatic grasp (a recent overview is found in [41]), enrichment of the haptic interface has received limited consideration. Therefore, in this work we investigate the potential of introducing an enhanced slip feedback for prosthetic interfaces.

2.2 Related work

Haptics research has undertaken various endeavors to provide a substitute for the missing tactile sense, pioneering with studies on eliciting physiological tactile

sensations through cutaneous electromechanical vibration and electrical stimulation [12] [79]. Tactile force displays have been an extensive focus of haptics research for prostheses [147]. Meek et al. [102] proportionally maps the exteroceptive force to the prosthesis users. They showed an improvement mainly in object manipulation for users provided with force feedback, as opposed to a low success rate for users engaged in open-loop manipulation tasks. Similarly, Patterson et al. [116] translated grip pressure from an object to hydraulic pressure in a cuff around the upper arm of the user. The authors compared various feedback modalities such as vibration, pressure, vision, vibration and vision, and pressure and vision. Combined pressure and vision feedback resulted in the smallest error in gripping a block, while pressure feedback alone performed better than vibration feedback alone in relaying grip pressure. Although both studies successfully argue that high performance in manipulation is sustained by one-to-one physiologically compatible stimulation, the feedback signals are less likely to stabilize the grip without the assistance of vision. In more recent work by Li et al. [89], force was mapped into vibration for multiple sclerosis patients in an effort to help them manipulate objects more efficiently. Depending on the level of patient impairment, the methodology consisted of relaying amplitude-based feedback proportional to the grip force, or event-cue vibration feedback, which alerted users when their grip force strayed from a safe-grasp force range. Under these conditions, patients could grasp and lift objects more successfully than they could without any feedback. The approach is viable for rehabilitation training in which the manipulation of a limited set of objects with known coefficients of friction is sufficient. Panarese et al. [114] provided grip force feedback to the toes and showed that participants in the study grasped a test object by appropriately regulating the grip force applied by a robot hand. Force feedback is relevant for characterizing the applied grip force of prosthesis wearers. However, grasp instability, such as slip, cannot be sufficiently prevented or overcome using this type of feedback scheme. It is not trivial to predict the weight or friction properties of everyday objects grasped with prosthetic hands in order to automatically and efficiently determine a threshold of force above which force feedback can be relayed or below which the user can be notified of the imminence of a slip.

Physiological studies showed that slip is a pivotal determinant in grip control [72] [10]. Slip, artificially generated by changing the load force on an object held in the human hand, was found to improve the agility of the grip response that depended on the load force rate [72]. This result is a prime indicator that the rate of slip may influence the grip response. Nonetheless, slip or motion cues feedback in prosthetic applications has not received much attention. Tsagarakis et al. [152] developed a device that embeds two miniature motors in a "V" configuration to generate sensations of relative lateral motion at the fingertip. Kim et al. [82] developed a number of multifunctional tactile feedback devices that can be used to provide feedback of contact, pressure, shear force, vibration, and temperature for users who have undergone targeted reinnervation surgery. For tele-manipulation, Edin et al. [14] devised a mechanism in which a user holding an instrumented object receives frictional information through solenoids mounted on the object to elicit physiological responses that resemble the responses observed during slips. These studies, however, do not examine the possible benefits of slip feedback for prosthesis or tele-manipulation users. Webster et al. [160] developed a tactile slip display for virtual reality applica-

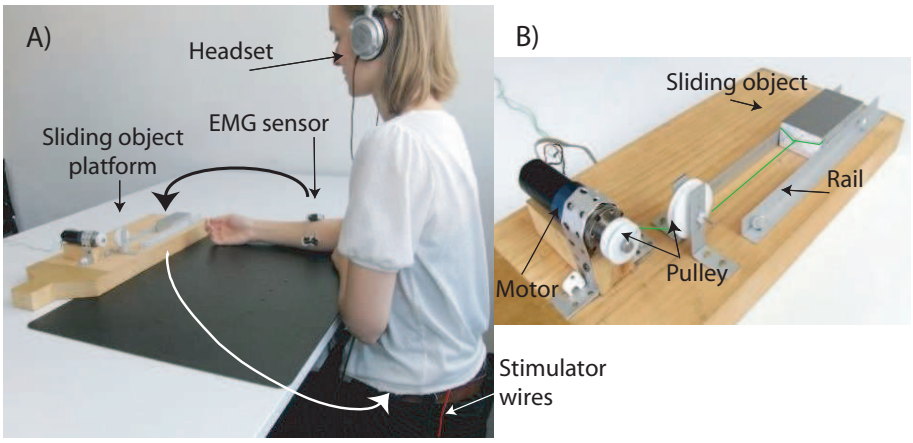

Figure 2.1: Experimental setup. A) The participant used electromyographic (EMG) signals to control the speed of a slipping object, while receiving visual or electrotactile vibration feedback. Auditory feedback removed the noise and controlled the time progress of the experiment. B) Details of the platform on which the motor-driven object slipped.

tions. The device reproduces the sensations of sliding contact and incipient slip through the rotation of a ball positioned under the user's fingertip. According to the authors' findings, slip and force feedback represent a better solution than force feedback alone for assisting participants in the manipulation of a virtual object with lower forces.

We present a preliminary study on the potential of slip speed feedback for grip force control. The evaluation of slip speed feedback is performed in simplified psychophysical closed loop experiments through a comparison with feedback that relays on-off information regarding slip occurrence and with visual feedback. Information about slip is transmitted by electrotactile vibrations whose frequency encodes the speed of a slipping object. The selection of this frequency-encoded slip feedback stems from the properties of an artificial ridged skin developed by our group [46]. The artificial ridged skin detects, through its morphology, both slip occurrence and velocity from the spectral features of the signal of one single force sensor embedded in the skin. The frequency extracted from the tactile sensor signal can be thus mapped into the frequency of a tactile stimulation signal, providing users with enriched and efficient slip information.

The remainder of the present chapter is organized as follows. Section III presents the materials and methods based on which our experiments were performed. Section IV describes and discusses the results obtained from the experiments. Section V delivers cross-study remarks, while conclusions are presented in Section VI.

2.3 Materials and methods

We devised a simplified closed loop system that simulates the slipping phenomenon in EMG-based prostheses. In what follows, the experimental setup and procedure, the control system, and the data analysis methods are presented.

2.3.1 Experimental setup

We opted to implement a physical experimental setup of the slip phenomenon, instead of a graphical one, in order to create a more realistic and intuitive environment for the participants of the study. Figure 2.1A depicts the experimental setup. A participant was seated in a relaxed position with his arm on a table with his palm facing upward at an angle of approximately 45 °. Muscle contractions were acquired from the participant's Flexor Carpi Ulnaris muscle through one wireless electromyographic (EMG) sensor (Noraxon Inc.). The sensor sampled the contraction signal at 1, 500 Hz. On the table in front of the participant, an object weighing 250 g was made to slip on a horizontal surface. A pair of rails kept the object moving in the same direction. The object was connected to a pulley of the DC motor of 16 mm in diameter through a non-deformable wire (Fig. 2.1B). The DC motor (Faulhaber DC-Micromotor 2642), driven by a speed controller (Atmel ATmega328P AVR microcontroller), dragged the object along the platform surface at a constant velocity. The participant received feedback about the slip of the object by vision or cutaneous electrotactile stimulation. We chose the latter type of stimulation due to its high controllability and long-studied characteristics [79]. An electrical stimulator, generating biphasic signals of tunable frequencies [143], transmitted the cutaneous stimulation through one pair of self-adhesive multilayer hydrogel electrodes of 5x5 cm size (PALS Neurostimulation electrodes, Axelgaard Manufacturing Co., Ltd.), thus mapping 1D information about slip. The electrodes were placed on the lumbar area of the back, symmetrically with respect to the spine. We chose this area because it has a low sensory load [129], and there is no crosstalk between the signal of the electrical stimulator and the EMG signal. Detailed properties of these electrodes for prosthetic applications were studied in [143]. White noise was sent constantly to the headset in order to remove potential sound patterns that may influence the experimental process. Potential vibrations from the DC motor were eliminated by a soft pad placed beneath the forearm of the participant. A PC collected the EMG sensor signal and, accordingly, sent control commands to the DC motor controller regarding the speed at which to drag the object.

2.3.2 Experimental procedure

Nine unimpaired volunteers ranging in age from 26 to 34 years participated in three experiments, after having read the instructions and having given their consent. The number of participants was computed using the G*power analysis program [55]. Prior to commencing the study, ethical clearance was provided by the Swiss Association of Ethics Committees (KEK).

The participants were tasked with stopping an object from slipping by contracting their muscle based on the sensory information received from a feedback modality. This closed loop simulated the control of an EMG-driven prosthetic hand, the grip closure of which is regulated proportionally with respect to the user-dependent intensity of the EMG input signal over a fixed time period [53]. Consequently, the grip closure affects the slip or slip velocity of a held object. Hence, a weak grip closure allows an object to slip, and a strong grip may crush the object. However, an optimum hand closure can stop the object from slipping. The participants were instructed to contract their muscles without

moving their fingers too much, in order to simulate an amputee to some extent. The performance of participants in stopping slips was evaluated in a comparative study that consisted of three experiments. In each of these, participants received sensory information about slip through a unique type of feedback:

Visual feedback

The participant was watching the object slipping on the horizontal surface. The participant visually assessed the velocity of the object and contracted the muscle in order to stop the slip.

Slip occurrence feedback

The participant was deprived of visual stimuli by wearing a sleeping mask. Regardless of the slip velocity of the object, the feedback received by the participant consisted of an electrical stimulation signal of constant frequency, notifying the participant that the object was slipping. If the object stopped moving, the stimulation became inactive. Upon receipt of the feedback, the participant contracted the muscle and attempted to stop the slip.

Slip speed feedback

The blindfolded participant was provided with an electrical stimulation signal whose frequency was linearly associated to the slip velocity. Therefore, the tactile display carried not only information on whether the object was slipping, but also information on the slip velocity. The stimulation became inactive when the object did not slip. After recognizing the slip velocity, the participant decided the contraction intensity that would stop the object.

The overall 27 experiments (three feedback modalities for nine participants) were crossbalanced such that no systemic learning pattern would emerge. The rest interval between two consecutive experiments was at least one day for each participant. Each experiment consisted of 40 sessions, whereas one session was composed of potentially three phases, during which the participant attempted to stop the object from slipping. Therefore, the total number of phases could range from 40 to 120 phases, depending on the performance of the participant.

The main parameters that were taken into account in the design of the experiments were the electro-vibration frequency, the EMG intensity and the speed of the object. Prior to all experiments, we conducted a perception survey with the participants in this study, during which they were asked to characterize their perception of a set of electro-vibration frequencies generated by the electrical stimulator. As revealed by quantitative research [51] and observed in the subjective survey, nonlinearities in the perception of vibration frequencies are present. To avoid this issue in achieving the aim of the current study and to ensure a fairly linear mapping between slip speed and vibration perception, we opted to have a low number of stimulation frequencies. Among the tested frequencies, four rates of stimulation were found to relay distinctive and fairly linear vibration perceptions. At the beginning of the experiment, the participants undertook an EMG-intensity calibration phase, in which they were requested to contract their muscles with a minimum force and then a maximum comfortable force. Based on the findings of the survey on stimulation frequencies, the values within these

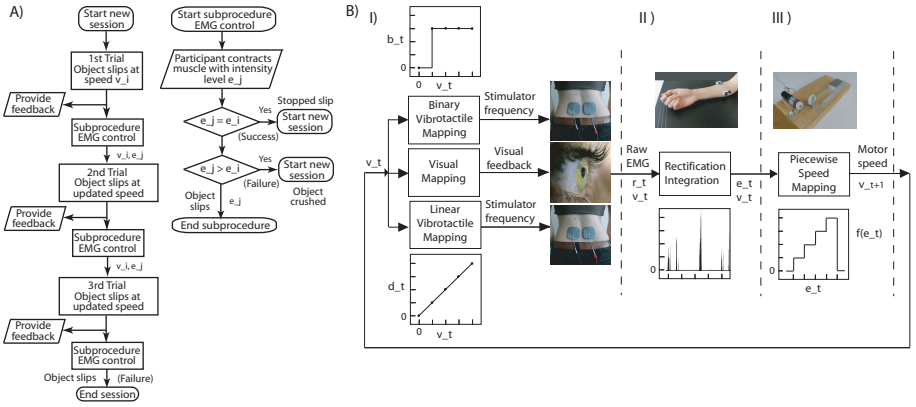

Figure 2.2: Experimental procedure and control. A) Diagram of the experimental procedure within a session. One session consists of three phases in which the participant attempts to stop the slip. Speed v_i is associated with and expects a contraction level e_i, whereas e_j is the actual contraction level input by the user. Stopping an object that slips at speed v_i requires a muscle contraction level of $e_j = e_i$ (success). B) Schematics of the control flow for the task of stopping the slipping object. I) Given that the object slips at initial velocity v_t, the participant receives notification by vision or slip occurrence feedback (b_t) or by slip speed feedback (d_t). II) The participant attempts to control slip by inputting a muscle contraction. The acquired EMG signal, r_t, is rectified and integrated into e_t. III) Function f maps a muscle contraction level to the speed change that it can cause to the object. Depending on e_t and on velocity v_t, the velocity of the object changes to v_{t+1}.

two EMG intensity limits were segmented into four equal contraction intensity intervals (levels). Furthermore, these levels were linearly associated with four velocities at which the object was set to move. Consequently, the closed loop experiment used four levels of muscle contraction linearly associated with four slip speeds of the object, which were, in turn, linearly associated with four frequencies of electrical stimulation. The numerical details of these parameters are provided in the following subsection.

As a short training exercise, the functionality of the closed loop interaction is explained to each participant, in five sessions that consisted of a random selection of feedback types and slip speeds. The additional purpose of these sessions is to associate the values of the electrical stimulation with the visual assessment of the slip speeds when the participants are blindfolded during the experiments involving the two electrotactile displays.

A diagrammatic description of one experiment in terms of the sessions is provided in Figure 2.2A. When a session began, the object slipped at a velocity randomly generated from the set of four possible velocities. As a response to the slip notification relayed by a certain feedback modality, the participant contracted his or her muscles in an attempt to match the contraction intensity level with that linearly associated with the actual velocity of the object. Depending on the contraction intensity level of the participant and the velocity of the object, the following situations may occur within a session: 1) the contraction intensity level matched the speed level, in which case the object was stopped (successful session); 2) the contraction intensity level was higher than the level

corresponding to the actual speed, in which case the object was assumed to be crushed (failed session); and 3) the contraction intensity level was lower than the level corresponding to the actual speed, in which case the object continued to slip at a reduced speed (the session proceeds to the next phase). The movement velocity of the object, altered by the input contraction intensity level, was updated at the beginning of each subsequent phase. The following subsection contains further details about the control of the experimental procedure. In addition to the slip feedback, the participants received auditory cues that control the course of the experiment and also informed participants regarding their performance. The auditory cues denoted the beginning of a session/phase, instructing participants of when to contract their muscles, and notified the participants of successes or failures in stopping the slipping object at the end of a session. One phase lasted four seconds, while the pause between phases was one second. Approximately five seconds elapsed between consecutive sessions, which was necessary to manually relocate the object at the starting position for the experiment with visual feedback. The four-second interval for response time was chosen to ease the participants' task by providing a relatively large amount of time to assess slip velocity and react to it. Although in natural-object manipulation, muscle contraction continuously modulates the state of the slipping object, participants of this study could relax their muscles during the inter-phase pause. The procedure was justified by measures to avoid muscle exhaustion along a minimum of 40 contraction phases. The procedure can also be thought of as describing an artificial interface between muscle activity and the prosthesis controller that offers large freedom in the design of a shared control scheme for manipulation.

2.3.3 Control system

The control system coordinating the phases of the experiment was implemented on a PC and is depicted in Fig. 2.2B. In an experimental phase, an object was made to slip at one of four rates 1.8, 3.2, 4.6, or 6.0 mm/s. These rates are in the set $V = \{v_i\}$, $i \in \overline{1:4}$. The relation between the rates is $v_j = v_i - 1.4 \cdot (i - j)$, where $i, j \in \overline{1:4}$. The four specific values were chosen to comply with the space constraints of the experimental platform and with the session time requirements of the experimental procedure. Slip information was relayed to the participants either by visual feedback or by electrotactile feedback (Fig. 2.2B.I). For experiments with electrotactile feedback, the cutaneous vibration frequencies selected in the preliminary survey are in the set $H = \{4, 36, 68, 100\}$ Hz. In particular, slip occurrence feedback at time t was defined as a piecewise function:

$$b_t = \begin{cases} f_b & : \quad v_t \neq 0 \\ 0 & : \quad v_t = 0 \end{cases}$$

with $f_b = 68$ Hz $\subset H$ for all participants. This stimulation frequency was extracted from the empirical frequency set as a value close to the median of the set. Essentially, this modality is confined to only conveying feedback messages on whether slip occurred. In case the object was slipping (speed $v_t \neq 0$), the stimulator transmits one frequency signal, f_b, otherwise the stimulation is inactive. The slip speed feedback at time t was designated by a discrete linear mapping, $d_t = l_d(v_t) \subset H$, and contains frequency-encoded information about absolute values of the slip velocities. Based on the values of the experimental

velocities and vibration frequencies, the linear function $l_d = 22.85 \cdot v_t - 37.14$ was derived. Thus, low vibration frequencies correspond to low slip velocities, and high vibration frequencies correspond to high slip velocities. The intercept factor, -37.14, is a consequence of the empirical linear design of the slip speed feedback function.

As mentioned previously, at the beginning of an experiment, the minimum, e_{min}, and the maximum comfortable contraction, e_{max}, were stored. The values within these two limits were segmented into four equal contraction intensity intervals (levels) corresponding to the four possible velocities of a slipping object. We denoted the set of EMG intensity levels as $E = \{e_j\}$, $j \in \overline{0:5}$, where we included level e_0 for the case of an input intensity below e_{min} and level e_5 in order to represent the input intensity above e_{max}. Within each experimental phase, as a response to the slip information received, the raw EMG signal, r, acquired from the muscle contraction, was rectified, and its integral was computed in order to obtain the EMG intensity e_j (Fig. 2.2B.II).

The participant could alter the slip velocity of the object by contracting the muscle at a relevant intensity level, $e_j > e_{min}$. The piecewise function $f : E \to V \cup \{0, \infty\}$ maps the contraction intensity level to the velocity change that it can cause (Fig. 2.2B.III):

$$f(e_j) = \begin{cases} v_i & : \quad j \in \overline{1:4} \wedge i = j \\ 0 & : \quad j = 0 \\ \infty & : \quad j = 5 \end{cases}$$

Depending on the current slip velocity $v_t = v_i \in V$ and the contraction intensity level $e_t = e_j \in E$, the new speed assigned to the object is given by the relation:

$$v_{t+1} = \begin{cases} v_t - f(e_t) & : \quad f(e_t) \leq v_t \ (1) \\ 0 & : \quad f(e_t) > v_t \ (2) \end{cases}$$

where $v_{t+1} : V \to V \cup \{0\}$. If $v_{t+1} = 0$, the object is stopped ($v_{t+1} = 0$ mm/s), and the session finishes as a success (condition (1) with $f(e_t) = v_t$) or failure (condition (2)). Otherwise, the object continues to slip at a lower velocity (condition (1) with $e_t > e_{min}$) or at the same velocity (condition (1) with $e_t = e_{min}$). The new speed, v_{t+1} is updated in the subsequent phase. If after all three phases, $v_{t+1} \neq 0$, then the session finishes as a failure. For example, if the current speed of the object is $v_t = v_4 = 6.0$ mm/s and the muscle contraction level is e_3 (the value is user-dependent), then the speed in the following phase (if the current phase is not the last phase) is $v_{t+1} = v_4 - v_3 = 6.0 - 3 \cdot 1.4 = 1.8$ mm/s$= v_1$.

2.3.4 Data analysis

The data obtained in the experiments was stored in files and included the raw EMG signal of the participant, indexes for sessions and phases, the expected muscle contraction level corresponding to the slip speed of the object, the actual muscle contraction level of the participant, and the EMG intensity per phase. Comparison of the three different feedback modalities requires several performance measurements to be derived and applied to the data:

Promptness to stop slip

Success refers to a session in which the participants are able to stop the object, i.e., the participants respond with a muscle contraction level that corresponds to the given slip velocity of the object. In contrast, failure refers to a session in which: 1) the slip speed was not altered because the contraction level was below the minimum contraction value or 2) the slip speed was only decreased as a result of insufficient muscle contraction or 3) the slip was stopped at the cost of "crushing" the object due to excessive muscle contraction. One of the performance measures in the present study is the promptness to overcome slip, i.e., how many attempts (phases) participants needed to stop the object. The definition may be pertinent to prosthetic interfaces that are predominantly coarse compared to the dexterity of the human hand. The most prompt response characterizes a session in which slip was overcome from the first phase, whereas the least prompt response stands for a session in which the moving object was not stopped in any of the three given phases. For each of the three feedback modalities, the following variables were quantified: the percentages of successes in the first phase, the second phase, and the third phase, as well as the percentage of failures to stop the object within the three phases.

Success-to-EMG-intensity ratio

The success-to-EMG-intensity ratio provides a measure of profit from the feedback modality, taking into consideration both success and the expense in effort (EMG input). Success refers to the percentage of success in stopping the slip of the object within an experiment (across all sessions). The EMG signal intensity accounted for the effort of the participant to overcome the slip of the object during a session. The EMG intensity within a phase, denoted as e, was computed with respect to the e_{min} and e_{max} contraction intensities, after having rectified and integrated the EMG input signal. Subsequently, the average EMG intensity invested per session by a participant is designated by the following value

$$I_{EMG} = \frac{1}{N} \cdot \sum_{i=1}^{T} \frac{e(i) - e_{min}}{e_{max} - e_{min}}$$

where N represents the total number of sessions, and T represents the total number of phases ranging from 40 to 120.

Hence, the success-to-EMG-intensity ratio of a participant becomes:

$$P = \frac{\sum_{i=1}^{N} success(i)\%}{I_{EMG}} \tag{2.1}$$

Contraction level deviation

The contraction level deviation measured the degree of variability in the input contraction levels with respect to the expected contraction level. The types of contraction variation are described by the matrix S in Fig. 2.5A. We computed the joint probability distribution matrix, $p(e_j, v_i)$, with $e_j \in E, v_i \in V$, for a participant, to which we further applied the mask matrix $S : E \times V \rightarrow \{L_1..L_9\}$. The contraction level deviation, $D(k) \in \mathbb{R}$ with $k \in \{L_1..L_9\}$, was thus derived

as:

$$D(k) = \frac{\sum_{i,j;S(e_j,v_i)=k} p(e_j, v_i)}{\sum_{i,j;S(e_j,v_i)=k} 1}, \tag{2.2}$$

where the numerator represents the total number of instances of L_k-type contractions exerted by the participant, while the denominator is a normalization factor representing the total number of L_k-type contractions appearing in the mask matrix.

Reaction time within a phase

We examined participants' reaction time to slip, within a phase, in order to present considerations for the design of "human-in-the-loop" control interfaces. It is worth noting that the reaction time to slip within a phase was not a control parameter in the design of our experiments, thus participants did not regulate it for best performance. Therefore, the response time provides only an indication of an unconstrained time standard for voluntary reaction to a tactile stimulus. We computed the reaction time to slip as the duration between the onset of a phase and the rise of the EMG signal above a threshold of 90% of the EMG signal amplitude corresponding to the lowest slip speed.

2.4 Results and Discussion

In this section we provide statistical evidence about the efficiency of the three feedback modalities.

2.4.1 Promptness to stop slip

In the present study, we investigate how quickly, in terms of phases, the users can stop an object from slipping, depending on the feedback modality and the slip velocity of the object. Figure 2.3A shows the results for the nine participants for the case in which the speed of the slipping object was 1.8 mm/s. Single factor analysis of variance (ANOVA) for three levels corresponding to the three feedback modalities showed a similarity in performance in the first and the third phases, regardless of the feedback type. Discriminatory effects depending on the feedback appeared only in the second phase, as confirmed by $F(2, 24) = 3.77$ and $p < 0.05$. The result shows that the visual feedback and the slip speed feedback led to a higher rate of success relative to the slip occurrence feedback in the second phase. At a slip velocity of 3.2 mm/s, the feedback modality did not generally play a significant role in the first phases, as illustrated in Fig. 2.3B. However, in the third phase of a session, the participants receiving vision and slip speed feedback achieve better performance in stopping the slip of the object before the session finishes. The single factor ANOVA with three levels yielded $F(2, 24) = 8.80$ and $p < 0.01$. As the slip velocity increased, the feedback modality imposed a gradually higher discrepancy on the performance of the participants. Identical analysis (ANOVA) for performances recorded at a slip velocity of 4.6 mm/s, indicated, by $F(2, 24) = 4.45$ and $p < 0.05$, that in the second phase feedback has a discriminative effect on the performance (Fig. 2.3C). In particular, the slip speed feedback and vision yielded improved results for the users. The significance of the feedback

modality became even higher for a high slip velocity (Fig. 2.3D). In the first phase of the session, at a slip velocity of 6.0 mm/s, it was far more likely that participants receiving slip speed feedback were able to stop the object. The same analysis of variance yielded $F(2, 24) = 10.37$ and $p < 0.001$. A simple regression was conducted in order to determine the performance of the participants in the first phase at a higher speed of slip. For each participant, we fit a regression curve (a polynomial of degree less than three) to the percentage of success versus slip speed (the goodness of the fit was $R^2 > 0.95$). Based on the fitted curve, we computed the performance of each participant at a slip velocity of 7.4 mm/s. The results, $F(1, 10) = 5.57$ and $p < 0.05$, provided by ANOVA with two levels, revealed that the slip occurrence modality, opposite to the slip speed feedback, would not support a prompt response to slip. Another measure relevant to promptness is the percentage of failures to stop the slip within the first three phases. A feedback modality that endorses promptness should decrease the number of such failures. At first three slip velocities, differences in the effect of the feedback modalities were not present. However, at a slip velocity of 6.0 mm/s, failures to stop the object within the first three phases were considerably more frequent with the slip occurrence feedback than with the slip speed feedback: $F(1, 16) = 20.81$ and $p < 0.001$ (ANOVA with two levels). We performed a regression analysis to investigate if this discrepancy maintains as the slip velocity becomes higher. For each participant, we fit a regression curve (a polynomial of degree less than three) to the percentage of failures to stop the object within the first three phases versus slip speed (the goodness of the fit was $R - square > 0.95$). Based on the fitted curve, we computed the degree of failure to stop the object within the first three phases at a slip velocity of 7.4 mm/s. At a speed higher than 6.0 mm/s, ANOVA identified the slip occurrence feedback as the worse modality: $F(2, 21) = 7.37$ and $p < 0.01$ in case of the ANOVA with three levels, and $F(1, 14) = 25.02$ and $p < 0.001$ in case of the ANOVA with two levels (slip occurrence and slip speed feedback). These results suggest that, as the speed of slip increases, the rate of failure to stop the slip within the first three phases drastically increases (and consequently the promptness decreases) with slip occurrence feedback, as opposed to the rate of failure with vision or the slip speed feedback. We therefore predict that discrepancies between the slip speed and the slip occurrence types of feedback will escalate as the slip velocity becomes larger. The absolute values of the percentages of success were generally not high. The explanation may reside in the design of the experimental procedure. The three-phases session limit and six-input options lead to a 0.5 probability of stopping slip within a session. However, on a relative scale, the slip speed feedback yielded comparable or better results than vision. As indicated by the results of the present study, slip speed feedback favors a relatively more prompt response of the users in their attempt to overcome slip at an early stage.

2.4.2 Success-to-EMG-intensity ratio

For each feedback modality and each slip velocity, we computed the success-to-EMG-intensity ratio, as an indicator of the user's profit from the feedback in controlling the slip with an EMG-based prosthesis. The results obtained after having applied Eq. 2.1 to each participant, are shown in Fig. 2.4. The type of feedback modality provided to the user became critical as the slip velocity

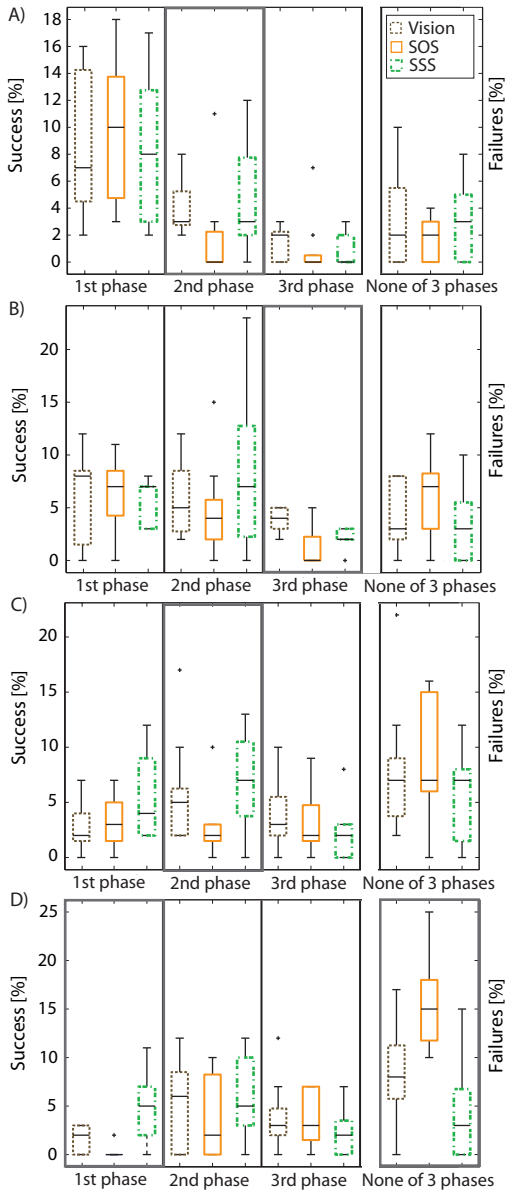

Figure 2.3: Promptness to stop slip relative to the slip speed and the feedback modality. The percentage of successes in the first phase (column 1), second phase (column 2), and third phase (column 3). The percentage of failures to stop slip within the first three phases (column 4). The slip speeds are: 1.8 mm/s (A), 3.2 mm/s (B), 4.6 mm/s (C), and 6.0 mm/s (D). Each column compares the three types of feedback modalities: vision (brown), slip occurrence stimulation, SOS (orange), and slip speed stimulation, SSS (green). The confidence interval of the results is 95%. The results show that at high slip speeds the slip speed feedback and vision, in contrast to the slip occurrence feedback, manage to stop slip in the early stages of its occurrence. Thick-border columns denote the conditions in which significant difference was found.

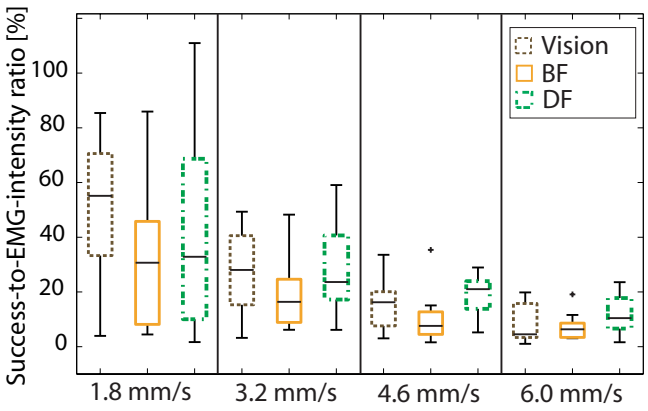

Figure 2.4: Success-to-EMG-intensity ratio relative to the slip speed and the feedback modality. The four velocities are: 1.8 mm/s (column 1), 3.2 mm/s (column 2), 4.6 mm/s (column 3), and 6.0 mm/s (column 4). Each column compares the three types of feedback modalities: vision (brown), slip occurrence stimulation, BF (orange), and slip speed stimulation, DF (green). The confidence interval of the results is 95%. The results indicate that the slip speed stimulation maintains a relative increase of the success-to-EMG-intensity ratio as the slip speed becomes larger.

increased. We performed single factor ANOVA with three and two levels in order to investigate the statistical significance of the results. Similar results across feedback modalities were obtained at the first two velocities. At a velocity of 4.6 mm/s, ANOVA indicated that feedback discriminated the rates of success over the EMG intensity, ranking the slip speed feedback as the most appropriate for the task of the experiment. Hence, the ANOVA with three levels yielded $F(2, 21) = 5.16$ and $p < 0.05$, and the ANOVA with two levels (slip occurrence and slip speed feedback) yielded $F(1, 14) = 10.67$ and $p < 0.01$. At a velocity of 6.0 mm/s, the success-to-EMG-intensity ratio is also enforced more efficiently by the slip speed feedback than by the slip occurrence feedback, as supported by the results of the ANOVA with two levels, $F(1, 10) = 9.22$ and $p < 0.05$. When slip occurs, optimally, the prosthesis user should not react with a grip force overhead to stop the object. A previous study reported that, upon slip, humans compensate with a minimum energy to stabilize an object in the hand [10]. In our study, as the velocity of slip increases, we could observe, more notably for slip speed feedback and vision, a higher rate of success and a more efficient use of the EMG intensity.

2.4.3 Contraction level deviation

In the present study, we investigated the types and distribution of errors in the responses of participants, accounting for their entire range of actual contraction intensity levels, in order to evaluate the efficiency of the three feedback modalities. The errors were defined as relative drifts of the actual contraction level from the expected contraction level. The types of errors are represented in more detail in Fig. 2.5A. Level L5 represents the successful match between the actual and expected contraction levels and also delineates the areas of low order (L1-L4) and high order (L6-L9) drift errors. The low-order drifts characterize the

phases in which participants responded with a contraction intensity one (L4), two (L3), three (L2), or four (L1) levels lower than that expected for the given velocity. The high-order drifts correspond to cases in which the participants crushed the objects responding with a contraction intensity one (L6), two (L7), three (L8), or four (L9) levels higher than what they were expected to input as corresponding to the given velocity. The drift errors with vision, slip occurrence feedback, and slip speed feedback were computed according to Eq. 2.2 for each participant and are illustrated in Fig. 2.5B, 2.5C, and 2.5D, respectively. Irrespective of the feedback modality, the figures reveal a trend of contraction drifts towards lower levels. This can be explained in part by the experimental procedure, due to which participants, if given a sufficient number of phases to stop an object, resorted to lower contraction levels to decrease the speed and avoid crushing objects.

Single factor ANOVA was conducted for the data collected during the experiments with the three feedback modalities across each level drift. Level L1 corresponds to only one case, according to which participants expected to respond with the highest contraction, actually respond with a contraction intensity below the allowable input contraction range. At level drift L1, we found significant disparate responses relative to the provided feedback, with two-level ANOVA (slip occurrence and slip speed feedback), $F(1, 10) = 4.56$ and $p < 0.05$. It appears that this type of drift was predominant for the participants who were provided with slip occurrence feedback. An excess of three-level drift toward lower contractions (level L2) predominantly occurred in the case of slip occurrence feedback as well, as supported by the ANOVA results, $F(2, 18) = 10.47$ and $p < 0.001$ (three-level ANOVA) and $F(1, 12) = 29.87$ and $p < 0.0001$ (two-level ANOVA, slip occurrence and slip speed feedback). At level L3, different effects depending on the slip occurrence feedback and the slip speed feedback were not present ($F(1, 16) = 4.08$ and $p = 0.06$). Vision and the slip speed feedback induced one-level drift contractions to a higher extent than the slip occurrence feedback. ANOVA with three levels yielded $F(2, 18) = 12.10$ and $p < 0.001$ and ANOVA with two-levels (slip occurrence and slip speed feedback) yielded $F(1, 12) = 16.60$ and $p < 0.01$. The correct choice for the contraction response is represented by level L5. In this case, the single-factor ANOVA revealed a significant difference between the slip occurrence feedback and the slip speed feedback. Thus, $F(1, 16) = 4.40$ and $p < 0.05$ favored the slip speed feedback over the slip occurrence feedback for the efficiency of stopping a slipping object. No significant differences were found for the high-order drifts. Generally, the contraction intensity levels were broadly scattered for participants receiving slip occurrence feedback and were more compactly distributed around the successful level for vision and the slip speed feedback.

2.4.4 "Human-in-the-loop" slip response time

It has been suggested that the body's exposure to sensory information during its participation in dynamic activities is fundamental to the development of self-perception [13]. This statement's implication for the embodiment of prostheses is central. While the previous sections presented feedback enhancements for "human-in-the-loop" slip control, we also considered its possible limitations by computing the participants' reaction time to slip within a phase as described in Section III D 4. The reaction time with respect to the feedback modality

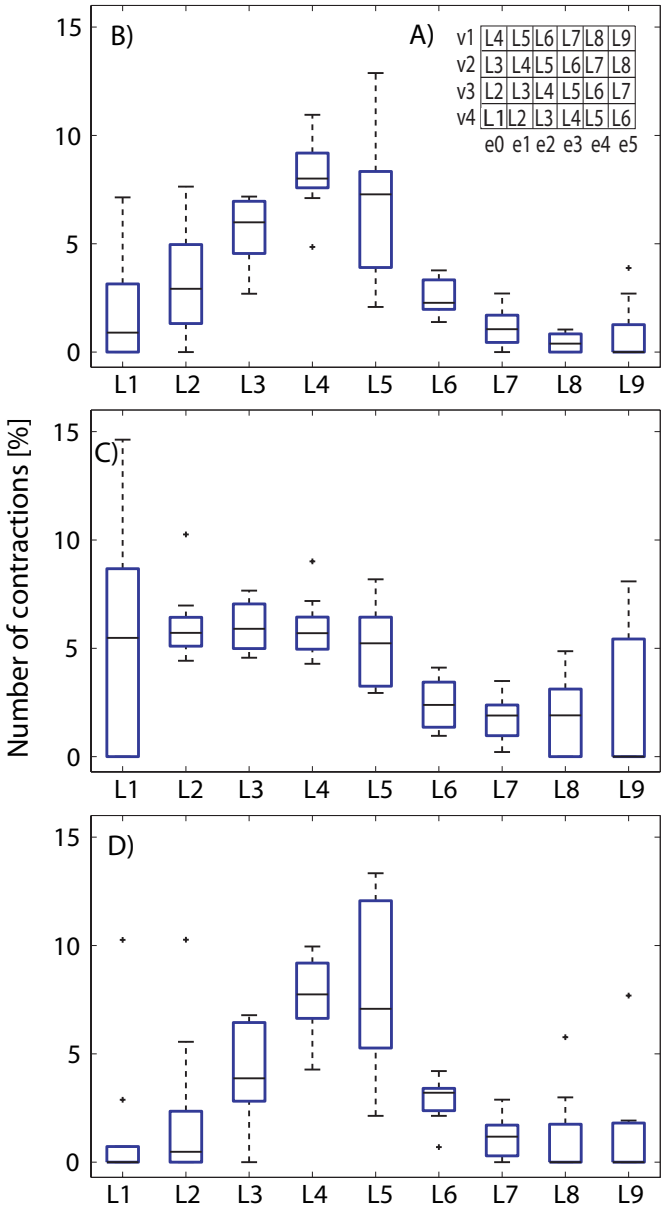

Figure 2.5: Level drifts of contraction intensity. A) Mask matrix for computing level drifts of contraction intensity based on the presented slip speed, v, and the actual contraction intensity level, e. Level L5 indicates the equality between the expected and the actual level of contraction intensity. The number of contractions (as a percentage) corresponding to each level drift for visual feedback (B), slip occurrence feedback (C), and slip speed feedback (D). The confidence interval of the results is 95%. The plots show that the slip speed feedback and vision, compared to the slip occurrence feedback, reduce the variation of muscle contraction input.

regardless of the slip speed is presented in Fig. 2.6A. The means of the reaction time were 1.71, 1.51, and 1.75 s with vision, slip occurrence feedback and slip

speed feedback, respectively. We applied a Kruskal-Wallis non-parametric test to the reaction time of all participants across the three feedback modalities. The test yielded $H(2) = 68.56$ and $p < 0.001$ by Chi-Square. We assumed that participants reacted faster when they received slip occurrence feedback because slip speed recognition was bypassed due to the lack of such information. The reaction time with respect to slip speed regardless of the feedback modality is presented in Fig. 2.6B. The means of the reaction time were 1.60, 1.64, 1.71, and 1.75 s for the set of speeds, respectively. The Kruskal-Wallis test yielded $H(3) = 21.90$ and $p < 0.001$ by Chi-Square. In general, the reaction time was the fastest when the slip speed was the slowest. A possible explanation stemming from our observations is that participants could easily recognize the smallest stimulus level and control its corresponding contraction level.

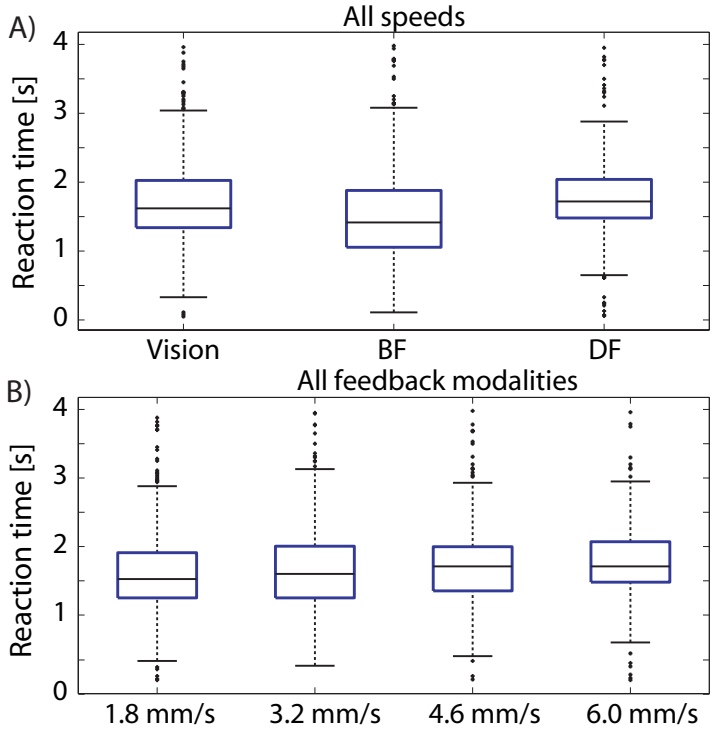

Figure 2.6: Reaction time to slip. A. Reaction time relative to the feedback modality (vision, slip occurrence feedback (BF) and slip speed feedback (DF)). B. Reaction time relative to the slip speed. On average, the reaction time to slip was in the range of $1.51 - 1.75$ s for all three feedback modalities and four slip speeds. The confidence interval of the results is 95%.

If we consider the average reaction time extremes of 1.51 s and 1.75 s, the slip of an object traveling at the maximum experimental speed of 6 mm/s can be stopped after a minimum distance of approximately 9 mm and 10.5 mm, respectively. Assuming a robot hand skin of length 80 mm (a regular size to cover the palm of a prosthetic hand), the two average reaction time extremes will be able to stop the slip of an object traveling at speeds of maximum 53 mm/s and 45 mm/s, respectively. These calculations ignored various factors that can affect slip control, such as the size and initial position of the object, the type of

grip (power, precision, etc.), the time to actuate a prosthetic hand, etc. Based on these results, we envision a hybrid control scheme for overcoming slip such that excessively high speeds of the slipping object are managed by local controllers of a prosthetic hand, whereas slower speeds are relayed to and managed by the prosthesis wearer. The benefits of this control scheme are twofold: (1) it enables automatic grasp control when the user's reaction time is slow or when there are technological limitations in the interface communication speed, and (2) it involves the user in the control loop, which is a sensorimotor prerequisite for a prosthesis embodiment.

2.5 General Remarks

Our study investigated the role of slip speed feedback for grasp stability with potential for prosthetic applications. General characteristics of the slip speed feedback include (1) quantitative information about slip events and (2) intuitiveness, through mapping speed to frequency, as opposed to sensory interfaces that require users to learn various stimulation patterns. Comparative performances of slip speed feedback and vision open up the possibility of dedicating vision to more suitable tasks.

A dexterous embodied prosthetic system may be developed by improving the control with slip speed feedback and by implementing a complementary autonomous controller that manages excessively high slip speeds. The improvement of user performance may be achieved with vision and the slip speed feedback by providing comprehensive training to users. In contrast, training with slip occurrence feedback could lead to limited or no improvement due to the lack of relayed information. In our study, learning did not take place for any feedback modality, probably because the training was only introductory and the experiments were short. We quantified learning by splitting the series of 40 consecutive sessions into two halves for each participant and computing the success percentage for each half. We applied a two-way ANOVA with replication, taking as factors the feedback modality and the time-dependent halves, across all participants. ANOVA yielded $F(2, 48) = 3.26$ and $p < 0.05$ for the feedback factor, $F(1, 48) = 1.37$ and $p = 0.24$ for the two groups of sessions, and $F(2, 48) = 0.21$ and $p = 0.80$ for the interaction effect between the two factors. These results indicate that although feedback modality influences success in stopping slip, there is no significant difference in the success ratio in time, and thus no learning effect occurred.

We may argue that an appropriate scheme to overcome slip of an object is to always input low contraction intensity levels and gradually decrease the speed of the object until the object stops. In which case, slip occurrence feedback should be sufficient. This hypothesis was rejected based on the experimental results, according to which, even when confronted with the lowest contraction level expectation, the participants receiving slip occurrence feedback recorded the highest percentage of crushes (8.89%, on average) relative to the other two feedbacks (in average, 4.98% for slip speed feedback and 2.81% for vision). A single-factor ANOVA with three levels comparing the three feedbacks yielded $F(2, 24) = 6.62$ and $p < 0.01$. Besides this result, the number of crushes was not significantly different across the slip occurrence and the slip speed feedback modalities, regardless of the slip speed.

Using the tactile display for practical applications entails a subsequent study of the feasibility range of the proposed feedback. This study is a prospective research avenue for our group. The setup must include a gripper with adequate sensors and must be evaluated in real-world grasp scenarios. In a setting where slip is influenced by gravitational forces, the slip speed is regulated by the material of the gripper, i.e., its coefficient of friction. The challenges that need investigation under these physical and computational properties of the prosthetic system in order to obtain an efficient user-response time to slip are: the time settings of the closed loop and consequent slip speed applicability constraints of the slip feedback, and the required user attention. With regard to time settings, the EMG acquisition window (currently set to a four-second phase time) must be reduced in order to allow a finer mapping to grip force. Extensions for incorporating more complex EMG acquisition and continuous mapping to grip force are widely researched [118]. The feedback display may need to integrate continuous mapping between slip speed and vibration frequency, and to cope with skin perception nonlinearities. We expect that the reduced EMG signal acquisition time or the extension of the sets of contraction levels, speeds and stimulation frequencies may decrease the absolute success rates in slip control with all three feedback modalities. However, we also expect that these changes would not distort the relative significance of the occurred performance trends. We transmit slip by discrete timed events that produce hight activation of brain areas [148] and less habituation than static stimuli [79]. The implementation of the slip speed feedback, currently based on electrical stimulation, can be substituted by alternative technologies found to display the same information in a more efficient way. Although the presented closed-loop interface is simple, it offers a framework that can be further elaborated toward clinical use.

We consider the slip speed feedback as a reverse force feedback, representing "negative" forces. Therefore, relaying slip speed information is as significant as relaying quantified continuous force information. These antagonistic grasp metrics may provide the prosthesis wearer with a gradient toward finding the optimal grip force.

2.6 Conclusions and Future Research

We proposed an intuitive slip speed feedback modality, for grip force control for prosthetic applications, that endorses rich dynamical tactile information such as slip occurrence and slip velocity. The proposed slip speed feedback boosts the promptness in overcoming slip, increases the success in controlling slip with a lower consumption of muscle contraction intensity, and ensures lower variability of the muscle contraction input. Overall, the slip speed feedback performed comparably to vision and demonstrated significant improvement over tactile displays that relay binary slip information. As a future work, we intend to investigate the applicability range of the slip speed feedback for grasp control with a prosthesis. Furthermore, we plan to relay both force and slip information in order to represent proprioceptive and exteroceptive stimuli, respectively. Provided with a quantitative measure of both, we expect that the prosthesis wearer will regulate the sensorimotor grasp transformations in an energy-efficient manner.

Chapter 3

The Role of Quantitative Feedback Guidance in Grip Force and Slip Speed

Distinct role of force and slip feedback in stable grasp

Relative to Chapter 2, Chapter 3 provides additional evidence of the distinct role of slip speed and force feedback for efficient grasp stability in upper-limb prostheses. The work in this chapter integrates haptic sensing from an artificial ridged skin, details of which are described in Chapter 4, with a graphical interface.

We investigate virtually-operated stable grasp under perturbation. By generating slip in a robot hand, we study the effects of guidance in energy-efficient grip and slip speed on users' grip response to slip. We evaluate physiologically the performance in grip control under physical grasp perturbation, such as slip, and computational noise, such as inaccuracies in the tactile sensor. Results show that the guidance in an object's friction-related properties, e.g., weight, leads to grip force intensities within safe margins against slip, whereas guidance in an object's slip speed leads to reaction times to slip that are proportional to the slip speed. Moreover, the combination of both feedback guidances suggests that the two types of information may be mutually exclusive and that, in the design of haptic interfaces and devices, they may need to be separated in order to reach an efficient grasp control.

[2]Parts of the material in this chapter represent a manuscript in process of submission: D.D. Damian, M. Fischer, K. Dermitzakis, and R. Pfeifer (2012) "The Role of Quantitative Feedback Guidance About Grip Force and Slip Speed" (to be submitted)

3.1 Related Work

It is agreed that successful artificial interfaces in prosthetics do not only depend on the success of the task, e.g., object manipulation, which can be achieved through a complex open-loop control. In addition, the haptic interface must also transfer the interaction information to the prosthesis wearer [101]. This approach is meant to address issues that have not yet been resolved completely: stability of the interaction with the environment through engineered interfaces, acceptance and sustainability of the prosthetic devices [95] [118]. Artificial sensing for humans encounters a two-folded challenge: the development of tactile sensors that acquire rich information from the environment, and the development of tactile feedback interfaces that transmit the environmental information back to the body of the prosthesis wearer. Robotics community has been carrying out extensive research on developing sensors for robotic sensing. A review on current technologies is presented in [41]. According to this survey, there is a growing trend for tactile sensors arrays. Nonetheless, only a part of them may be applicable to prosthetics due to deficiencies related to the ratio between information richness, sensor robustness and its energy-efficiency. Currently, a wide range of sensors have been engineered to transduce forces or slip detection [152]. Our approach to artificial sensing, proposed in [46], aims to build sensors that acquire rich information by using sensor morphology and less energy.

Mapping the environmental information to prosthesis wearers has been commonly achieved through the tactile display of forces on the human skin by various haptic technologies [102] [114]. Although force feedback can characterize the grip force, it can not be used exclusively for grasp stability through an artificial interface in real world scenario. This insufficiency mainly comes from the inability to predict the interaction properties because previous CNS models are no longer accurate through an artificial control interface [72]. There is physiologic evidence that grasp stability in upper-limb prosthesis may not depend only on relaying information about grip force [72] [10]. According to these studies, slip is a pivotal determinant in grip control. Slip, artificially generated by changing the load force on an object held in the human hand, was found to improve the agility of the grip response that depended on the load force rate [72]. This result is a prime indicator that the rate of slip may influence the grip response. Nonetheless, slip feedback in prosthetic applications has not received much attention. Tsagarakis et al. [152] developed a device that embeds two miniature motors in a "V" configuration to generate sensations of relative lateral motion at the fingertip. Kim et al. [82] developed a number of multifunctional tactile feedback devices that can be used to provide feedback of contact, pressure, shear force, vibration, and temperature for users who have undergone targeted reinnervation surgery. For tele-manipulation, Edin et al. [14] devised a mechanism in which a user holding an instrumented object receives frictional information through solenoids mounted on the object to elicit physiological responses that resemble the responses observed during slips. These studies, however, do not examine the possible benefits of slip feedback for prosthesis or tele-manipulation users. Webster et al. [160] developed a tactile slip display for virtual reality applications. The device reproduces the sensations of sliding contact and incipient slip through the rotation of a ball positioned under the user's fingertip. According to the authors' findings, slip and force feedback represent a better solution than force feedback alone for assisting participants in the manipulation of a

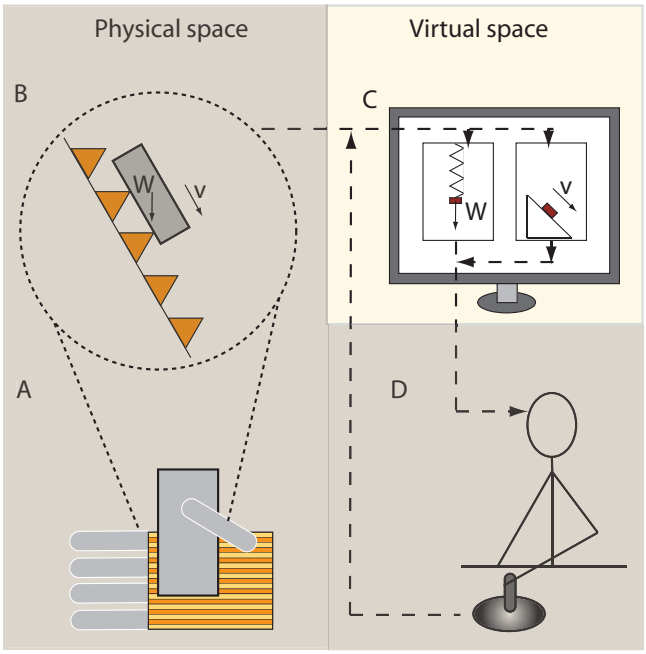

Figure 3.1: Schematics of the experimental setup. A. The artificial ridged skin on which an object of weight W slips with speed v. B. The screen displaying to the participant graphical information about grip force or slip speed feedback. C. Participant controls the slip via a joystick. D. The robot hand controlled by the user.

virtual object with lower forces. Grasp stability has been studied as a physical process [18]. From a physiological approach to stability, grasp may be defined as a region of minimum for both grip forces and slip speed values. As such, quantitative information about these antagonistic grasp metrics, e.g., force and slip, can provide the prosthesis wearer with a grip force adjustment guidance. This way, the prosthesis wearer avoids exerting excessive force that can crush an object or involve unnecessary energy use, or insufficient force that leads to object drop. In this study, we investigate the role of feedback about grip force and object slip speed in regulating the grasp process. The two metrics should be especially significant for learning grasp models with a prosthetic interface that is prone to generating perturbations. In a psychophysical experiment, we vary the weight and the speed of an object slipping in a robot hand. In order to detect slip speed, we use a ridged artificial skin, similar to the one developed in [46]. Therefore, our study offers an integrative view upon the grasp by connecting tactile sensors and haptic interfaces for a complete description of the grasp process. Consequently, we also investigate the influence of the variance in the tactile sensor output to the grasp performance. The remainder of the present paper is organized as follows. Section II introduces the materials and methods supporting our experiments. Section III describes the obtained results, which are discussed in Section IV. Finally, conclusions are presented in Section V.

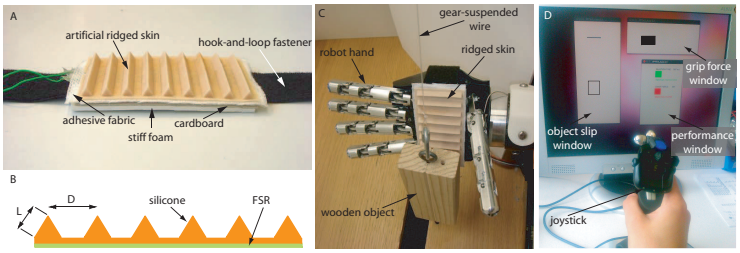

Figure 3.2: Elements of the experimental setup. A. Artificial ridged skin. B. Schematics of the artificial ridged skin illustrating the main components. The triangular side $L = 6$ mm and the inter-ridge distance $D = 10$ mm. C. Artificial ridged skin mounted on the robot hand and the slipping object. D. Screen showing feedback guidance and performance feedback.

3.2 Materials and methods

3.2.1 Experimental setup

The schematics of the experiment is depicted in Fig. 3.1. Information about the grasp of a slipping object on a skin (Fig. 3.1B) mounted on a robot hand (Fig. 3.1B) is selectively displayed virtually, in terms of object's weight or slip speed, to a user that controls the grasp through a joystick. The main parts of the experimental setup are shown in Fig. 3.2. The artificial ridged skin (Fig. 3.2A) is an extension of the skin developed in [46]. The artificial skin was built from silicone (Neukasil RTV 28) mixed with colorful adhesive agent (Neukasil binder A140 beige). The fluid was solidified into a 3D mask built by rapid prototyping. The artificial skin featured uniformly distributed ridges that are 10 mm apart one from the other. The ridges have a equilateral triangle shape with a side of 6 mm. The artificial ridged skin had a length of 90 mm and width of 4 mm, suitable to be mounted on the robot hand. Underneath the silicone patch, one single force sensor (FSR) (Interlink Electronics) acquired the force profiles as the object slips over the ridges. The signals from the FSR sensor were collected by a DAQ system and input to a PC for real time processing. The artificial skin was mounted on the robot hand described in [28] (Fig 3.2B). The robot hand was not actuated during the experiment, rather it was used as a ramp surface for the slipping object. The robot hand was mounted on a wooden cubic frame, and its palm fixed at an angle of about 45° through a system of pulleys attached to the wooden frame. A wooden rectangular object of $170 \times 50 \times 25$ mm length was used as the slipping object. We regulated the weight of the object by adding external weight attached to the bottom of the wooden object. This way, we also maintained the shape of the held object invariant to the weight. The two weights for the object were of 200 and 1000 grams. A DC motor mounted on the wooden cubic frame drove the object at a constant speed, being controller by a microcontroller. The participants were seated in a chair in front of a computer monitor. The robot hand setup was placed at their left side and was not visible to them. Information about the user's grip force or object's slip speed was displayed graphically on a computer screen (Fig. 3.2C). Participants could exert control over the grip force or slip by manipulating one-degree-of-freedom of a joystick with their dominant hand.

They were also deprived of environmental noise by wearing headphones during the experiment.

3.2.2 Experimental procedure

Seven unimpaired volunteers ranging in age from 23 to 35 years participated in three experiments, after having read the instructions and having given their consent. Prior to commencing the study, ethical clearance was provided by the Swiss Association of Ethics Committees (KEK). The task of the participant is to stop a slipping object with an optimal grip force. Within an experimental session, an object slipped over the artificial ridged skin at a constant speed. We used three values for the real speed of the object: 10, 30 and 50 mm/s. The slip speed of the object was generated randomly at the beginning of each session. The participants are relayed with feedback information about the interaction between the robot hand and the object (virtual grip force or physical slip speed or both). Participants could control slip by pulling the handle of the joystick from the neutral position toward the user in order to increase the grip force virtually. By pressing a button on the joystick, they confirmed the value of the grip force that they decided to be suitable to efficiently stop slip. This mapping would in reality control a robotic hand closure that tightens the grip. Twenty-four such sessions represent one experiment. We conducted a total of three experiments in which in which participants were relayed with three distinct feedbacks. Prior to all experiments, we defined the efficient grip force for each weight of the slipping object relative to the physical setup. We determined the value of the joystick displacement that corresponds to the slip margin, T_g. The object started to slip for joystick displacements below this threshold. The efficient grip force was thus set as the interval between the experimental threshold, T_g, and an addition of 50 joystick displacements units, $T_g + 50$.

The graphical interface included selected feedback information about user's grip force or object's slip speed during a session and information about user's performance at the end of each session (Fig. 3.2C):

Grip force feedback

The grip force was graphically displayed by the horizontal expansion or contraction of a filled rectangle. The displacement of the joystick was proportionally mapped to the length of the graphical rectangle, normalized based on *a priori* information about the range of joystick displacement and the range of robot fingers flexion around the experimental object. The relation, $F_g = (J_x * 800)/32767\ [JU]$ expresses the grip force in terms of joystick displacement units, JU.

Slip speed feedback

The slip speed information, extracted from the frequency in the force signal of the artificial ridged skin, was linearly mapped to the speed of a rectangle moving vertically on the screen. We automatically collect the force signal from the artificial skin as the object slips over the first five ridges of the skin, that is, along 50 mm of skin. We applied the FFT to this force signals. The extracted peak frequency of the signal was used to compute the slip speed of the object

according to the relation $v = f/D$, where v is the computed slip speed, f is the frequency of the force signal and D is the inter-ridge distance. Given the computed slip speed and the length of the object still in contact with skin surface of the robot hand, the user had to react within a limited time, in order to stop the slip before the object leaves the surface of the robot hand. For the experimental object, the maximum reaction time to slip was $Rt_{max} = 120/v\ [s]$.

Grip force and slip speed feedback

Both grip force and slip speed feedback were graphically shown to the participants.

Performance feedback

At the end of each session, the performance in adjusting the grip force within the safe margins against slip, and in reacting in time to stop the slippage, was displayed to the user. The performance result related to grip force could take one of three values. If the grip force of the user resided within the safe margins against slip, $T_g <= F_g <= T_g + 50$, then participants were shown the message "Efficient grip force", the joystick displacement value, and a graphical green-colored square. Overshooting the optimal grip force, i.e., $F_g > T_g + 50$ showed users, apart from the displacement value of the joystick, the message "Object was crushed" and a red-colored square. Lastly, when the joystick displacement was lower than that corresponding to the efficient grip force, i.e., $F_g < T_g$, participants were alerted about slip by being shown the displacement value of the joystick, the message "Object is still slipping" and an orange-colored square. The reaction time to slip was relayed to users as a binary performance result. We compared the users' reaction time to slip with the maximum computed time until the object falls from the robot hand, Rt_{max}. Thus, apart from the value of their reaction time to slip, users were shown the messages "Optimal reaction time" associated with a green-colored square, and "Object fell" associated with a red-colored square, for successful and failed reaction time, respectively.

Participants were provided with training consisting of two sessions for each experiment, in which they could experience random slip speeds and a virtual weight whose slip margin, T_g, was defined by a joystick displacement of 350 units. The order of the three types of feedback across all participants varied, in order to cross-balance each experiment. After each session, the experiment assistant relocated the object to the initial position with a controlled movement of the motor.

3.3 Results

3.3.1 Grip force response

Figure 3.3ABC shows the grip force response with respect to the two weights of the object and the three types of feedback guidance modalities. The horizontal dashed lines represent the interval of optimal grip force between the two grip force thresholds defined in the calibration process. Figure 3.3A shows the grip force response of participants provided with force feedback guidance only. Noticeably, with this type of guidance, the response from the participants were

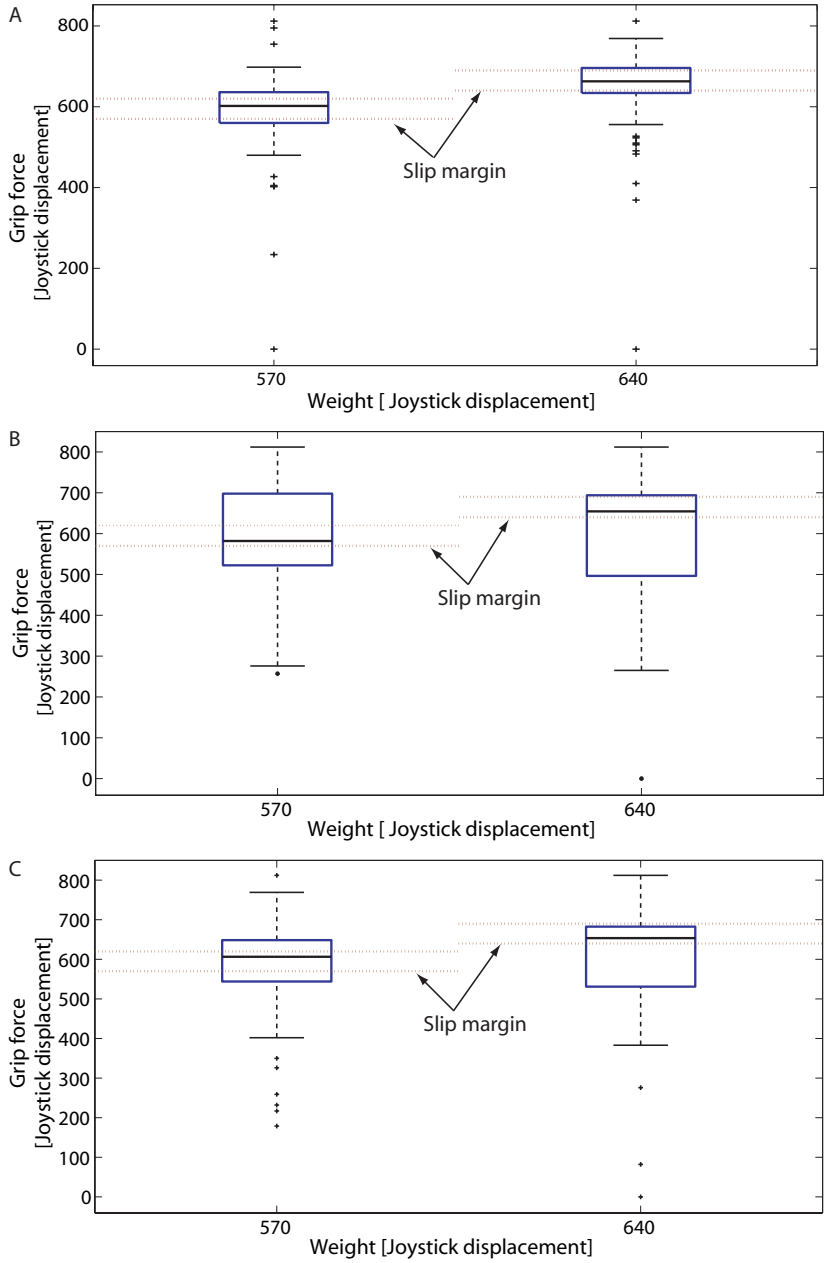

Figure 3.3: Grasp force with respect to object weight with force feedback guidance alone (A), slip speed feedback guidance alone(B), force and slip speed feedback guidance combined (C). Slip margin designates the grip force level under which the object starts to slip. This level was determined empirically with the robot hand platform.

mostly condensed within the optimal grip force region. The non-parametric Kruskal-Wallis test was applied, yielding $H(1) = 16.18$ and $p < 10^{-3}$. Figure 3.3B shows the grip force response of participants provided with slip speed feedback guidance only. Although the average grip force resides within the optimal grip force, the force response has a large variance. Kruskal-Wallis test yielded $H(1) = 2.03$ and $p = 0.15$, suggesting there is no significant difference in the participants' response for grip force, regardless of the object's weight.

In Fig. 3.3C, the grasp force with respect to object weight with force and slip speed feedback guidance is presented. Kruskal-Wallis test yielded $H(1) = 4.35$ and $p < 0.05$, suggesting that there is a significant difference in the grip response depending on the object weight presented.

We applied a Kruskal-Wallis non-parametric test to the users' grip force responses at object weight of 570 JU across all feedback guidances. The result showed that there is a significant difference($H(2) = 38.57$, $p = 10^{-8}$), whereas the Tukey multi comparison test particularly indicated that the significant difference appears between the grip response with slip speed feedback guidance and the other two feedback guidances. Same analysis when the weight was 640 JU resulted in no significant difference, i.e., $H(2) = 0.56$ with $p = 0.75$.

3.3.2 Response time to slip

The slip speed computed from the acquired force signal of the FSR was used to control the motion speed of the rectangle object displayed on the screen to the partipants. Figure 3.4ABC shows the reaction time with respect to the computed slip speed and the three feedback guidances. The violet dots represent the maximum reaction time. A reaction time to slip larger than this value implies that the participant was not sufficiently fast to stop the slip of the object while it was in the robot hand. Figure 3.4A, in particular, presents the reaction time corresponding to the force feedback guidance alone. The Kruskal-Wallis non-parametric analysis of variance test was used to determine significance between the groups of reaction time for the computed slip speed. The test yielded $H(4) = 12$, with $p < 0.01$ by Chi-Square. Tukey post-hoc method identified a significant difference only between the reaction time at slip speeds of 10 and 20 mm/s. Pearson correlation coefficient was -0.09 indicating that there is no correlation between the speed of the displayed slipping object and the participants' reaction time to slip. Figure 3.4B shows the reaction time with respect to computed slip speed with slip speed feedback guidance alone. We ran a Kruskal-Wallis test on the data, yielding $H(4) = 29.85$. The p-value, estimated by Chi-Square with four degrees of freedom is $p = 10^{-5}$. Tukey post-hoc method found that significant differences appear between the reaction time corresponding to slip speed of 10 mm/s and all other response times. Pearson correlation coefficient, computed between the slip speed of the displayed object and the reaction time to slip, was -0.40 suggesting that there is a medium negative correlation between the two variables. Figure 3.4C shows the reaction time with respect to computed slip speed with force and slip speed feedback guidance. The Kruskal Wallis test for the response time to slip yielded $H(4) = 10.64$ and $p < 0.05$. Furthermore, the Tukey multiple compare test indicated that significant differences in reaction time appear particularly between the speed of 10 and speeds of 30 and 40 mm/s. According to the Pearson correlation coefficient, -0.26, there is a low negative correlation between the response time

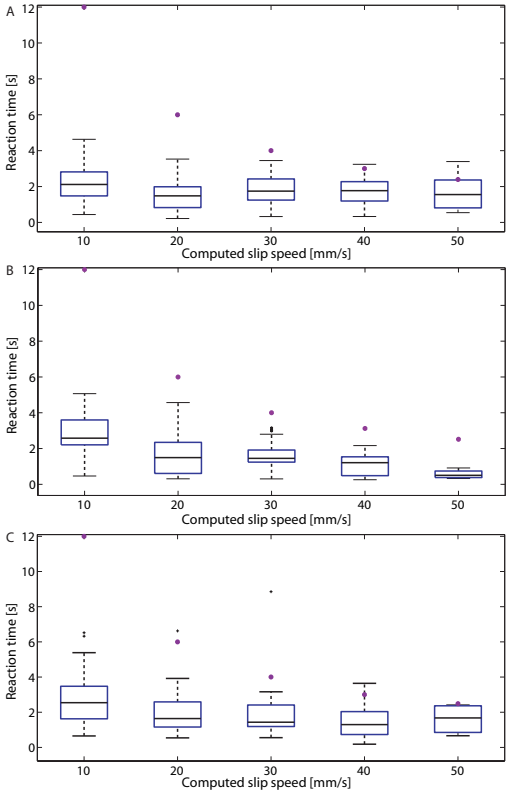

Figure 3.4: Reaction time with respect to computed slip speed with force feedback guidance alone.

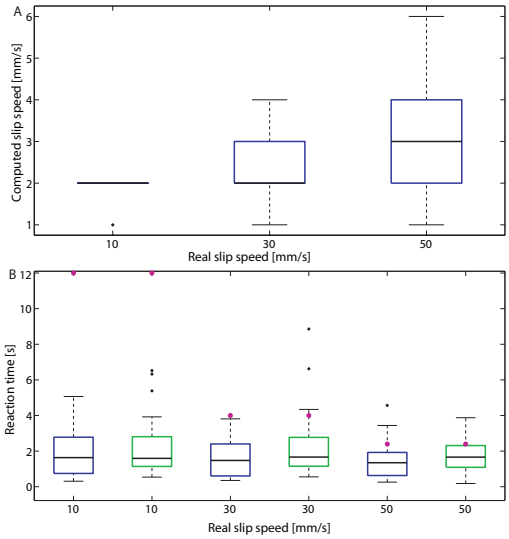

Figure 3.5: Reaction time with respect to actual slip speed with slip speed feedback guidance alone (blue) and force and slip speed feedback (green).

to slip and the moving speed of the graphical object.

3.3.3 Effect of slip speed detection variance

We evaluated the performance of the artificial ridged skin in detecting the speed of the slipping object. The mismatches between the real and computed speed are presented in Fig. 3.5A. Statistically, there is however a significant difference between the values of the computed speeds. The single factor one-way ANOVA yielded $F(2, 491) = 51.39$ and $p < 0.001$. We further investigated whether the variance in the slip speed detection significantly affects grasp stability. Figure 3.5B illustrates the reaction time to slip taking into account the real slip speed of the object. The errors, computed as a difference between the actual reaction time and the maximum reaction time (in violet bullets) for all conditions, showed no significant difference when Kruskal Wallis test was applied and were all classified as outliers.

3.3.4 Grasp success

We computed the rate of success in achieving a grip force within the optimal grasp region and a reaction time lower than the maximum response time to slip, depending on the feedback guidance, for all participants. The reaction time has been considered as a function of the real speed, in order to obtain an estimation of success closer to the potential real grasp scenario. Figure 3.6 shows the percentage of success to stop slip in time and reach an optimal grasp force. The highest success ratio for optimal grip force was obtained with force feedback guidance, whereas the highest success ratio for an in-time response to slip was achieved via the slip speed feedback guidance.

3.4 Discussion

The artificial ridged skin decreased its efficiency as the slip speed increases. While for slip speeds of 10 and 30 mm/s the performance was fair, slip speed of 50 mm/s had the largest variance. The post-processing of the acquired signals require several computations of the frequency to provide a value closer to the real slip speed. Due to a high slip speed, there are not sufficient frequencies computed over the acquired samples in order to yield a more accurate slip speed.

The analysis conducted for the grip force response clearly showed that the grip force can be adjusted with information about the normal force applied to the grasped object. Furthermore, the analysis performed on the grip reaction time, showed that the most significant and variate adjustments on the reaction time took place with slip speed guidance alone or with force and slip speed guidance combined. Slip speed feedback has been found to improve the success in finding the optimal grip force in [42], featuring agility, energy efficiency and less response variability. The current result further contributes by indicating that feedback about slip speed regulates the reaction time to grasp. The result finds physiological support in studies performed with human users holding an object in their healthy hand [72].

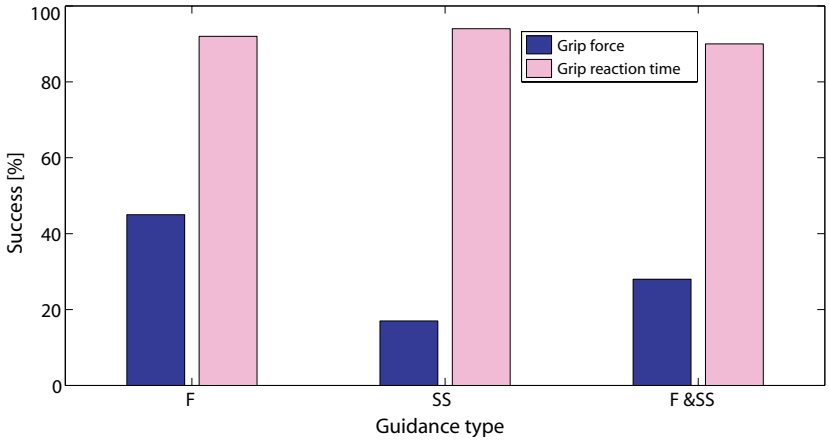

Figure 3.6: Success to stop slip in time and reach an optimal grasp force, relative to force feedback guidance (F), slip speed feedback guidance (SS) and the combined feedback guidance (F&SS).

The rate of success, as computed for grip force and grasp reaction time for each feedback shows that the highest percentage of success in finding an optimal grip force is achieved with the provision of grip force guidance alone, and the highest percentage of success in responding to slip in time is achieved through slip speed guidance alone. The fact that the combination of the two types of feedback did not result in highest success scores may suggest that the two types of information are perceived in a mutually exclusive manner, and providing them at the same time is distracting and inefficient. Investigating this hypothesis in more details is a valuable research avenue with potential for neuroscience and the design of haptic devices. The resulting performances do not consider parameters such as object size and geometry or its initial position in the hand. It is worthy to note that issues arise with smaller objects for each the reaction time should be even faster. For such cases, the ridged skin's features should be improved for more accurate slip detection of high speeds.

Because the FSR is prone to hysteresis, we didn't use it to describe grip forces. We therefore used the joystick to linearly describe the grip force. In contrast, slip detection uses the frequency spectrum, which is not prone to hysteresis.

3.5 Conclusions and Future Research

The study presented in this chapter is two-fold. First, we developed an artificial ridged skin and tested its potential to extract enriched information (force, slippage detection, slippage speed) from the interaction with a slipping object using one force sensor. The approach aims to offer high information bandwidth to cost ratio, as well as to reduce the complexity (energy, weight) of prosthetic hands. The evaluation of the artificial ridged skin was performed under theoretical and practical conditions. Secondly, we investigated tactile feedback guidance (force, slippage speed, force and slippage speed) that can lead to optimal grasp during object slippage. The evaluation was performed in a psychophysical ex-

periment with human participants in a combined real and virtual environment. This study also connects the tactile sensing and display systems. The results show that the artificial ridged skin is a promising tactile sensor for extracting information related to slippage. Furthermore, the results suggest that force and slippage speed feedback may enable an optimal reaction time and grip for overcoming slippage. The study supports a better understanding of the requirements for stable grasp with prostheses. As a future work, we will increase the performance of the artificial ridged skin and test grasp stability in real-world tasks by using a force and slip speed haptic device developed by our group [45].

Chapter 4

Artificial Ridged Skin for Slippage Speed Detection in Prosthetic Hand Applications

Artificial ridged skin for detection of force, slip occurrence and speed

In this chapter, we present in detail an artificial ridged skin able to detect force, slip occurrence and speed using minimal resources.

The human hand is one of the most complex structures in the body, being involved in dexterous manipulation and fine sensing. Traditional engineering approaches have mostly attempted to match such complexity in robotics without sufficiently stressing on the underlying mechanisms that its morphology encodes. In this work, we propose an artificial skin able to encode, through its morphology, the tactile sense of a robotic hand, characteristic to slippage events. The underlying layout consists of ridges and allows slippage detection and the quantification of slippage speed. Such encoding of slippage signal becomes suitable for relaying tactile feedback to users in prosthetic applications. This approach emphasizes the importance of exploiting morphology and mechanics in structures for the design of prosthetic interfaces.

[3]Parts of the material in this chapter previously appeared in: D.D. Damian, H. Martinez, K. Dermitzakis, A. Hernandez Arieta and R. Pfeifer (2010) "Artificial Ridged Skin for Slippage Speed Detection in Prosthetic Hand Applications", *IEEE/RSJ International Conference on Intelligent Robots and Systems (IROS)*, pp. 904 - 909.

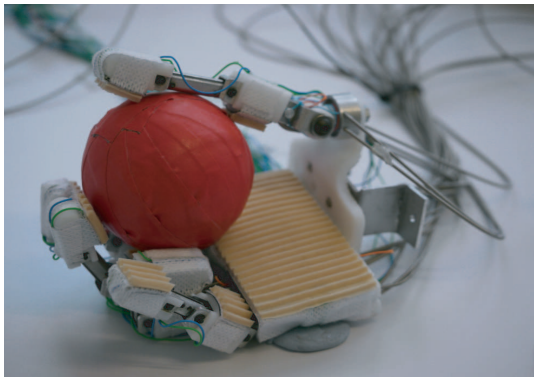

Figure 4.1: Robotic hand equipped with artificial ridged skin.

4.1 Related Work

Haptic technology has gained interest in robotics as the means for enabling a major sense through which robots can perceive the environment and interact with it. In prosthetic applications, restoring the feedback loss is crucial for the normal functions of the human, in regards to the body awareness and its control or environment perception [132]. Slippage sensing is a prerequisite for stable grasp and fine object manipulation [75]. A wide range of interesting tactile sensors have been developed for slippage detection which use a variation of transduction principles. Cotton et al. [38] developed a thick-film piezoelectric sensor for slippage detection. When slippage occurs, the film tilts and produces vibrations causing changes in the value of the piezoresistors. Yamada et al. [167] built a skin featuring rounded ridges equipped with strain sensors in between to detect slippage due to sensor deformation. Slippage information is extracted from the velocity and acceleration of the strain gages deformation. Tremblay et al. [151] used nibs on top of the skin surface which vibrate when an object starts to slip. Accelerometers placed inside the artificial skin capture the vibration and convey slippage notification. Schmidt et al. described in [140] a sensor made from capacitive membranes on top of which brushes of fibers were placed. Such sensors are able to detect slippage on a robot hand by fibers vibration. In [54], slippage is detected by a sudden change in the three-axial force sensor which Edin et al. developed. The technique used is to embed three metal-based strain gages at the tip of the fingers in the three axial directions. Optics is an additional option in detecting slippage, according to [112]. Using conical feelers on rubber sheet surface, Ohka et al. acquired an image of the contact area and of the feelers displacement to determine the surface normal and shear forces. Other method for detecting slippage is to consider tactile information as a tactile image and use motion detection algorithms [100]. An array of identical electrical circuits is sensitive to temporal and spatial changes, and thus identifies microvibrations produced by slip. A survey on the state of tactile sensing in robotics was done by Dahiya et al. in [41] where various such technologies are comprehensively discussed.

Prosthetics requirements are not trivial. They stem from the need of correlating machine interfacing technology with human afferent and efferent mech-

anisms. The demands enumerate light devices, which entail less or smaller electronics and less wires, fast communication which further assumes low algorithmic complexity, intuitive feedback modalities and intuitive feedback signals. Feedback modalities are assumed to relay meaningful information in accord with the mechanism of skin receptors. Our contribution aims at developing tactile sensing able to relay enhanced information about slippage events, while diminishing much of the electronic and algorithmic complexity often required in other tactile sensing approaches. We propose an artificial ridged skin which encodes, through its morphology, the slippage detection and slippage speed for a robotic hand. The features of the tactile signal can readily be converted to pulses patterns suitable for tactile feedback in prosthetics. The current approach emphasizes the importance of morphological properties, as a mean to outsource computational costs to mechanical structures. Pinpointing the role morphology plays, we can use it to filter meaningful information for the user and consequently to mitigate his cognitive effort in interacting with a prosthetic device. A careful design of the sensing interface is decisive in achieving a smoother human-robot integration.

In the following sections, we will present the tactile sensing system we developed, detailing its features, the results in creating an interface for prosthetics and close with a discussion about the contribution of this work and future directions.

4.2 Artificial skin construction

The aim of this work is to build a tactile sensing system which takes into account the aforementioned demands in prosthetics. To accomplish this, we resorted to mechanical structures that are able to intrinsically encode information about the slippage of an object. We built a set of ridged artificial skins in which we discretely varied the distance between two consecutive ridges, D_{rr}, from 2.5 to $4mm$. The ridged artificial skin is built from silicone and transduces the surface events to a force sensing resistor (FSR) beneath. Figure 4.2 depicts a sample of the silicone ridged skin, the standard FSR sensor, and illustrates the process of construction. The ridged shapes of the skin were obtained by solidifying the silicone into an ABS ridged mask which was built by rapid prototyping. The transverse sectional shape of the silicone ridge is an equilateral triangle, with the side $L = 2.5mm$. The thickness of the pad on which the ridges lay is $1mm$. The FSR sensor size is 4x4cm, measuring a force sensitivity from $100g$ to $10kg$. In between the FSR sensor and the ridged patch we placed a fabric imbibed on each side with a different type of glue to match the adhesive properties of both parts that were blended. The components are not expensive, and the construction process makes the skin sample easy to replicate.

4.3 Artificial skin model

The morphology of the skin in the interaction with a slipping object leaves an imprint on the FSR signal, as depicted in red in Figure 4.4 b). We modeled the signal acquired by the FSR sensor in two representative cases within the slippage phenomenon. In the first case, the object presses on the ridges, without

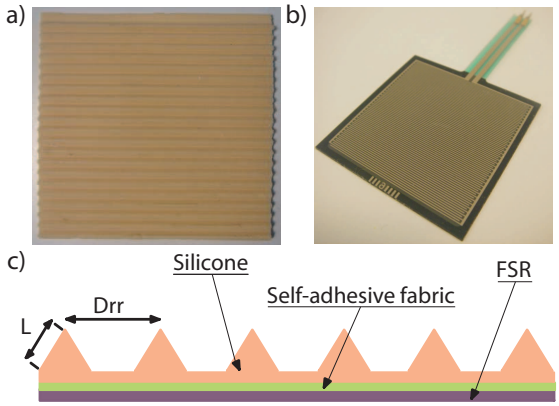

Figure 4.2: The fabrication process of the ridged skin. a) Sample of ridged skin. b) Force Sensing Resistor. c) Artificial skin layers.

deforming them laterally as in Figure 4.3 a). We premise that this case accounts for the valleys of the FSR signal. In the second case, the object makes contact with the first ridge in its direction of slippage, as described by Figure 4.3 b). The ridge deforms laterally and opposes to the object movement. Our assumption is that the FSR signal peaks are attributable to the extra-force needed to surpass the ridge in the moving direction. In Figure 4.3 c), a detail on the forces acting on the sliding object is illustrated. Considering the slippage velocity constant, we can extract the following relations:

$$\begin{aligned} P - F_{r1} &= N \sin\gamma + F_{r2} \cos\gamma \\ &= N \sin\gamma + \mu N \cos\gamma. \end{aligned} \tag{4.1}$$

In this equations, P represents the force that pulls the object along a slipping direction. F_{r1} and F_{r2} denote friction forces, μ is the friction coefficient equal to 0.7813, and $\gamma = 60\,^\circ$ is the angle of the triangular ridge. The silicone ridge opposes the movement of the object according to the value of force N. The FSR sensor underneath the ridged patch is able to detect normal forces, therefore we are interested in measuring the forces acting against this sensor. Thus the model of the FSR sensor can be formalized as in the equation bellow:

$$\begin{aligned} M(t) &= W(t) + N \cos\gamma \\ &= (1 - k\mu)W(t) + kP. \end{aligned} \tag{4.2}$$

The transduced value of M is modulated by the morphology of the skin. This evidence is embedded in the expression of $k = \cos\gamma/(\sin\gamma + \mu\cos\gamma)$. $W(t)$ represents the partial weight of the object gradually covering the area of the FSR during the movement. Its value depends on the ratio of the displacement between the moving object and the FSR sensor to the length of the object. Relation 4.2 was obtained by replacing N with its expression derived from equation 4.1. Eventually, the FSR model is mainly influenced by the object weight and the force transmitted by the extra-work of pulling force P. We experimentally tested the model in the setup showed in Figure 4.4 a). By measuring the FSR value when the object slips horizontally on a flat skin, we acquired the

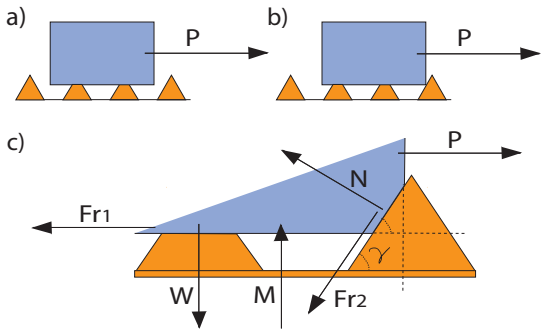

Figure 4.3: Force analysis at slippage. a) Object presses on the ridges. b) Object deforms laterally the first ridge encountered in the moving direction. c) Detail on the forces in case b).

value of transduced weight in time. To explain the effect of ridges on the extra-force in the FSR signal, we measured the pulling force on the object slipping over the ridged skin. The object was pulled by a DC motor at constant speed. The pulling force P was measured using a potentiometric force sensor wired in series with the object. We simultaneously acquired the values of the FSR and of the potentiometric force sensor during the slippage trial. Feeding the values from the time series of the signals into the model equation, we obtain the FSR model denoted in Figure 4.4 b). A Fast Fourier Transformation applied to the raw FSR signal (red) and to the FSR model (magenta) discloses that the two signals have the same frequency equal to $0.315Hz$. This is illustrated in Figure4.4 c) by the highest peak in the signals spectrum. The inaccuracies of the model stem from various reasons: (1) the friction force becomes larger as the moving object covers more of the surface of the FSR sensor, subsequently increasing the pulling force; (2) we ignore the elastic deformation in our model, which would also absorb energy from the moving object, and (3) the mechanical tolerance of the potentiometric force sensor which has a built-in spring. The above equations also apply for skewed orientation of the plane along which the object slips.

4.4 Structural properties of the ridged artificial skin

The bio-mechanical complexity of the ridges on the human hand is still an intriguing research topic. Their role is debated from sensing to dexterity [156]. The ridged structure offers better grip due to increased friction [29], it magnifies the pressure exerted by the manipulated object [56] and acts as a frequency filter for specific skin mechanoreceptors [139]. In this section, we present the characteristics of the ridged artificial skin we built, under different force conditions.

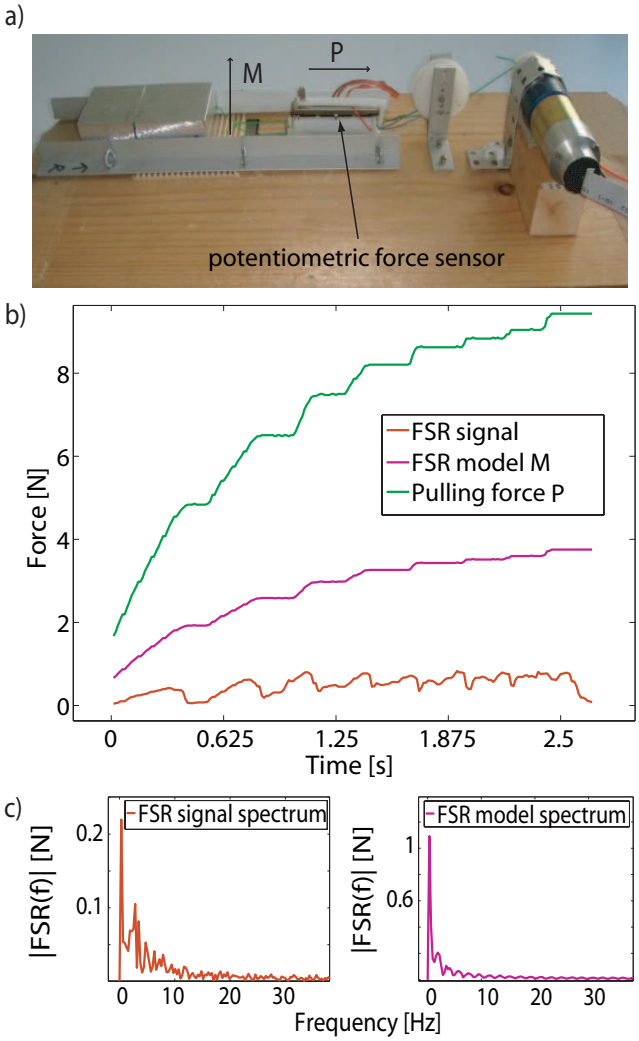

Figure 4.4: FSR model. a) Experimental setup for creating the model. b) Time series of raw FSR (red), pulling force (green) and resulting FSR model (magenta). c) Frequency spectrum of raw FSR and model FSR showing identical peak frequencies of $0.315Hz$.

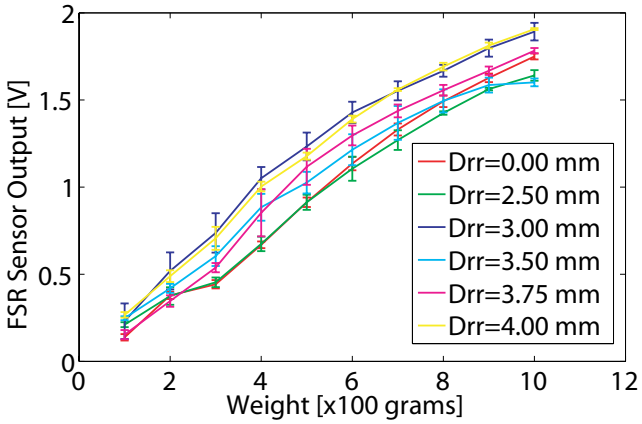

Figure 4.5: Distribution in voltage magnitude as a response to different object weights and inter-ridge distances D_{rr}.

Artificial skin as a force transducer

For a static characterization of the force, we tested several types of artificial skins while various weights were placed on top. The artificial skins had different ridge densities designated by the inter-ridge distance (D_{rr}). A flat skin (without ridges) was also used for reference ($D_{rr} = 0.0mm$). Four trials were performed for each skin and each weight. The data acquisition was made by a Texas Instruments DAQ system, sampling at $1000Hz$, and further analyzed in Matlab. Figure 4.5 depicts the voltage amplitude elicited by the skin patches when weights of 100 to $1000g$ were placed on top. For each weight, the data shows a relative increased voltage value with reduced ridge density. The maximum standard deviation was $0.13V$ for the skin with $D_{rr} = 3.75mm$, followed by the skin with $D_{rr} = 3.0mm$ with standard deviation of $0.11V$. The inter-ridge distance affects force measurement in that the contact surface distributes force according to the number of ridges supporting the object, when the object is larger than the sensorized skin patch. This implies increased force values for large inter-ridge distances and decreased force values when ridge density is high. These tendencies can be seen to some extent in Figure 4.5 if we ignore the two skins with high variance.

Artificial skin as a slippage detector

Grip disturbances can lead to the slippage of a grasped object. To stabilize the object in the hand, it is mandatory to detect such events. Additionally, slippage speed can provide preliminary cues to regulate grip force when the friction coefficient is known [75]. We conducted experiments with a sliding object to quantitatively evaluate slippage speed. We utilized six types of artificial skins and applied a total of three slippage velocities. To cover the entire surface of the artificial skin, we placed two FSR sensors beneath. The results are invariant to the number of FSRs and this grants skin efficiency even with one single FSR. However, there is no such standard sensor that has the size of the particular skin we built. In a typical experiment, an object was sliding horizontally across the artificial skin at a constant speed given by a DC motor running at preset

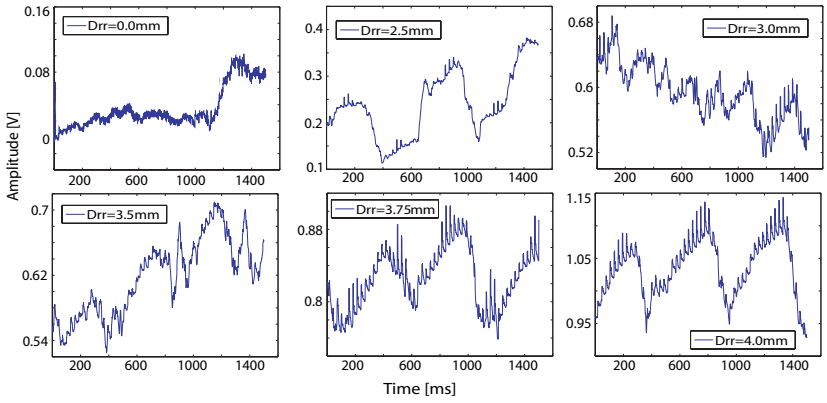

Figure 4.6: Time profiles for slippage signals generated by an object sliding at same speed over skins of different inter-ridge distances D_{rr}.

parameters. The skins were fixed to exclude extraneous vibrations. The data acquisition was made by the system described in 1) and a peak frequency was extracted from the spectrum of the data.

The time series in Figure 4.6 show the signature of the slippage signal with respect to the inter-ridge distance parameter, at a constant slippage velocity of $10mm/s$. In the spectrum, the ridge patterns gave rise to meaningful peak frequencies, in contrast to the flat artificial skin. The latter one maintained a low amplitude in time and the yielded frequency was being assigned, for most trials, the smallest frequency in the spectrum, regardless of slippage velocity.

Our model described in section III suggested that each time the sliding object encountered a ridge, the signal recorded a peak value. Thus, under slippage conditions, the skin patch behaves like a signal generator whose frequency f_s accounts for slippage speed v_o of the object and for distance D_{rr} between two consecutive ridges. Given a constant velocity, this relation can be expressed as follows:

$$f_s = \frac{1}{\Delta t} = \frac{v_o}{D_{rr}}.$$

where Δt is the period between two consecutive peaks in the signal. By statistically averaging the measured velocity of the moving object across experimental trials, we were able to calculate the ideal frequency. The results depicted in Figure 4.7 show values of peak frequencies extracted for the six skins and three velocities. They suggested that inter-ridge distance D_{rr} is an important parameter for the quality of frequency encoded information. Among all skins, the one with $D_{rr} = 4.0mm$ yielded discriminatory peak frequencies for each velocity. Furthermore, its mean value was the closest to the ideal frequency given by the formula above. The peak frequency was computed as an average over five experiments per skin per velocity.

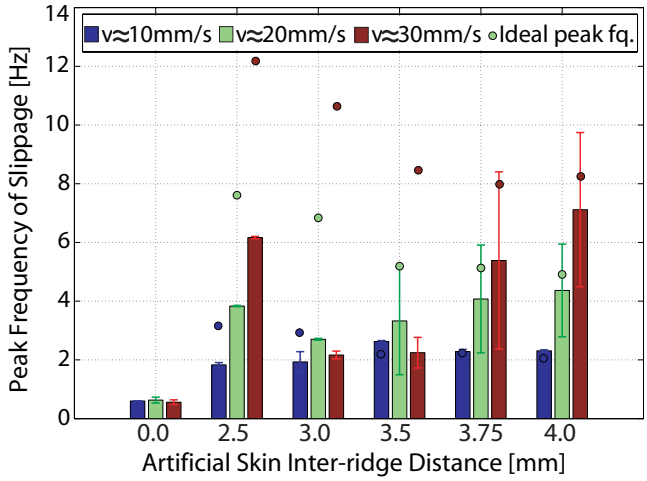

Figure 4.7: Peak frequencies of slippage signal at three velocities as elicited by skins with different inter-ridge distances D_{rr}.

4.5 Informational properties of the ridged artificial skin

In our experiments for prosthetics we utilize the robotic hand [7] depicted in Figure 4.1. Our goal is to achieve a fully integrated system, comprising of a user which can control a robotic hand via bio-electrical signals, and of a robotic hand which in turn is able to efficiently acquire information about grasping events and transmit it back to the user. In this section we describe the experiment to evaluate slippage detection in the robotic hand, and the implementation of a tactile feedback encoding, to complete part of this prosthetic loop, as illustrated in Figure 4.8.

4.5.1 Slippage detection in a robotic hand

This experiment was intended to test the robotic hand performance in slippage detection in a dynamical and noisy environment. The robotic hand is tendon driven and has 13 degrees of freedom. Its palm was equipped with a 8x4cm patch of ridged artificial skin. It was only this area of the robotic hand which was investigated for slippage detection, the fingertip skin was inactive. We conducted our experimental trials with the robot hand equipped with the ridged artificial skin of $Drr = 4.0mm$. Two FSR sensors underneath the skin recorded the surface events. The sensors values were acquired at $80Hz$. A Fast Fourier Transformation was run over the time series and a peak frequency was extracted. We used two types of objects, a rectangular and a cylindrical object. One object was slipping horizontally across the skin at a certain speed set by a DC motor. The robotic hand was programmed to automatically tighten the grip in order to hold the object in the palm. The motors of the robotic hand were actuated proportionally to the peak frequency to flex the fingers toward the object: motors flexed the fingers faster when frequency was high and flexed them slower when frequency was low. Stable grasp was discriminated as a stable

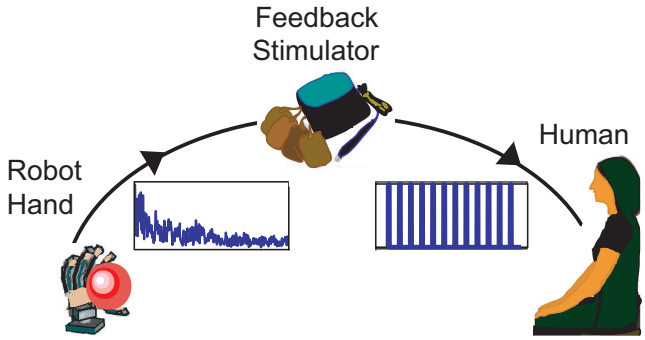

Figure 4.8: Schematics of tactile sensing system. Artificial skin encodes slippage whose speed is further encoded into vibration pulse frequency for stimulating user's skin in prosthetic applications.

signal over a period of 12.5 milliseconds, while slippage was classified mainly by a peak frequency occurring in a range spectrum of $[1, 20]Hz$. Figure 4.9 shows the performance of the robot hand in gripping and stopping an object from slipping away, when the object slided over its skin at six velocities. Ten trials per speed for each object were run. The success at sliding speeds lower than $10mm/s$ maintained higher than 90%. However, at slippage speeds larger than $17mm/s$, the performance degraded drastically. The rate of failure was higher for the cylindrical than for the rectangular object. One explanation is that the contact surface between the cylindrical object and the ridged skin is reduced compared with the rectangular object, thus decreasing the accuracy in detecting an appropriate slippage frequency. Systematic analysis to evaluate the relation between the slippage frequency and the slippage velocity was not conducted because it was not possible to control all the experimental conditions (noise from the motors, mechanical disturbances of the robotic fingers tightening around the object, etc).

4.5.2 Feedback encoding of the slippage signal

Based on the findings of our study, we propose an implementation for the feedback stimulation in prosthetics to relay information about slippage events to users. A promising prosthesis is one which combines the precision of the robotic device in mechanical events with the experience of the user capable of discerning best among contextual information. Tactile feedback provides to users notification on grasping events and decisional control over the reaction requested by such events. An automated prosthesis would deprive the user of sensorial and manipulative re-education, making the integration between the user and the prosthesis cumbersome. Thus, tactile feedback signal becomes of major importance for the prosthesis effectiveness [6]. One way to deliver the tactile feedback is vibrations. Vibration is the sensation produced by sinusoidal waves of objects that are put against the skin [80]. The response of skin mechanoreceptors is to signal an action potential to each cycle of the oscillation. This kind of mechanism is proposed to encode the slippage detection and speed to tactile stimulation feedback in prosthetics in order to alert the user to object slipping. This is possible due to the series of ridges which pulse when a slipping object

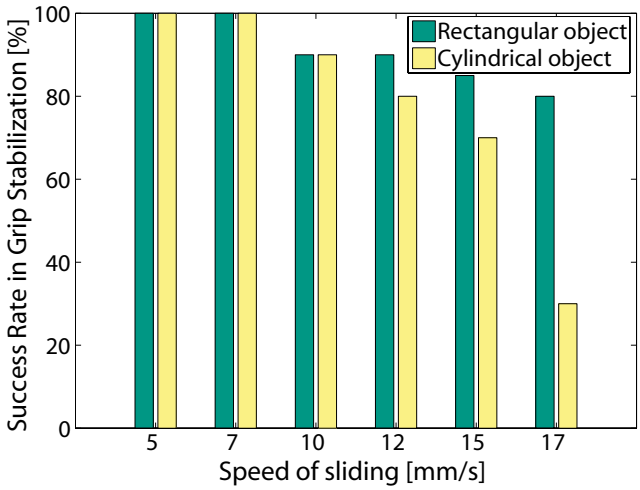

Figure 4.9: Performance in robotic hand grip stabilization, as a response to object slippage at six speeds.

makes contact with them. Therefore, slippage frequency extracted from the skin recordings can be readily converted to vibration frequency through linear mapping. In Figure 4.10, two instances of pulse stimulation patterns are presented (b)) for two slippage signals whose frequencies are equal to 2 and $4Hz$ (a)). The slippage frequencies were scaled onto vibration frequencies of range $[1, 150]Hz$ to meet somatosensory physiological constraints [79]. Additionally, the pulses have constant width to maintain same level of tactile stimulation intensity. This way, the vibration frequency information can be better decoupled from its intensity component [5], and the slippage speed better discriminated.

4.6 Discussion

In this section the design and the potential applications pertaining to the artificial ridged skin are discussed.

The ridge pattern

The design of the artificial skin ridges was minimal, drastically simplifying the properties of the biological hand ridges. We ignored the elliptical or curved arrangement of the ridges, and chose a linear one with same ridge orientation. Therefore, to avoid results of cases we did not treat, our experiments were performed with objects only sliding perpendicularly across the ridges. Otherwise, the accuracy in detecting the slippage frequency would decrease drastically.

The inter-ridge distance

The current setup is able to correctly detect slippage for objects heavier than $70g$, which slip at speeds lower than approx. $15mm/s$. The range of inter-ridge distances we used is justified by assumptions for sensing efficacy. We premised that a D_{rr} lower than $2.5mm$ would dismiss an accurate slippage sense, within

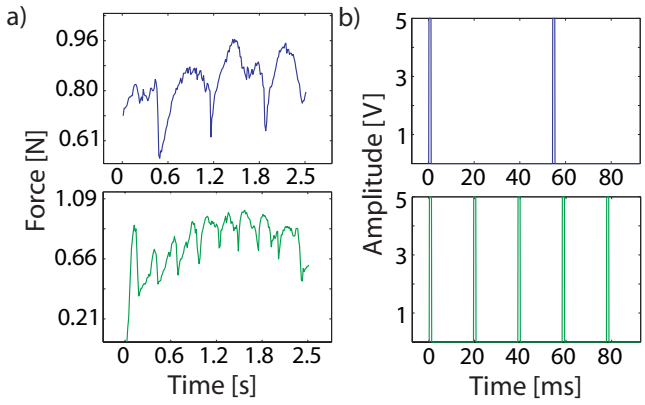

Figure 4.10: Feedback stimulation patterns. a) Two slippage signals with frequencies of $2Hz$ (top) and $4Hz$ (bottom). b) Expected stimulation pulses corresponding to signals in a).

the same trend as the skin with $D_{rr} = 2.5mm$. However, we hypothesize that the skin model can be replicated at smaller scales maintaining the same behavior if concurrently, the raw sensor it is used with has greater precision. On the other hand, a skin with D_{rr} greater than $4mm$ would make the slippage sense more coarse, taking additional time to compute the FFT and deliver the result in feedback stimulation.

The vibro-tactile feedback

For daily activities in which users are engaged, it is important that they receive not only on-off event information (on-off contact with objects, on-off slippage detection) about grasping events, but also continuous information on dynamical haptic events (slippage of an object, grasping force changes). We transmit continuous slippage by discrete timed events, according to neuroscience findings [148] which advocate that the brain responds better to discrete movements than to continuous actions. Such discrete stimulation, in contrast to static one, also suffers less from habituation [79]. The quantification of slippage speed within the stimulation supports the user perception of a slippage notification or alarm to which he should react with an appropriate grip. Apart from signaling slippage, this specific feedback pattern could also provide the users with morphological cues about the robotic device embedded to their body. Ultimately, we hypothesize that exposing the users to such dynamical and relevant information about the interaction with the environment would reinforce the incorporation of the robotic device into the body.

4.7 Conclusions

In this study, we showed that a careful consideration of morphology in the design of tactile sensing systems can lead to enhanced prosthetic interfaces, with reduced cost on the overall complexity of the prosthetic system. The ridges of the artificial skin allowed the encoding of slippage detection and slippage speed

quantification into a signal which can be readily postprocessed for feedback stimulation patterns in prosthetics. As a follow up, an investigation of other morphologies for the artificial skin, like spiral or concentric circular ridges will take place. Our preliminary results with circular ridges reveal that we can to an extent extract information about relative position of an object in the hand. Future work will also involve tests with human participants to evaluate the effectiveness of the proposed stimulation pattern in detecting slippage and adjusting grip.

Chapter 5

Artificial Tactile Sensing of Slip Speed and Position with Minimal Resources

Artificial ridged skin for detection of slip occurrence, speed and location

In Chapter 5 the capabilities of the artificial ridged skin presented in Chapter 4 are extended following the same principles of minimal resource usage.
We present an artificial ridged skin based on a single force sensor that detects the slip occurrence, speed and position of an object, subject to dynamic events, e.g. slip. The artificial skin features parallel triangular ridges that are arranged in a non-uniform configuration. An evolutionary algorithm generates an optimal distribution of ridges in terms of the accuracy and resolution of the slip speed and position detection. Real experiments with skins generated by the evolutionary algorithm show a successful detection of slip speed and position for slip speeds lower than 60 mm/s. Our results introduce the concept of "economical tactile sensing", defined as the enhancement of tactile information using minimal resources by exploiting the morphology of the artificial skin. The concept is pertinent in prosthetic applications because it can enable a high ratio of information to resources, and it is promising for robust, light and energy-efficient tactile sensing systems. The presented work points toward design principles for efficient tactile sensing through morphology-based computation.

[4]Parts of the material in this chapter represent a manuscript in process of submission: D.D. Damian, T. Newton, R. Pfeifer and A.M. Okamura (2012) "Artificial tactile sensing of slip speed and position with minimal resources" (to be submitted)

5.1 Related Work

Although humans experience a wide range of sensations, sensory psychophysics was found to be described by mainly four attributes: location, timing, intensity and modality [80]. Tactile sensing research focuses efforts into developing sensors that mimic the functionality of the mechanoreceptors found in the human body. Current challenges include both developing sensors that provide the aforementioned modes of information and synthesizing these channels of information into a coherent and meaningful picture of environmental stimuli. Successfully implementing these sensing capabilities into robotic devices, such as robotic or prosthetic hands, would endow robots and prosthetics users with refined grasp control and enhanced surfaces exploration.

To date, interesting technologies for artificial sensing have been developed, featuring various transduction methods, arrangement and scale of the sensing elements.

Force sensors have been studied extensively [40] [41] and incorporated into numerous commercially available products, e.g. force sensing resistors (FSR) [69], QTC-based sensors [21], etc. Furthermore, the research in tactile force sensing is currently shifting toward distributed sensors, such as tactile arrays, that cover a large surface of the robot hand. A few examples include all-body sensors [94] [141]. In the latter work, interconnected triangular shapes cover the non-flat surfaces of robots such as ICub, Nao, and Kaspar. Local chips integrate groups of sensor inputs to reduce the number of wires and to compensate for the hysteresis and sensor drifts. A force sensor array for fingertips is proposed in [26]. This sensor consists of a matrix structure (24.36×34.9 mm) with 64 sensitive sites based on FSR technology. The maximum resolution is about 1 mm and the minimum resolution is about 5 mm. Evaluated on a glove, the force sensor provides good repeatability and sensitivity, although further research is needed to address sensor linearity and hysteresis.

Inspired by the variety of multi-modal sensory capabilities of human skin mechanoreceptors, distributed heterogeneous tactile sensors have been developed. Takamuku et al. [150] developed an artificial skin that embeds two types of sensors (strain gauges and polyvinylidene fluoride (PVDF)) between two silicone layers. This skin has been proven to discriminate between a number of textures during squeezing and tapping. An alternative design for tactile sensors is presented in [162]. The artificial skin features a rigid core equipped with an array of electrodes surrounded by a weak conductive fluid. The volumetric flow path can be differentially measured by each electrode to acquire information about force magnitude, direction or object shape.

While force is useful for characterizing grip intensity, in robotic/prosthetic hands, slip speed is relevant for characterizing grasp disorders. Johansson and Cole [73] offer a prime indication that slip speed may affect our grip response. Slip, artificially generated by changing the weights of an object held in the human hand, was found to influence the reaction time and intensity of the grip response depending on the weight change ratio. Slip sensing is a prerequisite for stable grasp and fine object manipulation [75] [10]. In a recent haptics study, slip speed has been shown to boost the agility of overcoming slip, increase the success in controlling slip with a lower consumption of muscle contraction intensity, and ensure lower variability of the muscle contraction input [42].

In robotic grippers, the typical procedure for slip detection is to identify

extraneous perturbations or patterns of vibrations in the signal. A 18×18 mm sensor for detecting slip is presented in [103]. Four FSRs placed in different regions of this surface acquire the position of the force and its activation in time through rubber cylinders that cover them and transduce the external force. Cotton et al. [38] developed a sensor based on thick-film piezoelectric material shown to detect incipient slip for a friction coefficient of 0.3. In [15], a miniature silicon sensor (1.5 mm $\times$1.5 mm μm) is composed of four integrated piezoresistors that are used independently to acquire the three components of an external applied force. This sensor was shown to detect slip with a delay from a minimum of 24.5 ms to a maximum of 44 ms in the majority of experiments. Optics becomes an additional option in detecting slip. "Tactile" images, defining grasp postures, are processed to determine changes indicating slip. Using conical feelers on the surface of a rubber sheet, Ohka et al. [112] acquired an image of the contact area and of the feelers displacement to determine the surface normal and shear forces. Another method for detecting slippage is to consider tactile information as a tactile image and use motion detection algorithms [100]. An array of identical electrical circuits is sensitive to temporal and spatial changes, and thus can be used to detect microvibrations produced by slip. Currently, sensor technology provided qualitative measures of slip, e.g., slip detection, but not quantitative, e.g., slip speed. Tactile arrays contain location information (individual sensor addressability), and thus slip speed could potentially be detected - nonetheless, this feature has not been given much attention.

Current sensor technologies are primarily concerned with increasing sensing accuracy and augmenting grasp performance. While this research trend has vastly improved the design and understanding of sensor arrays in the context of robotic grasp, it has done little to address the energy efficiency of these relatively complex structures. While the literature offers a plethora of designs and mechanisms for tactile sensors, few studies discuss the impact of numerous factors, such as the space and number of embedded electronics, distributed computing, networking, integration of sensory data, wiring, crosstalks, robustness, power consumption, ease of manufacturing, cost, and maintainability, on the usability and feasibility of the proposed artificial sensing solution. In particular, the spatial arrangement and the transduction method used in the development of tactile arrays are factors of high concern in a dual quest of high spatial resolution and high sensitivity. The amount of wired interconnections associated with tactile arrays represents an impediment to dexterity due to the increased amount of time required to scan and transmit the readings from the array's taxels. Indeed, processing a large amount of data has been considered a major challenge in the field of sensor fusion. Although work has been done in the local pre-processing of the data (compensation of temperature and drifts, data preselection, etc.) by affixing local microcontrollers, the technological limitations of data buses hinder the number of taxels that can be used in tactile arrays or efficient computations on the acquired data. The sensory transmission time imposes another limit on the number of taxels, as the speed of transmission depends on the time needed to scan and multiplex the sensor elements of the array. Power consumption is also a major concern, as for instance in prosthetic hands which are expected to function consistently over long periods of time. Clearly, there is a positive correlation between the number of taxels and the power consumption of the artificial sensory system. A large number of taxels intrinsically affects the robustness of the system due to the interconnections

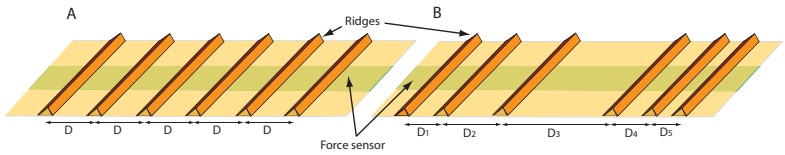

Figure 5.1: Arrangement of ridges on the artificial skin equipped with a force sensor. A. Uniform distribution of ridges. B. Non-uniform distribution of ridges. Ds represent the inter-ridge spacing. For the skin in case A, the inter-ridge distances are identical (D).

between the taxels and potential crosstalks. Redundancy could be the positive flip side of this issue.

Towards the development of efficient tactile systems, our approach to tactile sensing systems is to exploit the structure and the space of the artificial skin's materials in order to increase the sensory information at low cost, with respect to design complexity and energy consumption. Our approach was motivated in part by the work of Vincent et al. [157] and Pfeifer et al. [123] which advocates that engineering techniques primarily make use of energy, whereas biological systems primarily exploit structure, space and information. This latter strategy could be incorporated in the development of novel sensors to achieve an optimal trade off between information density and resource consumption. We present an artificial skin that detects stimulus slip occurrence and speed, location, and force (implicitly, due to the use of a force sensor), using a single force sensor. The latter feature, normal force, was investigated in static events in a previous work [46] and will be ignored in this study. The underlying approach is based on exploiting a non-uniform arrangement of parallel ridges whose consequence is the multiplexing of multi-sensory information into one data channel. Enhancing information while reducing the underlying resources finds priority especially in prosthetic applications, by reducing the circuitry, and therefore improving the system's robustness, while reducing energy consumption and overall complexity.

5.2 Concept for object slip speed and position detection

Consider a surface with uniformly distributed ridges (see Fig. 5.1A). A force transducer underneath the surface can intercept the force applied by an object slipping on top of the skin. As the object moves across the surface and hits a ridge, it gives rise to a peak in the force signal produced by the transducer. Given a constant spacing D and assuming a constant speed, v, we can determine the slip speed from the relation $v = D/T$, where T is the time period between the peaks in the force signal [46].

Although the homogeneous pattern of ridges enables the detection of the slip occurrence and computation of the slip speed, the ridge arrangement does not allow the detection of the dynamic location of the object on the skin surface. As long as the spacings have constant length and the speed is also constant, the time period between peaks is the same, regardless of where the object is on the skin. One possibility for detecting location is to change the distribution of the ridges on the surface of the skin such that the spacing information is a unique

feature (see Fig. 5.1B). Assuming again that the speed of the object is constant, we can detect three consecutive peaks and the time periods corresponding to their inter-ridge spacings

$$\begin{cases} T_i &= \frac{D_i}{v} \\ T_{i+1} &= \frac{D_{i+1}}{v} \end{cases} \tag{5.1}$$

The position can be determined by matching the T_{i+1}/T_i ratio with the prior knowledge of the ratio of two consecutive spacings, provided that the T_{i+1}/T_i ratio is unique. After determining the location, the speed can be computed from an equation in relation 5.1. All subsequent speeds and positions can be detected or updated by applying the same procedure to any following force peaks. Based on this concept, our study investigates a morphological design in terms of the ridge configurations of an artificial skin, that maximizes the ability to accurately detect the speed and position of a slipping object with reduced resources.

5.3 Skin design

The design of a skin which efficiently acquires rich environmental information (i.e., slip occurrence, speed and position of an object) was first investigated in simulation. A force signal corresponding to the ridge layout of an artificial skin was simulated and analyzed to produce a single score measuring the performance of the ridge layout with respect to the detection of position and velocity. The skin design process can be broken into four stages: (1) The simulation of FSR data as a function of ridge distribution; (2) The detection of position and velocity using the data generated in part (1); (3) The determination of a single score associated with the relative success of the detection in part (2); (4) The search and selection of the optimal score/skin. The following is a detailed explanation of each stage listed above.

5.3.1 Force data simulation

Given a distribution of ridges in the form of a vector D whose entries correspond to inter-ridge distances in millimeters, we simulated FSR data in response to an object slipping at speed v over the surface of a skin with inter-ridge spacings specified by D. Thus our goal was the construction of a function, $s(t) = f(D, l, t_0, v, SR)$ whose arguments D, l, t_0, v and SR represent the inter-ridge spacings, the length of the skin, the initial time, the velocity of the slipping object and the sampling rate of the FSR, respectively. The output $s(t)$ is the simulated signal of interest. For this generic simulation of the force data, the values of the inter-ridge spacings and speeds were chosen randomly, while we considered $t_0 = 0$, $SR = 400$Hz, and $l = \sum D$.

To implement f, we assumed that the FSR would respond primarily to the collision of the object and a ridge. Specifically, each collision was modeled piecewise to produce an exponential rise and decay in the profile of $s(t) = \bigcup_i c_i(t)$ given by

$$c_i(t) = \begin{cases} \kappa\alpha(t - t_i)e^{-\beta(t-t_i)} & [1] \\ \kappa(\alpha - c_{i-1}(t_i))(t - t_i)e^{-\beta(t-t_i)} + c_{i-1}(t_i) & [2] \\ \kappa\alpha(t - t_i)e^{-\beta(t-t_i)} & [3] \end{cases}$$

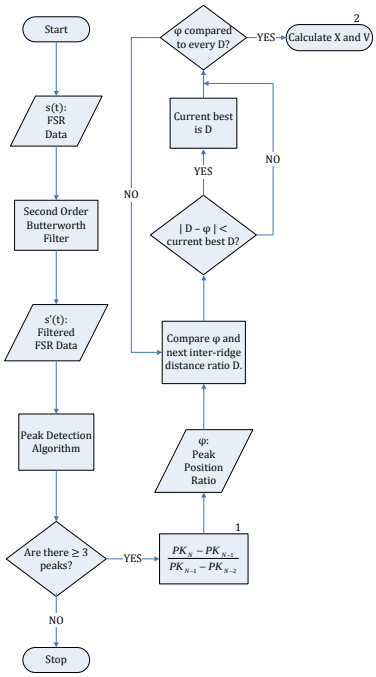

Figure 5.2: Algorithm for testing the design parameters of the skin. Based on a simulated force signal, $s(t)$, the algorithm reconstructs the position, X, and speed, V, of a slipping object. The distance between consecutive detected peaks, PK, are subjected to a ratio computation described in step 1, and compared to ratio of inter-ridge distances, D, which are known *a priori*. The performance in detecting the position and speed is used as a criterion for the ridge distribution selection (step 2).

$$[1] : t - t_i < 1/\beta \text{ and } i = 0$$
$$[2] : t - t_i < 1/\beta \text{ and } i \neq 0$$
$$[3] : t - t_i \geq 1/\beta$$

where $\kappa = e\beta$, α is the peak height reached by $c_i(t)$, t_i is the time at which the object encounters the ith ridge, and where each $c_i(t)$ is the ith portion of $s(t)$ (between ridge i and ridge i+1).

For each $c_i(t)$, the values of α and β were randomly selected from a fixed interval to simulate the non-deterministic nature of the real system. In addition, high frequency noise was randomly sampled from a repository of real data aquired from the FSR and added to $s(t)$. Last, low frequency white noise was generated in software and also added to $s(t)$ to produce the final signal used in the analysis of skin performance.

5.3.2 Detection of position and speed

To evaluate the anticipated performance of a skin, we devised an algorithm to extract the position and velocity of the slipping object at time t from the simulated signal $s(t)$.

The algorithm, depicted graphically in Fig. 5.2, begins by applying a second order Butterworth bandpass filter to $s(t)$, the raw simulated FSR data, to remove high and low frequency noise. The filtered signal, $s'(t)$, is then fed to a peak detecting subalgorithm which finds the points at which the filtered signal protrudes beyond its immediate surroudings by some predetermined threshold. In principle, each peak corresponds to a ridge on the skin; the times at which these peaks occur is stored in a vector PK. If the number of peaks found is fewer than three, the algorithm terminates as there is insufficient information to continue. If more than three peaks are detected, the algorithm considers consecutive triplets among the entries of the vector PK and calculates the ratio of the difference between the times at which these consecutive peaks occur as

$$\varphi = \frac{PK_k - PK_{k-1}}{PK_{k-1} - PK_{k-2}}$$

where $k \leq N$ and N is the size of PK. Since velocity is assumed to be constant, this ratio of time differences should be equal to the corresponding ratio of spatial differences between the last three peaks. Because we have a priori knowledge of the inter-ridge spacings, D, we may simply calculate the ratio of each successive pair of inter-ridge distances $\delta_i = D_i/D_{i-1}$, $i \leq N$, and compare the result to φ. If φ and δ_i match within some threshold for a given i, we have sufficient information to calculate the position and velocity of the slipping object. In particular, we calculate position as

$$x_k = \sum_{r=1}^{i} D_r$$

. Velocity may be computed as

$$v = \frac{D_i + D_{i-1}}{PK_k - PK_{k-2}}$$

Thus we extract the position and speed vector of a slipping object at time t corresponding to a ridge location given simulated FSR data, $s(t)$:

$$X = \{x_k \mid 3 \leq k \leq N\},\ V = \{v_k \mid 3 \leq k \leq N\}$$

.

5.3.3 Skin scoring

Because we had advance knowledge of the position and speed of the slipping object in simulation, it was straightforward to compare the output of the algorithm described in the preceding section to the actual values. However, due to the addition of random noise introduced into the simulated FSR signal, the detected peaks could identify either positions of ridges, as permanent features of the skin, or high intensity noise, as transient features of the skin. Therefore, it is not sufficient to simply compare the known values of X and V to the values calculated by the algorithm over a single trial to determine a metric for skin performance. To account for these confounding factors, we devised a system of performance evaluation in which, for a given skin, we generated signals corresponding to each set of three consecutive peaks and a velocity. The velocities,

v was considered in the range of 10 to 100mm/s with a discrete step of 5mm/s. The preceding algorithm was subsequently applied to each signal and the known position and speed was compared to the position and speed returned by the algorithm. If the algorithm correctly identified both speed and position within a predetermined margin of error, the skin was awarded one point, otherwise no point was awarded. The error tolerance in finding the position was one tenth of the skin length under three considered peaks and the error tolerance in finding the velocity was one tenth of the considered velocity. The points earned for each three consecutive peaks and velocity, were summed and then normalized by the total number of trials (the total number of consecutive peaks triplets multiplied by the total number of velocities considered). Moreover, for each type of skin described by the simulated force signal, this evaluation process was repeated five times and finally the evaluation score was averaged across these five trials. In this way, we were able to define a sliding scale of performance for skins in simulation.

5.3.4 Skin selection

The scoring described previously characterizes a simulated force signal corresponding to a random distribution of ridges on a skin. The optimal distribution of ridges (spacings) was determined by evolutionary programming. The optimization function finds the optimal sequence of spacings that fit onto a certain length of the skin. A genetic algorithm was run on various configurations of skin spacings whose score was quantified with respect to two objective functions: the accuracy of speed and position detection, and the resolution of speed and position detection. The genetic algorithm (GA) was programmed to maximize both variables. The sensing accuracy is defined as the minimal error in detecting the slip speed and position. This score is ascribed after running the algorithm presented in subsection B. The considered slip speeds reside in the discrete range of $10 - 100$ mm/s (with a discrete step of 5 mm) and considered positions represent positions of ridges. The sensing resolution is defined as the number of ridges in the configuration of the skin. The skin length was chosen to be 84, to roughly approximate the width of a human palm. The length of a chromosome, i.e., the number of variables over which the GA was applied, was 13, $\Delta = \{D_1, D_2, ..D_{12}, N\}$. The series of D_i with $i = 1 : 12$, represents values (in millimeters) for the spacings. The maximum number of spacings, 12, was computed based on the maximum number of different spacings whose sum equals the length of the skin. $N \leq 12$ represents the number of spacings considered as candidates for the skin. For each run, the GA selects the first N spacings D_i, with $i \leq N$, from the 12 possibilities. If the number of spacings, N, was less than 12, the last $12 - N$ values in the set were ignored. The population of the chromosome takes integer values in the range of 3 to 81 mm for any variable component. These range boundaries represent the minimum and maximum values for a spacing such that we have at least three ridges (two spacings) and the sum of the spacings is 84. Within one generation of a population, two are chosen as elite, $0.6 - 0.7\%$ of the remainder of the chromosomes are subjected to selection, and the rest are mutated.

We designated the parameter α as the weight regulator for the two objective functions: the accuracy, A, and the resolution, R, of location and slip speed detection. Hence, the selection function to be optimized is $F = \alpha \cdot A + (1-\alpha) \cdot R$.

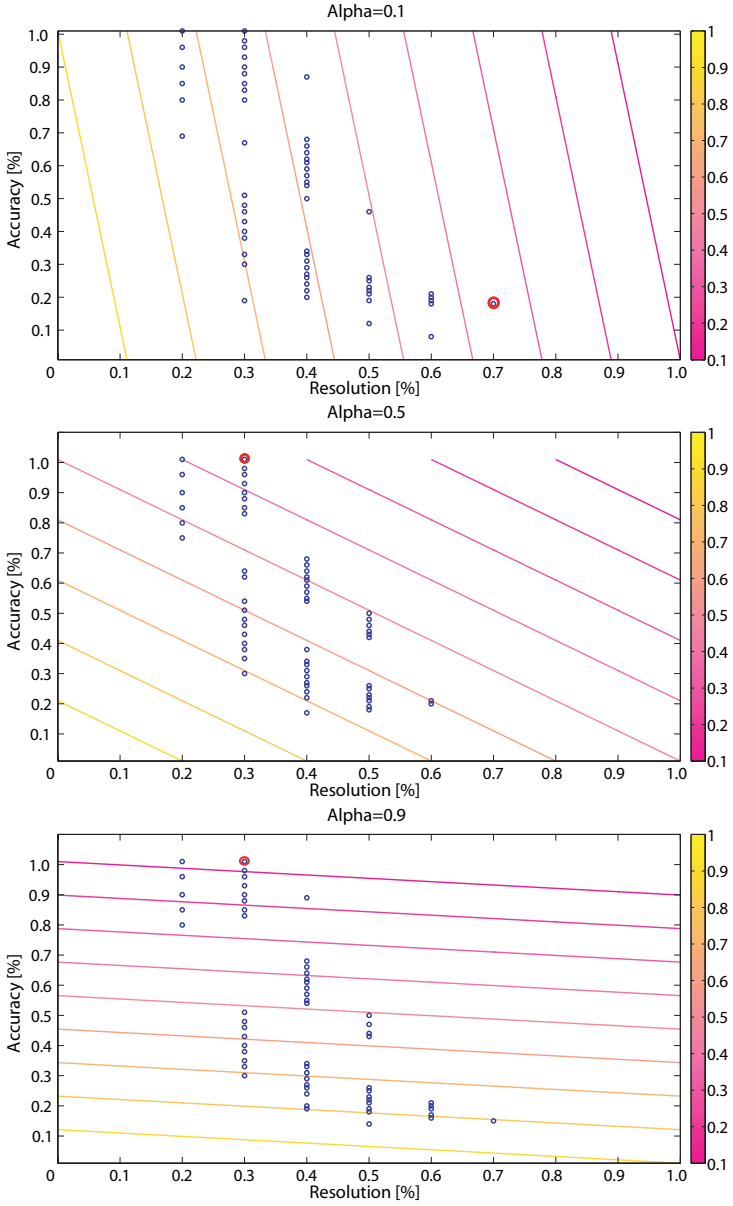

Figure 5.3: Search space of the evolutionary algorithm with respect to the two objective functions, accuracy in speed/position detection (Accuracy, A) and ridge distribution (Resolution, R). The search space is shown for skins with $\alpha = 0.1$ (A), $\alpha = 0.5$ (B) and $\alpha = 0.9$ (C). The blue circles represent local minimums, while the red circle represents the local minimum determined by the evolutionary algorithm. The lines represent the linear fitness function as a function of α.

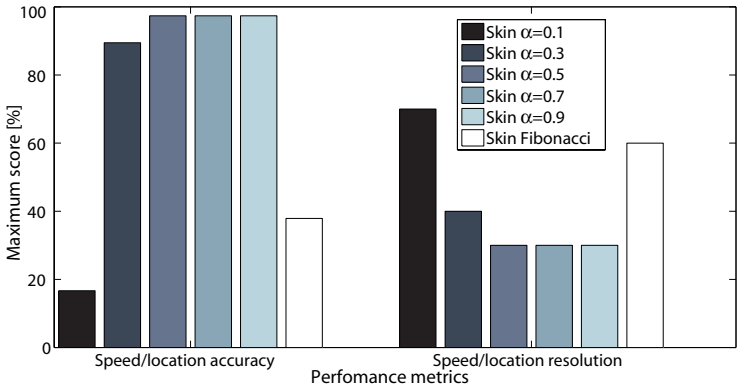

Figure 5.4: Score of six skin spacings configurations. The two groups represent the two criteria for the selection of the spacings: accuracy and resolution of detection of speed and position.

We ran the genetic programming algorithm for weights $\alpha = \{0.1, 0.3, 0.5, 0.7, 0.9\}$. For each weight, the GA was run for 96 hours. Figure 5.3 illustrates the search space of the evolutionary algorithm for three values of α: 0.1, 0.5 and 0.9. The axes represent the two objective functions : accuracy and resolution of speed and position detection. The lines in each plot represent the expression of the fitness landscape, depending on the resolution and accuracy, weighted by α. The color of the linear function represents the smooth fitness function, F. The blue circles denote the selected solutions during the runs of the evolutionary algorithm. The best solution over 96 hours for the arrangement of the spacings is represented by a red circle. A comprehensive description of the results of the GA is presented in Table 5.1. An additional skin was used as a reference for performance comparison, which is listed as the last entry in the table. The optimal skins generated by the GA are compared with the skin whose configuration of spacings is determined by the Fibonacci numbers, $\{5, 34, 21, 8, 3, 13\}$. This specific configuration yielded the highest score among other permutations of Fibonacci sequences on which the location and slip speed detection algorithm was applied. The sum of this skin's spacings is 84. The choice of the Fibonacci skin was motivated by properties associated with the Fibonacci series. According to one of these properties, within a restricted space, there exists a spatial arrangement that grants a high resolution of constitutive elements and, simultaneously, biologically-optimal distances between the elements [52]. The score for each objective function for the six skins is presented graphically in Fig. 5.4.

We chose to use a genetic algorithm in the determination of an optimal distribution of inter-ridge spacings for the following reasons: (1) The variables that are optimized are discrete; (2) A second order derivative for the spacing sequence does not exist; (3) The number of variables is unknown (we randomly select the number of spacings); (4) The score assigned to a skin is computed by an algorithm which uses noise from real data and determines statistically the accuracy in slip speed and position detection; (5) Although the fitness function is linear, as seen in the gradient in Fig. 5.3, it is difficult to determine analytically what kind of spacings sequence fulfills the local/global minimum in the

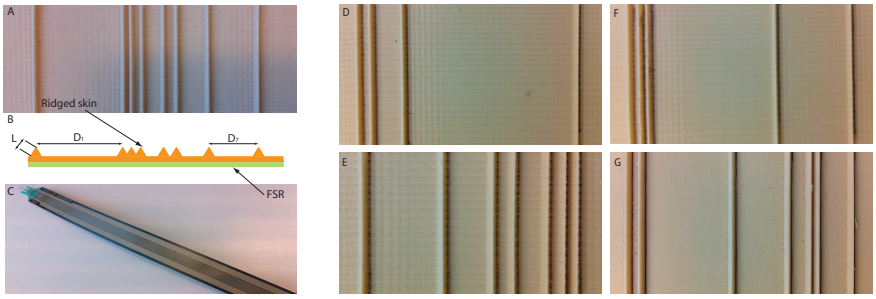

Figure 5.5: Real ridged skins. A-C. Skin components and fabrication. A. Example of silicone molded with triangular ridges. B. Transverse view of the layers of the skin. $L = 2.5$ mm. D_1 and D_7 are generic spacing values. C. Long force sensitive resistor. D-G. Example of the arrangement of ridges on the artificial skin. D. Skin with $\alpha = 0.5$. E. Skin with $\alpha = 0.3$. F. Skin with $\alpha = 0.1$. G. Fibonacci skin.

fitness space. This is due to the large number of possible spacing sequences ($\sum_{k=2}^{12} \frac{12!}{(12-k)!} = 1.3 \cdot 10^9$) and due to the criterion for the speed/position detection (e.g., high dissimilarity between consecutive time periods ratio in the force signal).

5.4 Experimental evaluation of artificial skins

We selected the three spacing configurations with the highest overall score, i.e., those corresponding to $\alpha = 0.1$, $\alpha = 0.3$ and $\alpha = 0.5$, as well as the Fibonacci configuration, for further experimental analysis of the artificial skins. In this section, the results of real experiments with artificial ridged skins based on these configurations are presented.

5.4.1 Artificial ridged skins

We built ridged artificial skins from silicone, which transduce surface events to a force sensor beneath (Figure 5.5A-C). The silicone patches were obtained from a mixture of the substance Neukasil RTV28 and the hardener Neukasil A140 (Altropol Kunsstoff GmbH) in a ratio of 10:1. The resulting paste was poured in an acrylonitrile butadiene styrene (ABS) mask built by rapid prototyping and cured by heat until the paste solidified. The transversal shape of the ridges was an equilateral triangle with the size of the side $L = 2.5$ mm, as described in [46]. The thickness of the pad onto which the ridges were affixed was 1 mm. As an active sensing element we used one FSR long sensor (Interlink Electronics), placed underneath the silicone patch. The FSR sensor has a sensitivity range of 100 g to 10 kg. The components are not expensive, and the construction process makes the skin sample easy to replicate. Figure 5.5D-G depicts four skin samples corresponding to $\alpha = 0.1$, $\alpha = 0.3$, $\alpha = 0.5$ and the Fibonacci skin.

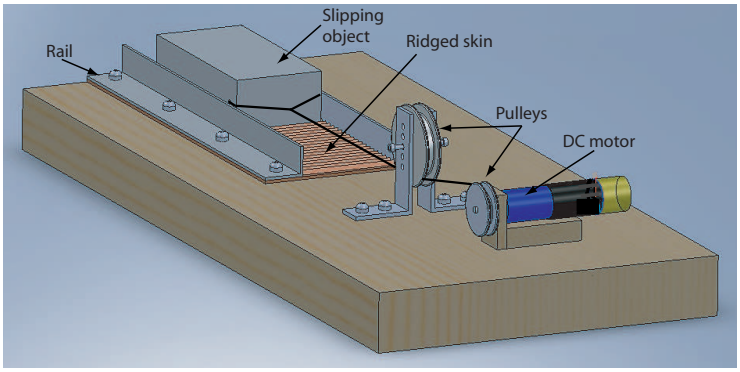

Figure 5.6: Experimental platform. The artificial skin is mounted on a wood platform. An object slips across the artificial skin, being driven by a DC motor along a pair of rails.

5.4.2 Experimental platform and procedure

The four artificial skins were evaluated using the experimental platform shown in Fig. 5.6. The artificial ridged skin was screwed on the platform under a pair of rails. A rectangular metal object of $25 \times 45 \times 90$ mm size was horizontally sliding across the skin, along the two rails. The object was dragged by a DC motor (Faulhaber DC-Micromotor 2642), driven by a speed controller (Atmel ATmega328P AVR microcontroller) through a non-deformable wire. The speed controller was implemented in Atmel AVR Studio to keep the angular velocity of the motor constant. A transparent acrylic bar was placed on top of the platform, having its inner ceiling at a height 35 mm from the surface of the platform. The bar inhibited vertical motion of the object as the object transversed a ridge while sliding. The bar had imprinted equidistant gratings to calibrate both the initial position of the object at the beginning of each experimental session and the images/videos of a Sony Cyber-shot DSC-T9 camera that monitors all experiments from atop. The entire platform was placed on a layer of foam and bubble sheet in order to remove extraneous environmental vibrations.

Data from the FSR sensor placed beneath the silicone patch was collected at a sampling rate of 400 Hz by a PC acquisition card (PC-Card-DAS16/16, Measurement Computing) and pre-processed by Tracer software. The experimental object was sliding on top of the skins at four speeds: 20, 40, 60 and 80 mm/s. For each artificial skin and each experimental slip speed, we conducted eight slip trials (128 trials in total). Video data was recorded and the object was tracked offline using the video analysis and modeling tool, Tracker [23]. Raw signals recorded from all four skins as the object slipped at 20 mm/s are presented in Figure 5.7. In this figure, the signal characteristics reveal high peaks associated with ridges that occur following large inter-ridge spacings and reduced amplitude for peaks associated with ridges that are preceded by reduced inter-ridge spacings. Additionally, there are extraneous peaks which occur when the object's front edge hits the surface of the skin and there is a positive angle between the surface of the object and that of the skin.

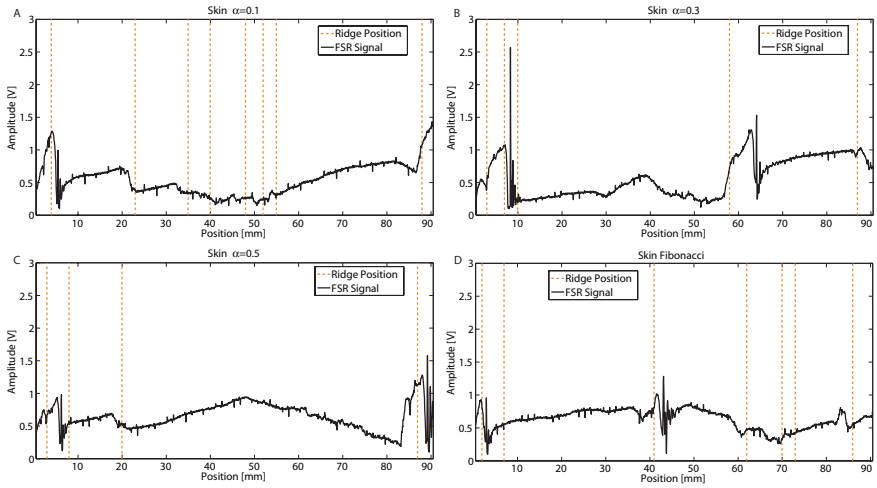

Figure 5.7: Raw signals and ridge distribution for four skins as the object travels at a speed of 20 mm/s. The skins are: A. $\alpha = 0.1$. B. $\alpha = 0.3$. C. $\alpha = 0.5$. D. Fibonacci Skin. The plots show the force valley and peak associated with each ridge. Additional valleys and peaks, which are not produced by the contact with a ridge, appear.

5.4.3 MMSE algorithm for detection of position and speed

As noted in Section IIIB, we developed an algorithm for detecting position and speed which we used in a simulated setting to identify high performing skins. However, this algorithm proved unsuitable for use on experimental data. This is because the simulated signal did not include models of a thorough dynamics between the object and the skin's ridges (e.g., size of the object, material of the skin, etc). Therefore we developed a new algorithm more appropriate to the real signals generated by the FSR. This new technique for determining the position and speed of the object was predicated on the assumption that there exists an affine mapping between any two data sets obtained from the same skin, modulo the presence of experimental noise. Thus, though a signal corresponding to a speed of 80 mm/s may be shifted and compressed in time when compared to a signal obtained at a lower speed, the relative geometry of these two signals should be similar. Experimentally, this assumption proved true over a wide range of speeds and over a large number of trials.

The geometric regularity of signals generated by a skin naturally suggests an algorithm that compares differing sets of data obtained from that skin. To this end, we devised a method in which portions of an unknown signal are compared systematically to a stored reference signal of known speed and spatial extent (see Fig. 5.8). Call this reference signal $r(t)$. The speed of the object that produced $r(t)$ is known; we shall refer to it as v_{ref}. Also, $r(t)$ is known to span the full spatial length of the skin.

The algorithm determines the speed and location of a slipping object at any time t, given a time window, $s(t)$, generated by that object from the time of initial slippage, t_0, to the present time t. Furthermore, we assume a finite range of possible speeds discretized by v_{step}: $\{v_{lower} \leq v \leq v_{upper} \mid v/v_{step} \in \mathbb{Z}\ \forall v\}$. For each possible speed v, our algorithm operates by assuming that $s(t)$ was generated at v, and interpolates the signal so that the density of data

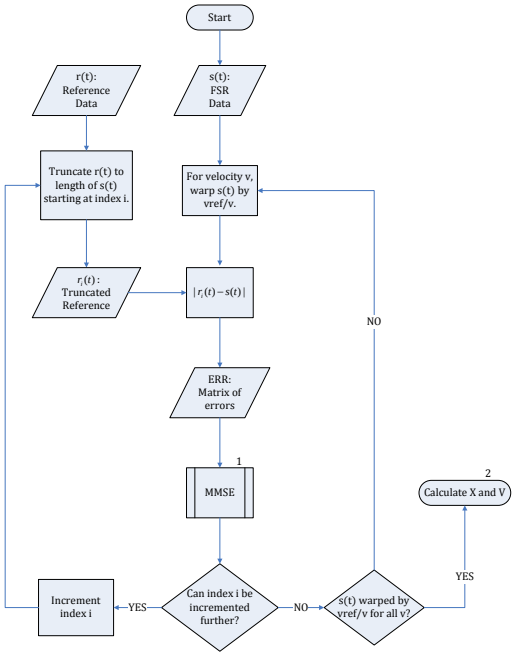

Figure 5.8: Algorithm for detection of position and speed from the real signal. The force signal is compared with a reference signal being stretched and compressed. For details regarding steps 1 and 2 see part IV section C.

points comprising $s(t)$ now matches that of $r(t)$. Alternatively, our algorithm compresses or dilates $s(t)$ in time by a "warping factor", $k = v_{ref}/v$, to match the density of data points observed in $r(t)$ given the assumption that $s(t)$ was generated at v. We shall refer to the warped signal as $s(kt)$. Having warped $s(t)$ by k, our algorithm slides $s(kt)$ over the length of $r(t)$ and at each point calculates a vector of errors, $\mathbf{e}$, equal to the difference between each point in $s(t)$ and the corresponding point in $r(t)$. The error vector $\mathbf{e}$ is stored as a row in a matrix ERR, whose rows correspond to $\mathbf{e}$ computed for different values of k. The arithmetic mean of $\mathbf{e}$ constitutes an unbiased estimator over the population of errors, and therefore we can calculate a single quantity, namely mean squared error (MSE) given by the expression $\text{MSE}(\bar{\mathbf{e}}) = \sigma^2/\text{size}(\mathbf{e})$, for each point of comparison between $s(t)$ and $r(t)$. For a given speed v, the index of the minimum value of MSE should correspond to the position of best fit for $s(t)$ in $r(t)$. Our algorithm thus implements a rudimentary form of minimum mean squared error (MMSE) estimation. Finally, repeating this process for each possible v and comparing the MMSE for each case to find the smallest overall MMSE, we determine both the location and speed of best fit.

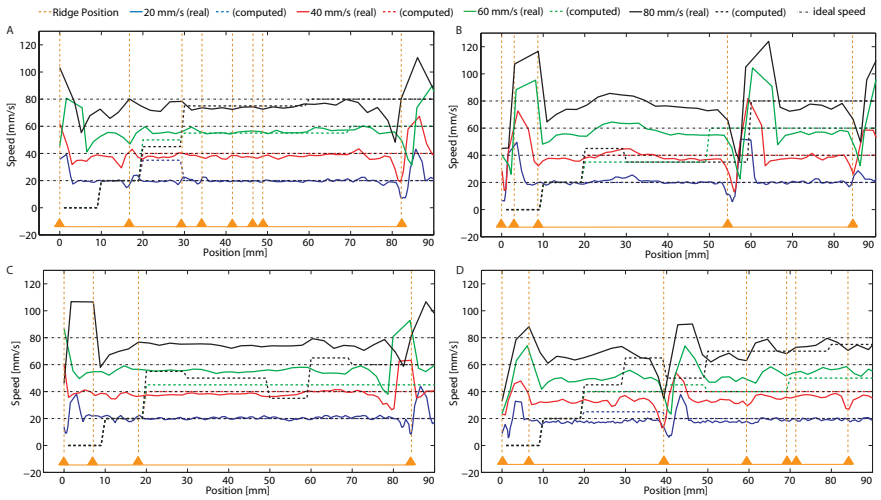

Figure 5.9: Real and computed speeds for four skins. The skins are: A. $\alpha = 0.1$. B. $\alpha = 0.3$. C. $\alpha = 0.5$. D. Fibonacci Skin. The object travels at a speed of 20 mm/s (blue color lines), 40 mm/s (red color lines), 60 mm/s (green color lines) and 80 mm/s (black color lines). The real speed is represented by a solid line, while the computed speed is shown with a dotted line. The vertical (orange) lines depict the positions of the ridges.

5.5 Results

Through our experiments, we have investigated the potential of artificial skins with non-uniformly distributed ridges to encode information about speed and position of a slipping object. In this section, we present the results of these experiments, highlighting slip signal characteristics and the performance of the analyzed skins.

5.5.1 Real speed fluctuation

As mentioned in the previous section, we tracked the object during its slip in all experimental trials. Although the speed of the motor was controlled to be constant, the velocity of the object, as extracted from the tracked data, fluctuated due to the dynamic interaction of the object with the compliant ridges. Figure 5.9 shows the ideal (control), real and computed speeds for one trial per speed per artificial skin. The trial depicted in the figure represents the one in which the computed speed error, calculated as the difference between the computed speed and the control speed, was minimal. In the case of the skin with $\alpha = 0.1$, the error between the real and the control speed was maximal at a position of 80 mm, having a mean of 5.27 mm/s and standard deviation of 0.27 mm/s. For the skin with $\alpha = 0.3$, the highest fluctuations in the real speed took place at positions of 50 and 80 mm. The means were 3.60 and 4.87 mm/s, with standard deviations of 0.42 and 0.29 mm/s, respectively. Relative to the skin with $\alpha = 0.5$, the highest fluctuation in the real speed took place at a position of 80 mm. The mean of the error was 15.00 mm/s, while the standard deviation was 0.23 mm/s. Regarding the Fibonacci skin, there were two main

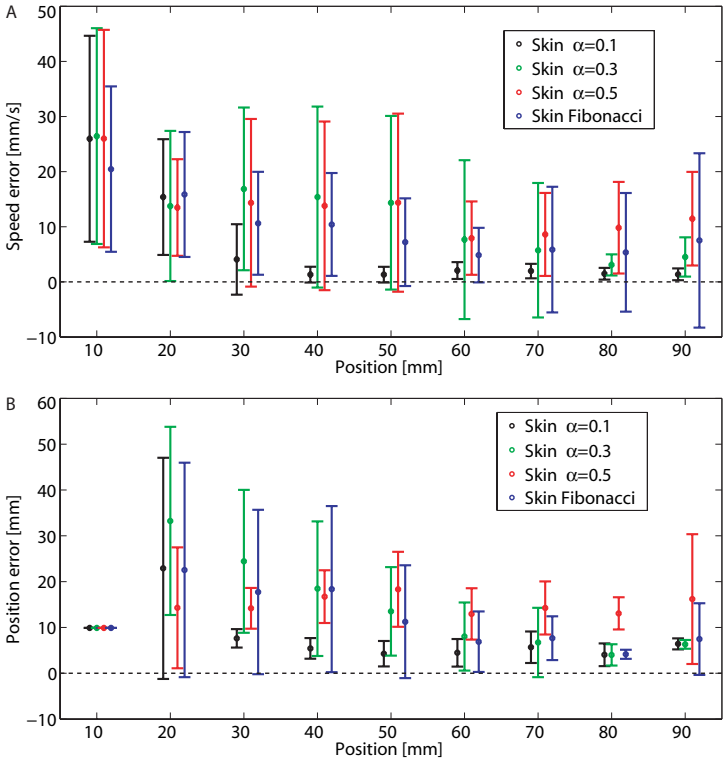

Figure 5.10: Velocity and position detection error for each skin. The morphology of the skin and the position of the object are two influential factors for the accuracy of the skins. The error bars represent the standard deviation.

peaks in the fluctuations of the real speed. At a position of 50 mm, the mean and standard deviation of this fluctuation were 6.30 and 2.43 mm/s, respectively. At a position of 70 mm, the mean and standard deviation of this fluctuation were 7.31 and 7.45 mm/s, respectively. The real velocity signal indicated that large fluctuations appear when the object hits a ridge that succeeds a large inter-ridge spacing. It also shows that the accuracy of the algorithm for slip speed and position detection decreases as the slip speed increases.

5.5.2 Influence of the ridge position on skin accuracy

We computed the detection error of the slip speed and position, for each individual skin, in order to investigate the effect of the ridge layout on the sensory information extraction. The results are depicted in Figures 5.10A and B, respectively. The errors were calculated as the absolute difference between the speed/position, computed by the MMSE algorithm, and the real speed/position measured from the video tracking, respectively. For each skin we applied single factor analysis of variance (ANOVA) to the speed detection errors across positions. Consequently, for each skin there existed significant differences in the slip speed errors across positions, with $F(8, 279) = 42.87$ and $p < 10^{-43}$ for the skin with $\alpha = 0.1$, $F(8, 279) = 9.58$ and $p < 10^{-10}$ for the skin with $\alpha = 0.3$, $F(8, 279) = 5.77$ and $p < 10^{-6}$ for the skin with $\alpha = 0.5$, and $F(8, 279) = 7.23$

and $p < 10^{-7}$ for the Fibonacci skin. The Tukey ad hoc test was performed subsequently. For each type of skin, the speed errors at position 10 mm were significantly larger than those at all other positions. In particular, in the case of the skin with $\alpha = 0.1$, the speed errors at position 20 mm were significantly larger than those at all other positions. For the skin with $\alpha = 0.3$, speed errors at position 70 mm were significantly lower than those at position 30 mm. Additionally speed errors at position 80 mm were significantly lower than those at positions 20 to 50 mm. Also, these errors recorded at position 90 mm were significantly lower than those at positions 30 and 40 mm. For the Fibonacci skin, the speed errors at position 20mm was significantly larger than those at positions 50 to 80 mm.

Similarly, single factor ANOVA applied to position detection errors confirmed that significant differences exist between these errors across all positions, with $F(8, 279) = 16.18$ and $p < 10^{-18}$ for the skin with $\alpha = 0.1$, $F(8, 279) = 25.17$ and $p < 10^{-28}$ for the skin with $\alpha = 0.3$, $F(8, 279) = 3.03$ and $p < 10^{-2}$ for the skin with $\alpha = 0.5$, and $F(8, 279) = 7.71$ and $p < 10^{-8}$ for the Fibonacci skin. According to the Tukey ad hoc test applied to the skin with $\alpha = 0.1$, the position errors at position 10 mm were significantly lower than these types of errors at position 20 mm, whereas these errors at position 20 mm were significantly larger than at all other positions. The same test applied to the skin with $\alpha = 0.3$ indicated that position errors at position 10 mm were significantly lower than those at positions 20 to 40 mm. Moreover, these errors at position 20 mm were considerably larger than those at positions 30 to 90 mm, errors at position 30 mm were considerably larger than those at positions 50 to 90 mm, errors at position 40 mm were considerably larger than those at positions 60 to 90 mm, and lastly, position 50 mm gave raise to considerably larger errors than those at position 80 mm. For the skin with $\alpha = 0.5$, there were lower position errors at position 10 mm than at positions 40, 50 and 90 mm. In the case of the Fibonacci skin, there were lower position errors at position 10 mm than at positions 20 mm. Furthermore, these errors at position 20 mm were considerably larger than those at positions 50 to 90 mm, errors at each positions of 30 mm and 40 mm were considerably larger than those at positions 60 to 90 mm. These results indicate two factors that may influence the accuracy of detecting slip speed and position. One is the number of samples that are available for computing speed and position. The errors in detecting either speed or position were generally smaller as the number of signal samples increases. This factor is analyzed in more detail in a following subsection. A second factor may be the distribution of the ridges on the artificial skin. As results from the Tukey tests and shown in Figures 5.10AB, large errors in speed and position detection appeared in the skin with $\alpha = 0.1$ at position 20 mm, which follows a region where no ridges are present. Similarly, large speed and position errors were more predominant between positions 20 and 50 mm of the skin with $\alpha = 0.3$, where no ridge-like feature was present, than between positions 60 and 90 mm. Notably for the skin with $\alpha = 0.5$, large position detection errors occurred between positions 40 and 50 mm. Given that the largest inter-ridge space lies between approximately 20 and 80 mm, the absence of large speed or position errors in the region 50 to 80 mm might be attributed to the force fluctuations, which consistently appeared after the object hits the flat surface of the skin with its front edge at an angle. In the case of the Fibonacci skin, large speed and position errors are found more predominantly between positions 20 and 40 mm

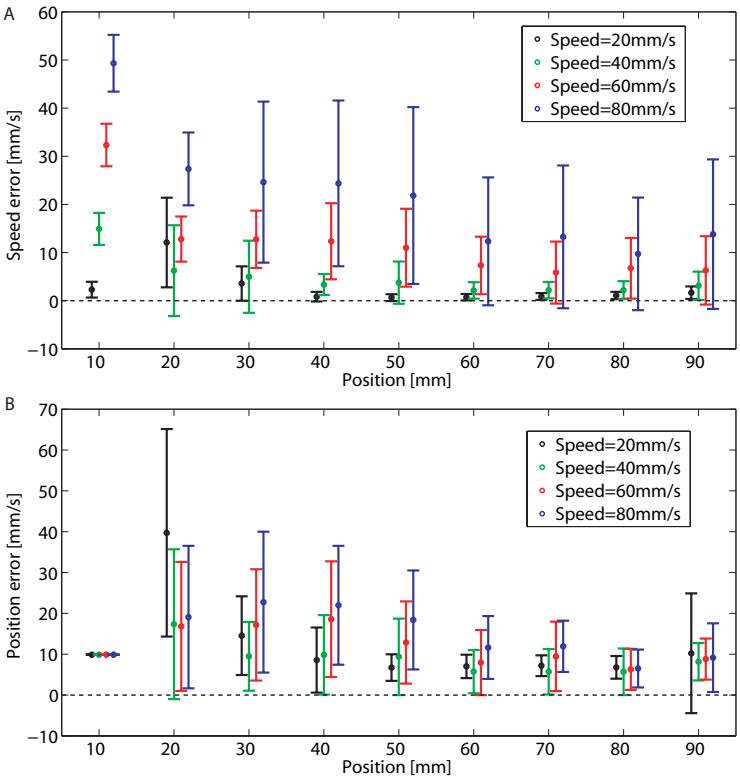

Figure 5.11: Velocity and position detection error for each velocity. Errors decreased as the slip speed decreased and as more samples of the force signal became available. The error bars represent the standard deviation.

than between positions 50 and 90 mm, where the ridges are more dense.

5.5.3 Influence of the speed on skin accuracy

The detection error of slip speed and object position for all skins at each speed is depicted in Figures 5.11A and B, respectively. The errors are calculated as the absolute difference between the speed/position, computed by the MMSE algorithm, and the real speed/position, measured from the video tracking. Firstly, the influence of the speed values, regardless of the slipping object position, was analyzed. Single factor ANOVA applied over the speed error measurements of all four types of skins across the speeds yielded $F(3, 1148) = 179.36$ and $p < 10^{-94}$, indicating that there is a significant difference between the speed detection performance depending on the slip speed value. The Tukey ad hoc method showed that significant differences in speed detection performance appear across speeds. In particular, there are significantly larger speed errors at speed 40 mm/s than those at all other speeds. Similarly, speed errors are considerably larger at speed 30 mm/s than those at all other speeds. Similarly, single factor ANOVA applied over the position error measurements of all four types of skins across the speeds yielded $F(3, 1148) = 10.44$ and $p < 10^{-6}$. The Tukey ad hoc test showed that position errors at speed 20 mm/s were significantly lower than those at all other speeds. Also, there were significantly lower position errors present at speed 30mm/s than at speed 40mm/s. In summary, the results show that the errors in speed detection increase with the slip speed.

5.5.4 Influence of slip distance on skin accuracy

We investigated the variation of error as the object slip distance increases. The absolute speed and position errors were computed over the distances $10-30$ mm, $40-60$ mm and $70-90$ mm and both single factor ANOVA and Tukey test was applied across these three distances. ANOVA applied to speed errors regardless of the type of skin and speed yielded $F(2, 1149) = 87.65$ and $p < 10^{-35}$, while ANOVA applied to position errors in the same conditions produced $F(2, 1149) = 50.07$ and $p < 10^{-20}$. Tukey ad hoc test in both cases indicated that the errors over the first third portion of the skin were significantly larger than the errors obtained over the rest of the skin, and the errors over the second third of skin were larger than the errors resulted from the slip over the third portion of the skin. This analysis applied for each type of skin showed that there exist differences in speed errors over the three distances. ANOVA's results were $F(2, 285) = 71.28$ and $p < 10^{-25}$ for skin with $\alpha = 0.1$, $F(2, 285) = 26.05$ and $p < 10^{-10}$ for skin with $\alpha = 0.3$, $F(2, 285) = 9.66$ and $p < 10^{-4}$ for skin with $\alpha = 0.5$ and $F(2, 285) = 19.05$ and $p < 10^{-7}$ for the Fibonacci skin. Regarding the Tukey test, the speed errors were considerably larger over the first distance than over the second and third distances, for the skins with $\alpha = 0.1$, $\alpha = 0.5$ and Fibonacci skin, whereas for the skin with $\alpha = 0.3$, speed errors were significantly larger on the first distance than all other distances, and errors were larger on the second distance than on the third distance. The position errors differed significantly over the three distances as well. ANOVA's results were $F(2, 285) = 27.18$ and $p < 10^{-10}$ for skin with $\alpha = 0.1$, $F(2, 285) = 43.61$ and $p < 10^{-16}$ for skin with $\alpha = 0.3$, $F(2, 285) = 3.77$ and $p < 0.01$ for skin with $\alpha = 0.5$ and $F(2, 285) = 14.37$ and $p < 10^{-5}$ for the Fibonacci skin. For the skin

with $\alpha = 0.1$, the position errors on the first distance were significantly larger than on the other two distances, according to the Tukey test. Furthermore, for the skin with $\alpha = 0.3$ and Fibonacci skin, the position errors were larger on the first distance than the other two distances, while these types of errors were also larger on the second distance than they were on the third distance. Finally, the position errors on the first distance of the skin with $\alpha = 0.5$ were significantly lower than those on the second distance. In conclusion, as the distance traveled by the object increases, errors tend to decrease due to the accumulation of available information provided by the FSR signal. In particular for the skin with $\alpha = 0.1$, at furthest 30 mm, most of the speed errors were below 4 mm/s, whereas the position errors were below 7 mm, regardless of the traveling speed. In the case of the skin with $\alpha = 0.1$, most of the speed and the position errors were lower than 8 mm/s and 8 mm, respectively, at furthest 60 mm. Regarding the skin with $\alpha = 0.5$, both speed and position errors exceeded a threshold of 10 mm/s and 10 mm for all distances. Lastly, for the Fibonacci skin, the speed errors were below 10 mm/s at furthest 30 mm distance from the slip starting point, whereas the position errors were below 10 mm at furthest 60 mm.

5.5.5 Artificial skins overall comparison

For each skin we computed the normalized root-mean-square deviation (NRMSD) of the errors in velocity and position detection. The results are summarized in Table 5.2. The NRMSD indicates that overall, the skin with $\alpha = 0.1$ performed better than the other three skins. Additionally, the average NRMSD values of speed and position detection over the four skins, suggest that slip speed detection is slightly more accurate than object location detection. In Fig. 5.12, the speed and position errors for the skin with $\alpha = 0.1$ are shown. Single factor ANOVA applied to the errors detected at the four velocities for this skin yielded $F(3, 284) = 13.26$ and $p < 10^{-7}$. According to the Tukey ad hoc test, significant error differences occur between slip at a speed of 20 mm/s and speeds of 60 and 80 mm/s, as well as between slip at a speed of 40 mm/s and speeds of 60 and 80 mm/s. Position errors are not significantly different, irrespective of the speed, with ANOVA results of $F(3, 284) = 1.94$ and $p = 0.12$.

5.6 Discussion

The organizing principle of this paper is the concept that sensory information can be augmented by intelligent design, such as novel arrangements of morphological features. Using one force sensor, it is possible to extend the sensing range such that, beyond implicit force information, slip occurrence, speed and position of a slipping object can be detected. We approached the design of the tactile sensor from a practical perspective. First, we simulated a force signal for ridged skins accounting for the presence of noise, the minimal inter-ridge distance found to generate a relatively distinctive peak (e.g., 3 mm), and a skin length constraint on the scale of a robotic/prosthetic hand. The simulated force signal was constructed using a simple model of the interaction between the slipping object and the ridges; an exponential peak in the signal was generated whenever the object's front end encountered a ridge. The modeling of the force signal excluded considerations about the geometrical or material properties of

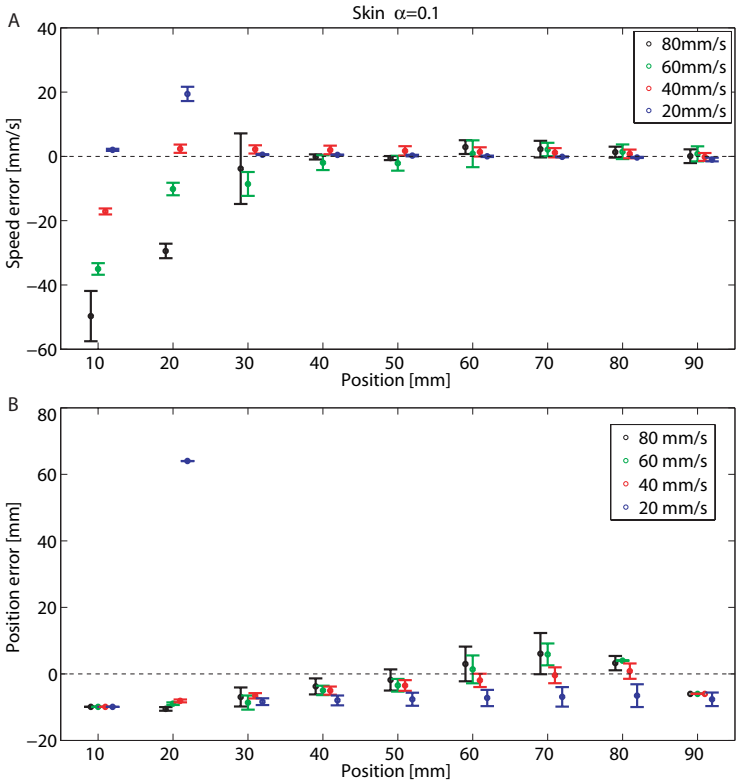

Figure 5.12: Velocity and position detection error for the skin with $\alpha = 0.1$. This skin performed the best among the four investigated skins. The error bars represent the standard deviation.

the object that would add to the dynamics of the interaction. This simplification is a cause of the different rankings of skin performance produced by simulation and real experiments. We expect that the optimal distribution of ridges on the skin surface as selected by the evolutionary algorithm changes depending on the number of runs of the genetic algorithm or depending on changes to the algorithm for detecting slip speed and location. For instance, future improvements to the MMSE algorithm may consider making predictions of the current speed and position by considering the detected values of these two parameters at multiple previous time points during the object's slip. Furthermore, the overall skin sensitivity, currently limited by the operational range of the FSR, can also be improved by replacing the FSR with a sensor which exhibits a wider responsiveness to pressure stimuli. However, the present work aims to provide a novel concept and a basic methodology for exploiting morphology for the enrichment of sensory information with minimal resources, rather than providing the best actual solution for an enhanced tactile sensor. The latter is in the hands of the designer for a given application; there are many possible permutations of materials, shapes and algorithms, all of which may contribute to the quality of the results depending on the specific scenario.

In slip scenarios occurring in uncontrolled conditions, slip speed is unlikely to be constant. Although in our experimental procedure the speed of the object was controlled by the DC motor, the slip speed was also modulated by the morphology of the skin. Therefore, during an experimental trial, the slip speed did not remain constant. Usually the speed decreased when the object encountered a ridge and subsequently increased having been released from the ridge's surface. For each control speed, Fig. 5.13 shows a sequence of nine means and standard deviations of the speed real and computed speed along nine positions, from 10 to 90 mm with a discrete step of 10 mm. Despite the fluctuations of the real speed, the detection algorithm managed to track the changes of the slip speed, as seen in the values of the means and standard variations of the computed speed in Fig. 5.13.

In the experimental procedure, the object always starts slipping from some initial position on the skin. However, we do not use this information in the MMSE algorithm to detect slip and position. The implementation of the algorithm is suitable for the slip speed and object position detection, regardless of the starting position of the slip.

Table 5.2 may suggest that skin performance increases with the number of ridges. However, it is apparent that taken to the extreme case in which we have a maximum number of ridges, i.e., a linear distribution of ridges with an inter-ridge distance equal to the minimum allowed, the performance will be extremely poor at least for position detection, since the profile of the transduced signal would presumably lack distinguishable features. Alternately, the performance depends on the arrangement of the ridges that gives rise to unique distinguishable features of the force signal during the interaction with the object.

The Fibonacci series is a pattern often occurring in nature. Biological studies [52] cite the arrangement of the leaves, sepals or florets in plants as examples and explain it as a pattern which is optimized to fit a maximal number of these plant elements in a constraint space. A similar formulation of space arrangement optimality may be attributed to the design of the artificial ridged skin; therefore we chose the Fibonacci skin as a reference skin for comparison. The results of our experiments show that the Fibonacci skin performed reasonably

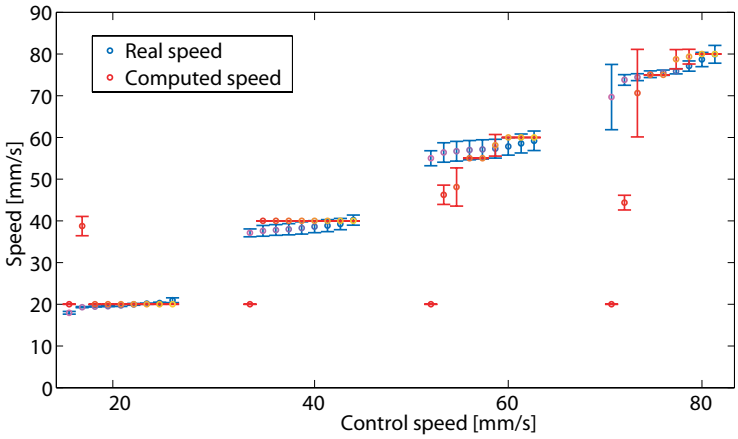

Figure 5.13: Real and computed velocity with respect to the control velocity for the skin with $\alpha = 0.1$. A. The ridges affect the velocity of the slipping object so that the real speed is not constant. B. The MMSE algorithm was able to detect non-constant speeds.

well. However, we speculate that a fundamental difference in the computational process and fitness function between the biological entities and the artificial transduction technique is the reason that the Fibonacci skin did not perform significantly better than the other skins.

In addition to the method outlined in the Section IV C, two alternate strategies for determining speed and location from the sensor data were investigated. The first, cross-correlation, produced consistently less accurate results than the MMSE algorithm and was therefore discarded as a candidate strategy for analyzing the data. The second method investigated was dynamic time warping (DTW). DTW is advantageous in the sense that it provides a metric for determining the similarity of two time varying signals independent of non-linear variations in the time dimension. Thus, our previously held assumption regarding constant speed could be relaxed. However, the time required to process data using DTW proved prohibitive. Therefore, this strategy too was rejected as a viable candidate. Implementing DTW in a streamlined and time-efficient way that meets the requirements of our problem remains an open avenue of future research.

5.7 Conclusion and Future Work

The concept presented in this paper is the augmentation of sensory information with reduced resources. This has been achieved by exploiting morphological cues, such as non-homogeneously distributed triangular ridges. Thus, using one force sensor, it was possible to extend the sensing range such that, beyond implicit force information, slip occurrence, speed and position of a moving object can be detected. The paper provides a basic technique for engineering tactile sensors based on this approach. In the future, we intend to extend the outlined principles to a 2D implementation of morphologically enhanced tactile sensing. We will also investigate various algorithms for information extraction that are

biologically inspired in order to gain more insight into designs generated by biological processes. The combination of morphologically-enhanced skins with distributed tactile arrays is another promising future strategy for increasing the bandwidth of sensory information.

α	***Skin spacings***	***Ridge absolute position***	***Max(A)***	***Max(R)***	***Min(F)***
0.1	$19, 12, 5, 8, 4, 3, 33$	$0, 19, 31, 36, 44, 48, 51, 84$	0.1667	0.7	0.3539
0.3	$4, 3, 48, 29$	$0, 4, 7, 55, 84$	0.8947	0.4	0.4663
0.5	$5, 12, 67$	$0, 5, 17, 84$	0.9737	0.3	0.3605
0.7	$7, 64, 13$	$0, 7, 71, 84$	0.9737	0.3	0.2211
0.9	$6, 20, 58$	$0, 6, 26, 84$	0.9737	0.3	0.0937
Fibonacci	$5, 34, 21, 8, 3, 13$	$0, 5, 39, 60, 68, 71, 84$	0.3789	0.6	–

Table 5.1: Results of GA.

	NRMSD		
Skin Type	***V[%]***	***P[%]***	***Avg. [%]***
$\alpha = 0.1$	0.21	0.15	**0.18**
$\alpha = 0.3$	0.32	0.24	**0.28**
$\alpha = 0.5$	0.38	0.20	**0.29**
Fibonacci	0.26	0.22	0.24
Avg. [%]	**0.29**	**0.20**	

Table 5.2: Normalized root-mean-square deviation (NRMSD) of speed (V) and position(P).

Chapter 6

Design and Evaluation of a Multi-Modal Haptic Skin Stimulation Apparatus

Haptic information artificially generated by a dynamical 2D contact with a skin

Chapter 6 is a preliminary study on the design of a force and slip speed haptic device and on the potential information that its stimulation signals could carry. Human grasping and manipulation are facilitated by cutaneous mechanoreceptors that provide information about contact location, pressure, and events such as making and breaking contact. A challenge in designing haptic feedback devices for the wearer of a prosthetic hand is simultaneous display of multiple types of haptic information. We present the preliminary design and evaluation of an apparatus for relaying multi-modal haptic information. The apparatus moves a set of contact points tangentially over the skin at a controlled speed, with controlled normal force. We apply this stimulus to an artificial skin instrumented with an embedded accelerometer, and characterize the resulting signals. Vibration frequency increases with applied normal force and tangential speed, whereas vibration amplitude increases with normal force and depends on skin properties. The results indicate that different forces and speeds can, under some conditions, be discriminated using vibration signals alone. Accurate identification of speeds is provided by series of vibration events that depend on the spatial distribution of contact points. This study motivates future work to perform human perception studies and create a wearable haptic display for prosthetics based on this concept.

[5]Parts of the material in this chapter previously appeared in: Dana D. Damian, Alejandro Hernandez Arieta and Allison M. Okamura (2011),“ Design and Evaluation of a Multi-Modal Haptic Skin Stimulation Apparatus”, *International Conference of the IEEE Engineering in Medicine and Biology Society (EMBC)*

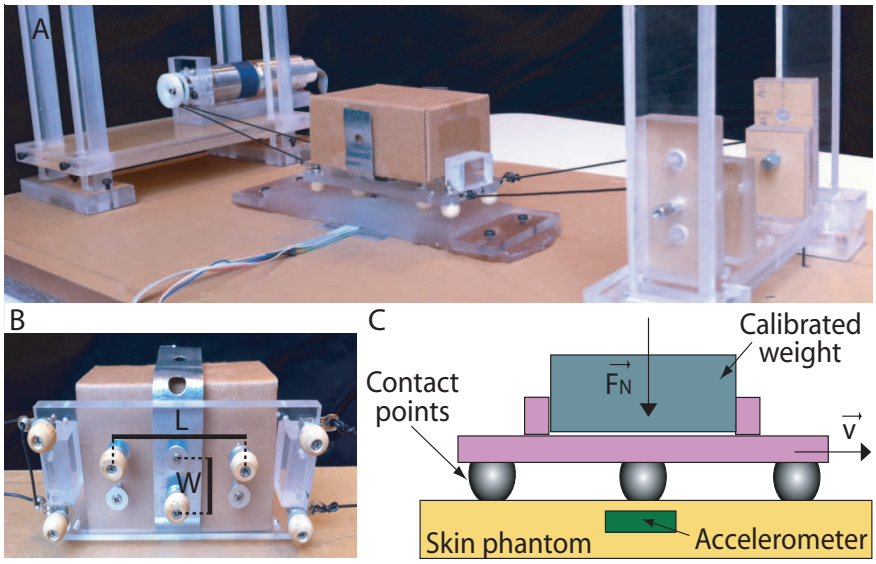

Figure 6.1: Experimental apparatus. A. Haptic device and artificial skin. B. Detail of the bead structure. C. Schematic of the experimental apparatus. A speed v and a normal force F_N are applied at three contact points.

6.1 Related Work

Human grasping and manipulation is enabled by a sensorimotor system that is able to access multi-modal haptic information in the human hand [10]. Dexterous manipulation tasks, such as slippage control and active exploration, in which the contact conditions between the hand and an object change, are expressed in complex spatial cues and forces acting on the skin. Pressure, stretch, and vibrations on the skin result from changing contact conditions, and elicit responses from various skin mechanoreceptors [77]. People wearing hand prostheses are deprived of contact/location cues and forces during object manipulation. They have to rely to a high extent on visual feedback, leading to fatigue and frustration [9].

Relaying spatial cues and forces through a haptic device could enable the prosthesis wearer to access rich, useful information about the changing state of contact between the artificial hand and a grasped or manipulated object. Such feedback may help the prosthesis wearer grasp, manipulate, and identify objects. As a result, grasp stability and dexterous manipulation can be achieved, while releasing some of the attention to vision currently needed.

In prosthetics research, haptic feedback has been used mostly to convey force during stable grasp. Vibrations have been extensively used as a means to display information about grasp force, e.g., [30, 79]. Force feedback has also been transmitted through mechanisms that push on the skin, e.g., [102, 116]. Conventional grasp force displays lack contact motion cues, but vibration signals elicited from force exertion can convey significant information about changing contact conditions and spatial distribution of surface features. This has been previously exploited in virtual environments and teleoperators, e.g., [84, 113]. Haptic devices that render contact location, slip, and shear have been developed

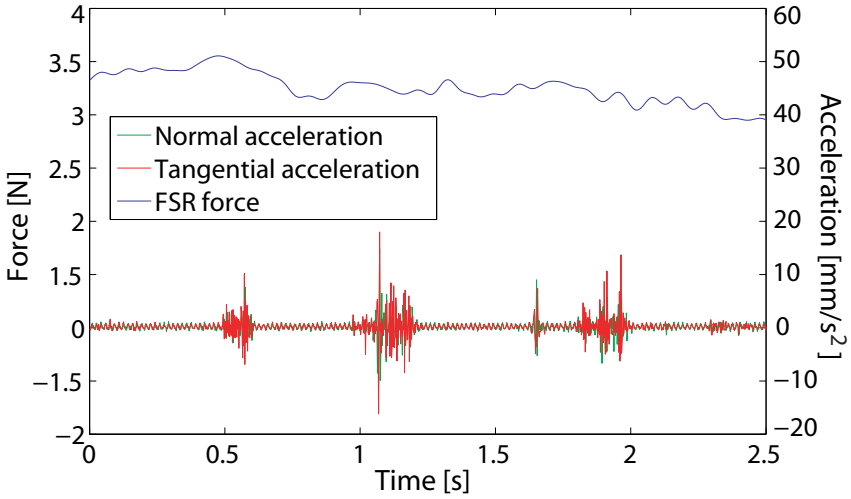

Figure 6.2: Raw signals recorded by the artificial skin. Force and acceleration on tangential and normal directions when contact points move at a speed of 18mm/s and carry a weight of 3N along the skin. The series of three vibrations correspond to three contact points distributed on a moving bar.

to display changing contact conditions [64], but existing devices are impractical for prosthesis wearers.

As a preliminary step toward designing a wearable haptic device that relays information about contact conditions, we present an apparatus able to generate spatial and force cues through moving contacts applied to the skin. The control parameters of the apparatus are the speed of a set of discrete contact points moving tangentially over the skin and a force applied orthogonally to the skin. The choice of the control parameters is motivated by human studies showing that grip forces are regulated by load forces [76], and tangential resistive forces convey texture information [87]. Recent work [42] found evidence that relaying information about slippage speed to prostheses users improved their ability to grasp a slipping object. In this paper, we describe the features of the signals generated by a multi-modal haptic apparatus and acquired by an instrumented artificial skin.

6.2 Experimental apparatus and procedure

6.2.1 Experimental apparatus

Haptic apparatus

The haptic apparatus, depicted in Fig. 6.1A, controls tangential speed and normal force applied to an artificial skin. An acrylic bar moves horizontally along the surface of the artificial skin and carries calibrated weights on top. Underneath the bar, wooden beads are mounted (Fig. 6.1B); the three beads in the center of this structure contact the artificial skin, and the others (of lower height) are placed at the corners of the structure for stability purposes. The three contact points are arranged in a zig-zag pattern, with $L = 48$mm and

$W = 15$mm, in order to maintain stability and equal distance to the center line of the artificial skin. Calibrated weights can be placed on top of the bar. A DC motor (Faulhaber DC-Micromotor 2642), driven by a speed controller (Atmel ATmega328P AVR microcontroller), drags the bar along the artificial skin at a constant speed. At its other end, the bar is connected to two counter-weights through non-deformable wires laid over two pulleys.

Artificial Skin

An artificial skin is used in this study as a surrogate for human skin. The skin (150x50x15mm) was built from plastisol (M-F Manufacturing), has a flat surface and was equipped with two sensors: an accelerometer (Freescale MMA7361L 3-Axis Accelerometer 1.5/6g, 400Hz (XY) and 300Hz (Z) bandwidth) and a force sensitive resistor (FSR) (40x40mm, Interlink Electronics). The accelerometer was placed 2mm beneath the surface of the skin, whereas the FSR was placed under the skin. The force and acceleration recorded by the two sensors are shown in Fig. 6.2.

6.2.2 Experimental procedure

The haptic apparatus controls two parameters: the speed of the contact points moving on the skin and the normal force applied to the skin through the calibrated weights. The contact points move at one of five possible speeds: 9, 12, 15, 18 and 21mm/s. Calibrated weights of 1, 3, 4 and 5N were used to apply normal force. At the beginning of an experiment, a speed command was sent to the microcontroller and a weight was manually placed on top of the bar. This paper focuses on the vibrations measured by the accelerometer; the FSR sensor was used to monitor the normal force applied through the weights. Data from the two sensors was collected at a sampling rate of 600Hz by a PC acquisition card (PC-Card-DAS16/16, Measurement Computing). A discrete vibration event occurs each time a contact point passes over the accelerometer. Both individual vibrations (associated with one contact point) and series of three vibrations (corresponding to three contact points) were analyzed. In order to characterize individual vibration frequency, weights of 1, 3 and 5N were used for applying normal force, whereas the contact points were moving at all experimental speeds. Individual vibration amplitude was measured under same speed conditions, while normal force was applied by weights of 3, 4 and 5N. Series of vibration events was analyzed in experiments in which weights of 3, 4 and 5N and all speeds were applied. The Euclidean norm of accelerations in the normal and tangential directions was used in subsequent analysis of the vibration signals. The peak frequencies of the individual vibration signal were extracted using the Welch power spectral estimation with an underlying Hamming window of 128 samples. The peak-to-peak amplitude was measured after smoothening the vibration signal with a Savitzky-Golay filter and applying a bandpass filter of 60 to 290Hz. The period between vibration events was determined by squaring the acceleration signals, applying a 2Hz FIR lowpass filter and Fast Fourier function. Seven trials per speed per weight (140 trials) were conducted.

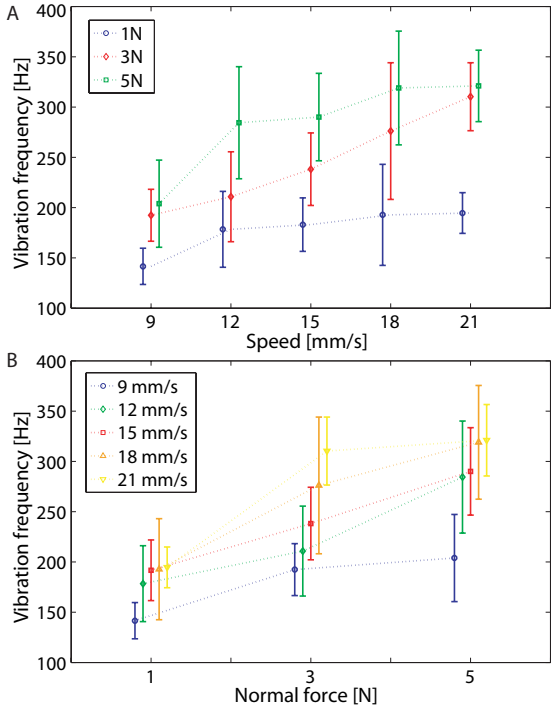

Figure 6.3: Vibration frequency with respect to tangential speed (A) and normal force (B). The frequency of vibrations increases with both the tangential speed and normal force.

6.3 Results

Individual vibrations

Vibration frequency was computed for each vibration event in each trial, and is plotted with respect to tangential speed of the contact points (Fig. 6.3A) and normal force applied to the skin (Fig. 6.3B). The results show that the vibration frequency increases monotonically and linearly with the tangential speed and normal force. For each speed, there was a significant difference in vibration frequency for normal forces of 1, 3 and 5N, as shown in Table 6.1A. Single factor analysis of variance (ANOVA) with three levels, corresponding to the three forces, yielded $p < 0.01$ for each condition shown in Table 6.1A. Tukey post hoc method indicated that significant differences appear between forces of 1 and 5N for each speed. ANOVA revealed a difference in vibration frequency for the tangential speeds of 9, 15 and 21mm/s at normal forces of 1, 3 and 5N. Each of the conditions yielded $p < 0.01$ and are shown in Table 6.1B. Tukey post hoc method found that significant differences appear between speeds of 9 and 21mm/s.

Figure 6.4 shows vibration amplitude with respect to tangential speed and normal force. The plots reveal trends according to which vibration amplitude linearly depends on the normal force and has a nonlinear dependence on the tangential speed. A single-factor ANOVA with three levels, corresponding to normal forces of 3, 4 and 5N, yielded significant differences ($p < 0.01$) for tan-

gential speeds of 12 and 21mm/s (Table 6.2A). Furthermore, Tukey post hoc method revealed that normal forces of 3 and 5N can be distinguished for these two speeds. ANOVA with five levels, corresponding to all experimental speeds, showed that these speeds can be differentiated for normal forces of 3, 4 and 5N, according to $p < 0.01$ for each of the experimental conditions. Details are provided in Table 6.2B. Tukey post hoc test indicated that significant differences appear between speeds of 9 and 15mm/s, and between speeds of 15 and 21mm/s,

A

Tangential speed	***p-value for comparison of 1, 3 & 5N***
$9mm/s$	0.006
$12mm/s$	0.003
$15mm/s$	0.0009
$18mm/s$	0.005
$21mm/s$	< 0.0001

B

Normal force	***p-value for comparison of 9, 15 & 21mm/s***
$1N$	0.001
$3N$	< 0.0001
$5N$	0.0002

Table 6.1: P-values from ANOVA for the vibration frequency as a function of tangential speed (A) and normal force (B).

for each normal force investigated.

Vibration event series

The series of vibration events provides spatial cues resulting from the distribution of contact points on the moving bar. An envelope applied to the raw signal featured low frequencies in the range of $0.3 - 1.0$Hz and was found to depend only on the tangential velocity (Fig. 6.5). Single-factor ANOVA with five levels, corresponding to all five speeds, yielded $p < 0.0001$ for each normal force. Tukey post hoc test found that significant differences occur between all tangential speeds. The ideal time between vibration events can theoretically be computed as the ratio of contact point distribution ($L/2 = 24$mm) to tangential speed. With respect to this ideal period, the normalized root mean squared deviation (NRMSD) for each speed is: 9% for 9mm/s, 9% for 12mm/s, 6% for 15mm/s, 10% for 18mm/s and 7% for 21mm/s.

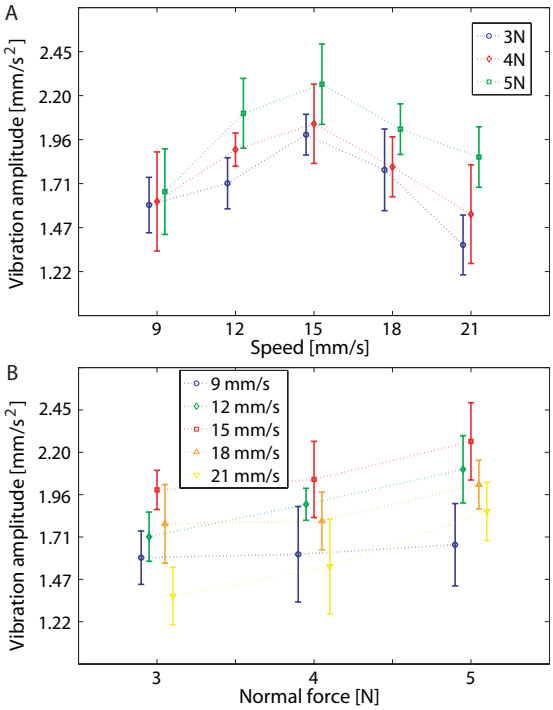

Figure 6.4: Vibration amplitude with respect to tangential speed (A) and normal force (B). Vibration amplitude varies linearly with the normal force and is influenced by the elastic features of the artificial skin.

A

Tangential speed	***p-value for comparison of 3, 4 & 5N***
$12mm/s$	0.001
$21mm/s$	0.002

B

Normal force	***p-value for comparison of 9, 12, 15, 18 & 21mm/s***
$3N$	< 0.0001
$4N$	0.002
$5N$	0.0001

Table 6.2: P-values from ANOVA for the vibration amplitude as a function of tangential speed (A) and normal force (B).

6.4 Discussion and conclusions

In this paper we presented a conceptual mechanical design and an objective experimental characterization of an apparatus proposed for relaying information about space/motion, forces and consequently vibrations acting on the skin. The experimental results suggest that vibrations elicited by a moving contact point on the skin are information carriers that integrate both force and spatial cues. The frequencies measured ranged from 125 to 375Hz, similar to the sensitive range of Pacinian corpuscles [41]. Analysis indicates that vibration frequency alone may enable discrimination between some speeds and between some normal forces. The results also show that vibration amplitude depends on the normal force. A cutaneous stimulation study [164] reported that the magnitude of perceived normal force increases as applied normal force increases from 1 to 5N. In our experiments, the vibration amplitude plotted with respect to speed was a parabola with a global maximum at 15mm/s. We surmise that this is a consequence of the resonant frequency of the artificial skin and may depend on various factors, e.g. material properties and thickness. The resonant frequency of the natural skin has been studied physiologically in [159] and its presence could be considered in the design of haptic devices. We found that vibration amplitude can be used to differentiate some speeds and normal forces. In addition, spatial cues resulting from series of vibration events display accurate information about the speed of contact points.

The characteristics of the haptic apparatus were obtained using an artificial skin instrumented with an embedded accelerometer. The artificial skin offers a degree of objectiveness in determining the signals generated by the apparatus. Further investigation will be carried out with human subjects to validate whether the obtained signals correspond to tactile afferent signals actually felt

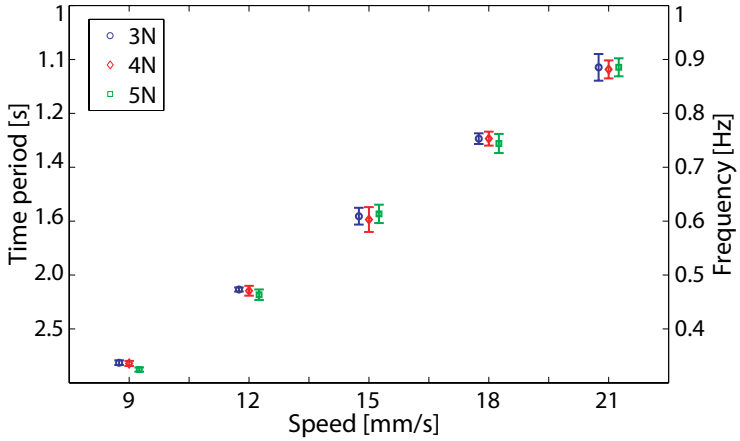

Figure 6.5: Time period and frequency of vibrations events resulting from the spatial distribution of contact points. The time period varies linearly with the tangential speed and does not depends on the normal force. The plot shows an accurate discrimination of speeds.

by the human skin.

The combination of multi-tactile variables, such as motion and normal forces, based on a set of contact points could play an important role in manipulation with prosthetic hands. Relevant tasks include controlling slippage by efficiently regulating grip forces and haptic exploration for object texture recognition. Our long-term goal is to build a haptic device for prostheses based on the proposed mechanism, and evaluate it in manipulation tasks.

Chapter 7

Force Feedback via Shaped Contacts

Influence of tactors shape on force feedback signals

Following up on the findings from Chapter 6, this chapter investigates the roles of soft tactors' shape in improving the haptic display of a normal force to the human skin.

Wearable haptic devices have potential application as a non-invasive method for proprioceptive and exteroceptive feedback for prosthesis users. In this chapter we present the preliminary design and evaluation of a haptic device for displaying grip force. Force is transmitted through the interaction of various shaped nubs mounted on a rotating belt with a rigid body contacting the skin. A force sensor was used to quantify the time-varying signals produced by the device, and a pilot study with human participants was used to identify user preferences. The effects of four different nub shapes were analyzed. The efficacy of the nubs in generating useful force sensations was considered with respect to several features: the nub's ability to relay force intensity and force frequency, force resolution, and smoothness/roughness. The force characterization conducted with the force sensor indicates that square-shaped nubs provide best force magnitude resolution. The user study showed that participants' preference for a particular nub shape correlates with the nub's ability to relay force magnitude, while the frequency of force fluctuation generated by rotating nubs is tightly coupled with nub's smoothness.

[6]Parts of the material in this chapter previously appeared in: Marvin Ludersdorfer, Dana D. Damian, Alejandro Hernandez Arieta, Rolf Pfeifer and Allison Okamura (2011), " Force Feedback via Shaped Contacts", *International Conference on Morphological Computation (ICMC)*

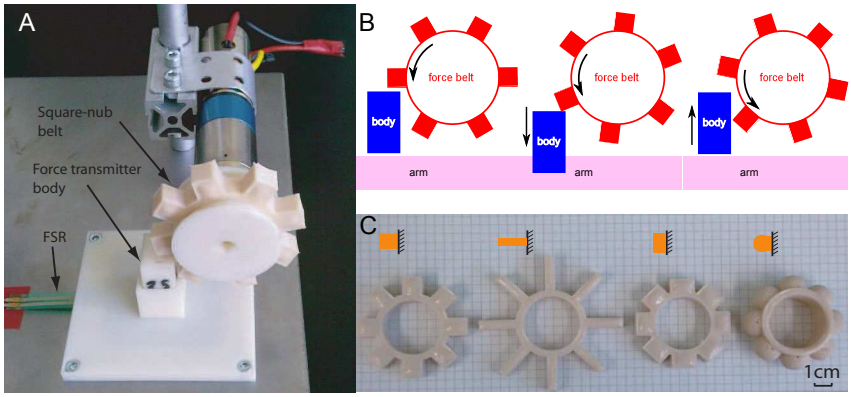

Figure 7.1: Experimental setup. A. The haptic device consists of a belt featuring nubs of various shapes rotated by a DC motor. By exploiting force generated by the moving nubs at contact with a rigid body, a normal force is transmitted at the base of the rigid body to represent grip force. B. Setup for human study. C. Nub types for the stimulating belt: square, long rectangle, wide rectangle and hemisphere.

7.1 Related Work

In recent years, there has been a considerable technological advancement in developing prosthetic hands with many degrees of freedom. However, current prostheses lack multi-modal, multi-degree-of-freedom haptic feedback to the wearer, making dexterous manipulation with prostheses difficult to achieve [10] [20]. Stabilizing an object in the hand entails a refined control of grip and load forces between the prosthesis and the held object [76]. In prosthetics research, haptic feedback has been used mostly for conveying grip force during stable grasp. Vibrations have been extensively used as a means of displaying information about grasp forces, through cutaneous electrotactile stimulation, e.g. [79], and vibrotactile stimulators (tactors), e.g. [30] [126]. Force feedback has also been transmitted via mechanical, e.g. [4] [114] and pneumatic, e.g. [116], push mechanisms in order to proportionally display exteroceptive force to the user. Mechanical push mechanisms have been implemented using servo-motors and linear actuators, while pneumatic push is achieved by regulating air pressure. Prior work shows increased performance of dexterous object manipulation when users receive haptic feedback, over cases without the additional feedback. In most related work, force feedback has been provided to the arm of the user, and in one case it was provided to the foot [114]. Our study evaluates continuously moving shaped contacts to provide mechanical force feedback, as means for displaying grip forces during manipulation. Various force profiles are generated by rotating belts featuring nubs of different shapes that transmit force to the skin. We implemented force feedback by contact during rotation of a motor in a single direction in order to make this a component of a novel compact haptic device that uses the two directions of one motor to relay various haptic sensations (The haptic feedback provided by the other motor direction is not addressed in this paper). We present a quantitative and qualitative description of the forces generated by the beltss nubs, conducted with a force sensor and a pilot user study, respectively.

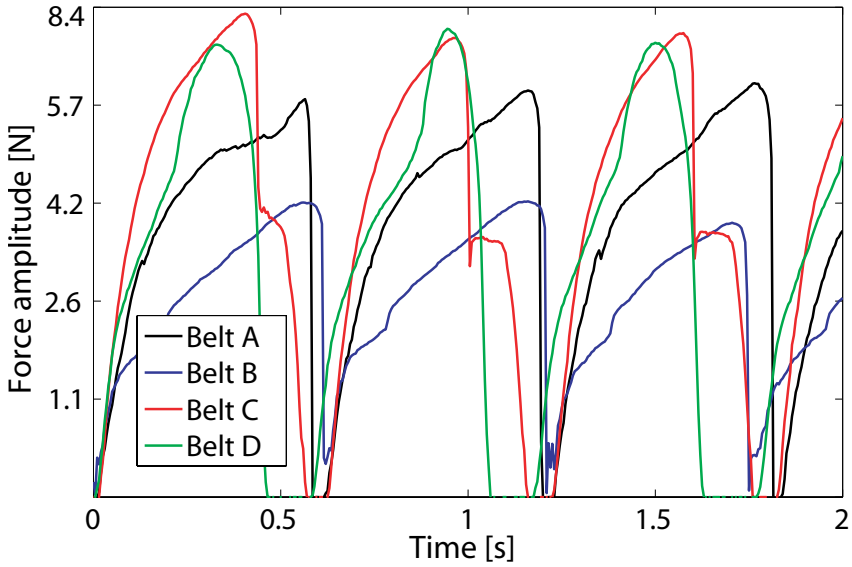

Figure 7.2: Raw force signals from belts with: square nubs (belt A), long rectangular nubs (belt B), wide rectangular nubs (belt C), hemispheric nubs (belt D). The signals were recorded with the motor rotating at a speed of 1.3 rad/s.

7.2 Prototype haptic device

The proposed haptic device is shown in Fig. 7.1A. A silicone belt covered by nubs is rotated by a DC motor (Faulhaber DC-Motor-Tacho combination) and contacts a rigid body through the nubs. The contact force captured by the rigid body during the rotation of the nubs is transmitted to the base of the rigid body, which contacts the skin. Various belts can be mounted on the device, each featuring a different type of nubs on the outer side. We test four nub shapes, as depicted in Fig. 7.1C: square nubs (type A), long rectangular nubs (type B), wide rectangular nubs (type C), and hemispherical nubs (type D). The silicone belts are obtained by solidifying silicone into an ABS (acrylonitrile butadiene styrene) mask built by 3D printing. The volume of the nubs is preserved across the four belt types. The horizontal distance between the outer diameter of the belt (measured without nubs) and the rigid body is 1 mm. The rotation speed of the belt, generated by the DC motor, is controlled by a HiBot TITechSH2 Tiny Controller board and a Solarbotics Compact L298 motor driver. The human forearm can be aligned with the base of the haptic device using a vertical sliding mechanism that lifts the belt and rigid body.

7.3 Experiments and results

The haptic device exploits the force created at the contact of the rotating nub with the rigid body. A normal force is transmitted to the base of the rigid body and captured by a sensitive receiver (force sensor or human skin). We tested the belts rotating at four speeds: 1.3, 2.4, 3.6 and 4.9 rad/s. The frequencies of force fluctuation associated with these speeds were 1.66, 3.07, 4.61 and 6.27 Hz. The

evaluation of the haptic device was conducted with (1) a force sensitive resistor (FSR) and (2) human users whose forearm was in contact with the base of the rigid body, as depicted in Fig. 7.1B. Signals from the FSR were acquired by a data acquisition system at a 200 Hz sampling rate. Examples of FSR signals when pressed by the four types of belts are illustrated in Fig. 7.2.

Evaluation by force sensor

Forty trials per speed per belt were run, and the average and peak force was computed. The results (Fig. 7.3) show that speed of rotation determines force magnitude for all four types of belts. Single factor analysis of variance (ANOVA) with four levels corresponding to four speeds showed that normal forces can be differentiated by speed. A significant difference in force amplitude was found between all speeds ($p < 0.001$). However, a linear monotonic relationship between speed of rotation and normal force (average or peak) existed only for type A and B belts. The peak force showed distinct values for speeds and belt types as well. Another four-level ANOVA conducted for each belt type yielded $p < 0.001$ across all speeds. Force amplitude resolution was computed for belts of type A, B and D, considering speeds 2.4, 3.6 and 4.9 rad/s. Type A belt has a considerable higher force resolution than type B and D belts ($p < 0.001$), based on a two-level ANOVA performed over measurements of both average and peak force.

Evaluation by user study

Three volunteers participated in the evaluation of the haptic device. The stimulation area was the ventral side of their forearm, where skin is glabrous. The device was enclosed in a box and the forearm reached it through a hole. The experiment had four sessions to test the four belts. During each session, participants were provided with ten occurrences of each experimental speed, presented in a random order (40 trials in total). The rotation speeds changed after each 8 s. The participants wore a noise-cancellation headset while a short sound marked the beginning of a new trial. The participants were asked to evaluate the relative force magnitude felt in each trial by a signed numeric value symbolizing the relative increase or decrease of the force magnitude from the previous to current trial. The users completed a post-experiment questionnaire that provided a qualitative evaluation of the sessions (belts). All users said that they rather used force frequency than force magnitude to interpret the intensity of the relayed force. Moreover, the users were asked to rate each session (belt) with respect to the following parameters: user ability to discriminate between various force magnitudes, force frequencies, and perception of smoothness/roughness of the force. The participants also ordered the sessions (belts) according to their preference for the overall characteristics of the sensations they received. For all participants, type D belt was found to be the least suitable in displaying various force magnitudes, whereas type A and B belts were the best (two votes and one vote, respectively). Two of the participants assessed that the set of force frequencies across belts were different; one participant evaluated them as identical. Regarding the smoothness/roughness of the relayed force, two participants said that the type D belt felt the smoothest. The other participant found a negligible difference in smoothness/roughness across belts. All three participants disliked

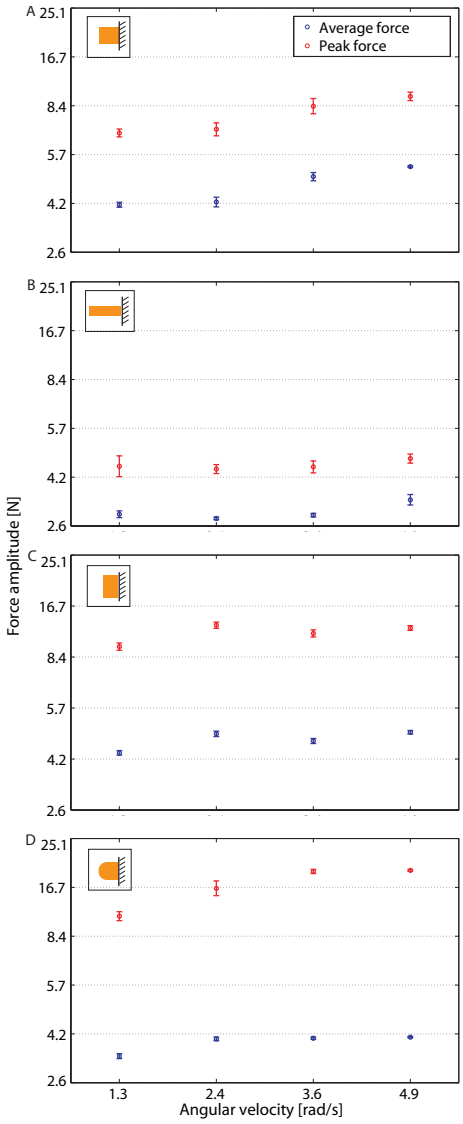

Figure 7.3: Mean and standard deviation of normal force relayed by four types of nubs and four speeds. Each plot correspond to a type of nub: A. Square. B. Long rectangle. C. Wide rectangle. D. Sphere. Nub shapes generate various force profiles.

	Participant 1				Participant 2				Participant 3			
	M	F	S	P	M	F	S	P	M	F	S	P
M	1				1				1			
F	0.8	1			0.8	1			-	1		
S	0.8	1	1		0.8	1	1		-	-	1	
P	1	0.8	0.8	1	1	0.8	0.8	1	0.4	-	-	1

Figure 7.4: Correlation coefficient for pair combinations of belt features: force magnitude (M), force frequency (F), force smoothness (S), and participants preference for the belt (P).

the sensation the type D belt induced. A correlation coefficient was computed for the combinations of the belt features investigated in this qualitative study. The results are listed in Table 7.4. There was a correlation between the rating of belts ability to relay various force magnitudes (M) and the order of user preferences for specific belts (P), as well as between the rating of belts ability to transmit various force frequencies (F) and the order of belts smoothness (S), which confirms the afore-mentioned observations.

7.4 Discussions and conclusion

The study considers the impact of the shape of a stimulus on force generation and is a preliminary inquiry for an efficient grip force display device. The belt with square nubs (A) yielded linear monotonic force magnitudes with respect to rotation speed and the highest force magnitude resolution, for both average and peak force. Compared to this belt, the one with long rectangular nubs (B) reduces both average and peak force. It provides a smoother force transmission due to a low average and peak force magnitude and low magnitude resolution. The belts with wide rectangular (C) and hemispherical (D) nubs amplify the force signal relative to type A belt. Type C belt produces a high duty rate by maintaining the contact with the rigid body over a relatively longer time. However, force magnitude does not increase significantly as speed increases. The type D belt provides more balanced force peaks than the rest of the belts, as seen in Fig. 2. The force increases linearly with the speed, and the increments of force magnitude are low. The pilot user study shows that force frequency, rather than force magnitude, was used as a force evaluation cue. The result indicates that frequency had a better tactile display resolution than force magnitude. However, a correlation between the preference for specific belts and their ability to display various force magnitudes was found. Interestingly, although the set of force frequencies was kept constant for all belts, two participants did not find them identical. The correlation found between the belt rating with respect to the users perception of various force frequencies and the belt rating with respect to perception of smoothness potentially indicates a tactile illusion according to which participants feel different frequencies when a skin contact of constant frequency changes its smoothness. In terms of force display by force frequency, there was no general agreement on which belt performs best. The relative high usability of belt A in displaying forces, generally rated by participants, may reside in the high resolution of force magnitude that this belt exhibits, as resulted from the FSR evaluation. We plan to examine belts of type A and B in further development of the haptic device. In particular, we will perform quantitative psychophysical studies that refine the design of the haptic device and extend the tactile variables displayed by the haptic device to the manipulated objects slippage speed.

Chapter 8

Wearable Haptic Device for Cutaneous Force and Slip Speed Display

Haptic device for force, slip occurrence and speed stimulation

Adding up on the studies of Chapter 6 and Chapter 7, this chapter presents the design and evaluation of a haptic device that relays quantitative information about normal and shear force on the skin with minimal resources.

Stable grasp is the result of sensorimotor regulation of forces, ensuring sufficient grip force and the integrity of the held object. Grasping with a prosthesis introduces the challenge of finding the appropriate forces given the engineered sensorimotor prosthetic interface. Excessive force leads to unnecessary energy use and possible damage to the object. In contrast, low grip forces lead to slippage. In order for a prosthetic hand to achieve a stable grasp, the haptic information provided to the prosthesis wearer needs to display these two antagonistic grasp metrics (force and slip) in a quantified way. We present the design and evaluation of a wearable single-actuator haptic device that relays multi-modal haptic information, such as grip force and slip speed. Two belts that are activated in a mutually exclusive manner by the rotation direction of a single motor exert normal force and tangential motion on the skin surface, respectively. The wearable haptic device is able to display normal forces as a tap frequency in the range of approximately 1.5-5.0 Hz and slip speed in the range of $50 - 200$ mm/s. Within these values, users are able to identify at least four stimulation levels for each feedback modality, with short-term training.

[7]Parts of the material in this chapter previously appeared in: D.D. Damian, M. Ludersdorfer, Y. Kim, A. Hernandez Arieta, R. Pfeifer and A.M. Okamura (2011), " Wearable Haptic Device for Cutaneous Force and Slip Feedback",*IEEE International Conference on Robotics and Automation (ICRA)*, (in press).

8.1 Related Work

Stability in grasping objects is defined as a load-to-grip-force sensorimotor transformation that ensures adequate safety margins against slip. Stable grasp with the human hand requires both anticipatory parameter control based on a predictive model in the central nervous system (CNS) and discrete-event sensory-driven control [72]. The latter type of control is specifically related to involuntary slippage scenarios and is based on sensory information to regulate the ratio between grip and load forces [10, 63]. With prior knowledge about the grasped object, proprioceptive cues, and incoming exteroceptive signals, such as force, pressure, motion and vibration, the CNS is able to integrate sensory information in order to ensure a grip force within safe margins. Prosthetic hands introduce an engineered sensorimotor interface that hinders the natural reliance on predictive models and is prone to generate significant perturbations in the grasping process. In such scenarios, stable grasp control becomes a sensorimotor transformation highly dependent on incoming sensory information, aimed at regulating the grip force and removing perturbations such as slip and excessive force that can damage the held object or involve unnecessary energy use.

At present, haptics research is taking various approaches to feed back sensory information to the user in order to restore grasp stability. The endeavor also undertakes the release of the current need of monitoring manipulative actions with vision, which is a leading factor in user rejection of prostheses (e.g., [9,161]) and a serious gap to attaining the integration of a prosthesis as part of the wearer's body.

Research on sensory substitution has focused on tactile grip force displays. Various works showed that vibrations can be successfully used as a display for grip force, e.g., [3, 89, 126]. The work of Kaczmarek et al. [79] represents a rich reference about the potential of using electrocutaneous or mechanical vibrations to excite mechanoreceptors of the human skin and generate various tactile sensations. An alternative approach is a one-to-one physiologically compatible stimulation, according to which grip force is relayed by means of a push mechanism onto the skin, e.g, [102, 114], or by a cuff around the arm to display grip pressure [116].

Although force feedback is relevant for characterizing the applied grip force of prosthesis wearers, the deprivation of motion cues cannot sufficiently prevent or overcome grasp instability. Physiological studies, e.g., [10, 72], showed that slippage is a pivotal determinant in grip control. Perturbations artificially generated by changing the weight or the slip speed of an object were found to upgrade the agility of the grip response and the ability to overcome slippage, according to early work of Johansson and Cole [72] and recent work of Damian et al. [42], respectively. Nonetheless, slip feedback in prosthetic applications has not received much attention. For grasp stability, Tsagarakis et al. [152] developed a device that embeds two miniature motors in a "V" configuration to generate sensations of relative lateral motion at the fingertip. Although the device is compact, mountable on the hand finger and supports the display of various motion speeds, its placement would imped the use of the healthy hand of prostheses users. Slip feedback has been proved successful in tele-manipulation and virtual reality. Edin et al. [14] devised a mechanism in order to transmit frictional information through solenoids mounted on a held object. The mechanism elicited physiological responses that resemble the responses observed with

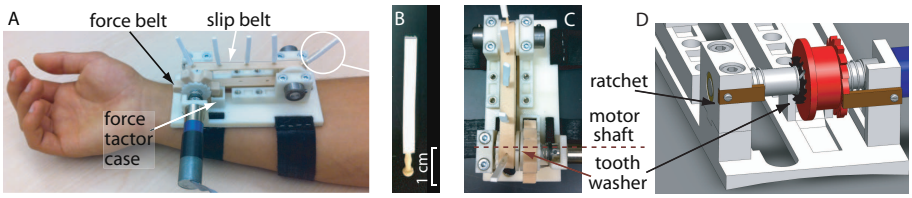

Figure 8.1: The wearable haptic device. A. The wearable haptic device mounted on the forearm. It consists of normal force and slip speed transmission belts. During motor rotation, the nubs on the force belt push onto the force tactor at its base to transmit normal force to the skin. Soft pins mounted on the slip belt contact the skin during the rotation of the belt. B. Detail of a slip pin made of wood and foam. C. Top view of the wearable haptic device showing the motor shaft on which a tooth washer mechanically enables the rotation of either the force or slip belt depending on the rotation direction of the motor. D. Front view of the CAD design of the wearable haptic device. The pulley of the slip belt is omitted to highlight various structural layers.

occurring slips. Webster et al. [160] developed a two-degree-of-freedom slip display that reproduces the sensations of sliding contact by means of the rotation of a ball positioned under the user's fingertip. According to the authors' findings, slip and force feedback, compared to force feedback alone, offer an improved assistance for the manipulation of a virtual object using reduced forces. Recently, the significance of multi-modal sensory substitution in prosthetic applications has been credited. Kim et al. [82] developed a multifunctional tactile feedback device that provides feedback on contact, pressure, shear force, vibration, and temperature. The device was evaluated with users that have undergone targeted reinnervation surgery.

Prompted by physiological findings and practical issues in prosthetics, we present a wearable multi-modal haptic device aimed at relaying grip forces and slippage. As such, the device displays normal forces and slip speeds, respectively. We evaluate the properties of the wearable haptic device and user ability to identify displayed stimuli in quantitative and qualitative studies.

8.2 The proposed wearable haptic device

8.2.1 General design specifications

The wearable haptic device is presented in Fig. 8.1. It consists of two main components: the normal force transmission belt and the slip speed transmission belt. The belts are made of silicone by solidifying the elastomer into an ABS (Acrylonitrile Butadiene Styrene) mask built by rapid prototyping. The two belts are activated in a mutually exclusive manner based on the assumption that if an object slips it means there is insufficient grip force, whereas if an object is tightly grasped, there is no occurring slip. Hence, we opted to use the rotation direction of a single DC motor (Faulhaber 1727U 012C, regulated by a HiBot TITechSH2 Tiny Controller board and a Solarbotics Compact L298 motor driver) in order to control either the force feedback belt or the slip speed feedback belt. The selection mechanism of the active feedback belt was achieved by means of a tooth washer mounted on the DC motor's shaft. On each side

of the tooth washer there is a pulley supporting a feedback belt, loosely placed on the motor shaft and pushed toward the tooth washer by a spring. The configuration of the washer's teeth constrains one pulley to rotate with the motor, while the other pulley is held fixed by a ratchet mechanism. The wearable haptic device is designed to be worn on the ventral part of the forearm. We exploit this flat area of the forearm in order to maintain the belts of the haptic device undeformed. The size of the wearable haptic device was determined from a forearm measurement pilot study conducted with 20 humans (4 females and 16 males). Based on the study and physical constraints of the components, the size of the wearable haptic device was set to 56 mm width and 127 mm length. Consequently, the haptic device weighted 209 grams.

8.2.2 Normal force transmission belt

Force belt design

The normal force transmission belt has an inner diameter of 15 mm and outer diameter of 22 mm. Six square nubs with sides of 7 mm cover the surface of the belt. The shape of the nubs was selected based on a previous study [93] in which the same force display mechanism was used. During the rotation of the belt, the nubs periodically push down a rigid body placed in a case at the base of the force belt. The size of the rigid body is $7 \times 9 \times 16$ mm. The contact force captured by the rigid body from the belt's nubs is transmitted to its base which in turn makes contact with the skin (see Fig. 8.2). We hereafter refer to the rigid body as the force tactor. The mechanism enforces the transmission of a normal force on a skin surface of 63 mm^2. Due to the elastic material of the nubs, the amplitude of the normal force varies with the speed of the motor rotation by exploiting the principle of momentum. This property was shown in [93] for force tactors pushing on a rigid surface. Similarly, the frequency of the normal force can be regulated by the rotation speed of the motor due to the uniform distribution of the nubs on the belt surface.

Force belt performance

Following up on the study in [93], we conducted experiments with the wearable haptic device in order to characterize the normal force stimulation to the human skin surface. The wearable device was mounted on the ventral side of the forearm of a single user, while the forearm was resting on a table with the ventral side facing up. A force sensitive resistor (FSR) was placed between the force tactor and the human skin. Three force recording sessions were conducted at a sampling rate of 200 Hz, each of them for 11 motor speeds (33 trials in total). Across the three sessions, the position of the force tactor with respect to the ventral side of the forearm was slightly changed. The average and standard deviation of the normal force amplitude and frequency were computed over five time segments of a trial. One time segment spanned over three seconds. In Fig. 8.3A the normal force amplitude is plotted with respect to 11 motor speeds. Although in the previous study [93] the force amplitude showed a linear dependence on the motor speed for a force tactor contacting a rigid surface, the measurements in the three sessions showed that this linear relation is no longer valid if the stimulation is transmitted to the human skin. From our experimental

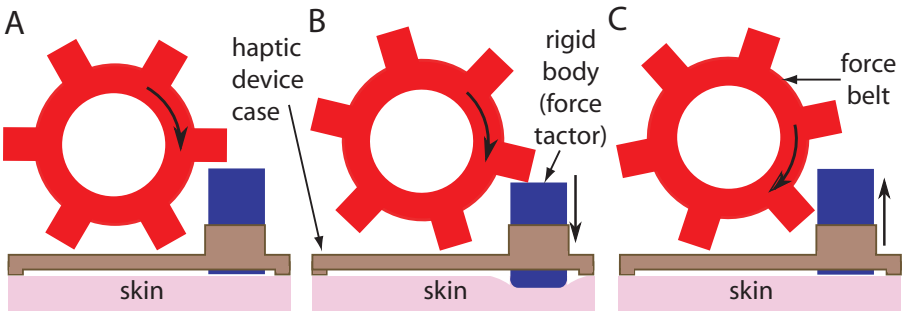

Figure 8.2: Mechanism for generating normal force to the skin. As the belt rotates (A) the nubs push the rigid body on the skin (B) and release the force (C) with a frequency related to the rotation speed of the belt.

observations, the variation of the normal force amplitude within one session and between sessions depended on the resistive forces between the force tactor and the skin due to the initial pressure exerted by the wearable haptic device's cuff around the forearm, and on the position of the force tactor with respect to the forearm featuring various softness of the skin. The frequency of the normal force pulses was computed by applying a Fast Fourier transform to each trial. Figure 8.3B shows a monotonic relation between the normal force frequency and the rotation speed of the motor, for angular velocities lower than approximately 8 rad/s. When the angular velocity exceeds this value, the wearable haptic device vibrates and the variation of the frequency increases.

8.2.3 Slip speed transmission belt

Slip belt design

The slip belt as shown in Fig. 8.1 is stretched over two pulleys of 15 mm diameter and 80 mm axial distance. The belt features soft pins that are uniformly distributed along the outer surface of the belt. As the pins are moving on the bottom side of the belt, they make contact with the skin. The design of the slip belt is based on a study [43] according to which spatially distributed moving contacts on the skin relay accurate information about the slip speed. The study also showed that the vibration generated by the moving pins at contact with an instrumented artificial skin enables the discrimination of some speeds. The pins are made of two materials. The base of the pins is made of wood and it features a groove that allows its fixation into holes of the silicone belt. The top of the pin is made of foam rubber. The combination of materials provides the pin with rigidness to transmit tangential force information, and softness to create contact sensation and ensure skin integrity. The length of the pin is 37 mm and the distance between the skin and the axis of the pulleys is 22 mm.

Slip belt performance

The slip speed was evaluated by running the DC motor at 14 constant speeds and measuring the time the slip belt took to perform a full turn. The results of these experiments, computed over five such trials, are depicted in Fig. 8.4. Slip

speeds in the range $50 - 200$ mm/s can be generated with high accuracy.

8.3 User study experiments

The human study evaluated the ability of users to recognize normal force and slip speed stimuli as generated by the wearable haptic device.

8.3.1 Experimental setup

Ten healthy volunteers (one female and nine males) with ages between 25 and 31 years (average age was 28.2 years) took part in the perception study. The study was approved by the Swiss Association of Ethics Committees (KEK). The participants gave their written consent to the experimental protocol. Among the participants, eight were right-hand dominant and two were left-hand dominant. The subjects were comfortably seated and the wearable haptic device was mounted on the dominant forearm. The dominant forearm was maintained in a normal and relaxed position along their body. Subjects did not see the device during experimental trials. A graphical interface on the monitor displayed the timeline of the experiment and buttons that controlled the self-paced experiment. A keyboard was used to collect participants' answers provided using the non-dominant hand. Audible cues were masked by noise-canceling headphones.

8.3.2 Experimental procedure

We conducted two experiments with users in order to evaluate the two tactile parameters that the haptic device is able to display: normal force and slip speed. A one-interval four-alternative forced choice procedure was used for each experiment. An experiment consisted of a training and a test phase. During the training phase, participants were presented with seven representations of each of the four stimuli levels (28 representations in total) in a random order. Subsequently, the participants were given the opportunity to display any of the stimuli levels at will, until they were confident in their recognition skill. The entire training phase spanned over five minutes in average. In the test phase, the stimuli recognition ability of the participants was evaluated across 100 trials. In each trial, a stimulus level was presented to the participants for five seconds. The participants identified the provided stimulus as "1", "2", "3" or "4" by pressing a key. Another key allowed the participants to voluntarily start the next trial and ensured a self-paced test during which they could take a break. There was no pause between the training and test phase. The participants were provided with a five minutes pause between the two experiments. The duration of a complete individual study (trainings and 200 evaluation trials) was approximately 45 minutes. The order of the two experiments was changed across participants in order to prevent a systematic learning bias between the slip speed and normal force feedback. Thus, odd-numbered participants were tested with force feedback first and slip speed feedback second, and the reversed for even-numbered participants.

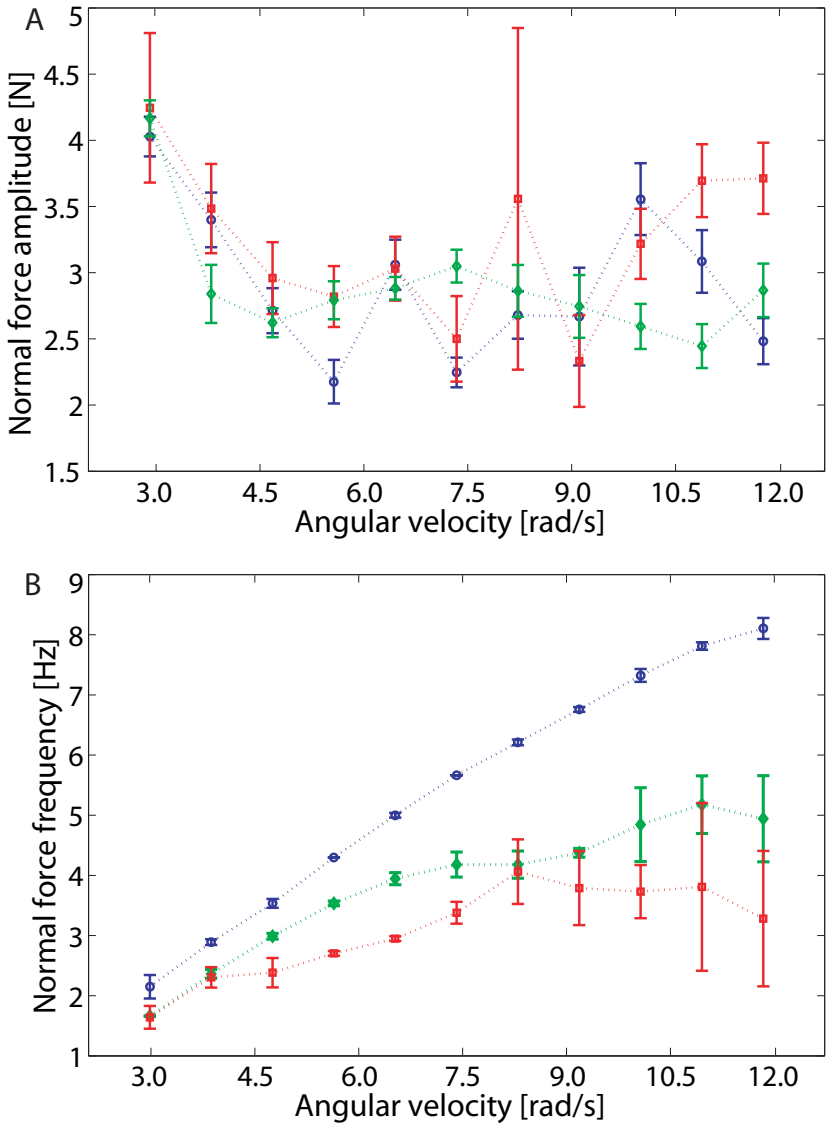

Figure 8.3: Characteristics of the normal force display with respect to motor speed. A. Force amplitude. B. Force frequency. The three colored curves designate three sessions of normal force recordings corresponding to three mountings of the wearable device on the forearm. The average and standard deviation of the normal force amplitude and frequency were computed over five trials for each speed. Normal force frequency, rather than amplitude, is reliably generated for angular velocities lower than 8 rad/s.

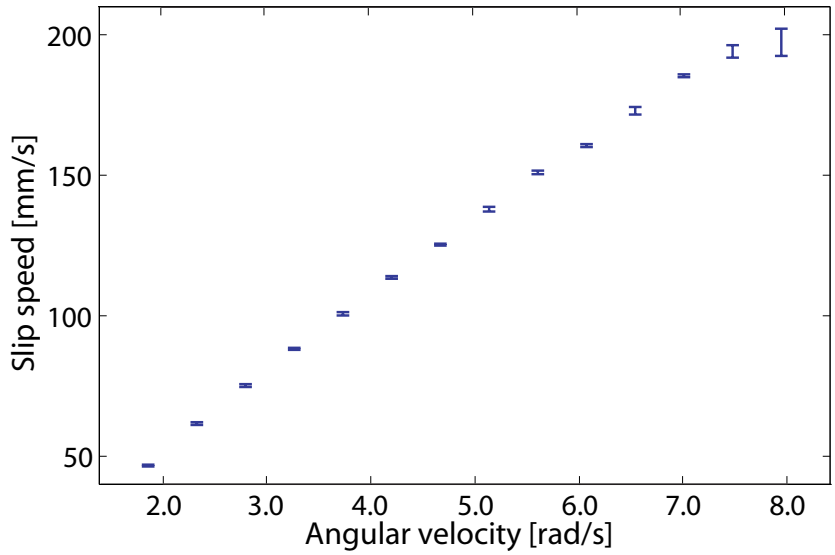

Figure 8.4: Characteristics of the slip speed display with respect to motor speed. The average and standard deviation of the slip speed values were computed over five trials. Slip speed is reliably generated at all investigated motor speeds.

8.3.3 Stimuli control

Based on the characteristics of the wearable haptic device, we displayed normal force by means of the normal force frequency and slip via slip speed. Most of the psychophysical literature has investigated the Just-Noticeable-Difference (JND) for human sensing of high frequency vibrations (exceeding 20 Hz), e.g., [99, 125, 133]. Given that the range of frequency output of the normal force display was below 8 Hz, physiological constraints found in these studies were not applicable to our experiment and could not be used for the choice of the normal force frequency levels. We therefore selected four angular velocities within the range for which the frequency of the normal force had low variation and monotonic relation with respect to the angular velocity ($3 - 8$ rad/s): 3.5, 5.0, 6.5 and 8.0 rad/s. As such, four normal force frequency levels, that are approximately equidistant, were generated. The JND for slip speed has received limited attention in haptic studies. Salada et al. [134] measured the slip speed sensitivity on the human fingertip at reference speeds of 80, 140, and 240 mm/s. The authors found that the slip speed sensitivity averages around 10% and is highly dependent on the texture of the stimulation surface. Gleeson et al. [61] used slip speed as a parameter to communicate a difference of contact location and thus relay direction. Their user study showed that speeds as slow as 1 mm/s over a displacement as little of 0.2 mm, displayed on the fingertip, were able to transmit direction information with an accuracy greater than 95%. To our knowledge there is no study on the JND for the ability of humans to perceive slip sensations on the forearm. Hence, four equally distant stimuli levels were selected within the entire interval of available speeds. The slip speeds chosen for the recognition experiment were 55, 100, 145 and 190 mm/s, corresponding to angular velocities of approx 2.00, 3.70, 5.30 and 7.00 rad/s.

8.4 Results

8.4.1 Quantitative evaluation

The analysis of the experimental data was performed using SPSS19 and Matlab. Figures 8.5A and 8.5B depict the confusion matrices for normal force and slip speed feedback, respectively. The rows indicate the stimuli levels presented to participants and the columns designate the actual identification response of the users. The values in the matrix represent the average and standard deviation percentages computed over the responses of all participants. Most errors involved the mismatch of the correct stimulus by only one level, for both feedback modalities. The identification rates of normal forces and slip speeds are depicted in Figs. 8.6A and 8.6B, respectively. The recognition success for the normal force and slip speed levels was computed over all ten subjects. The horizontal lines in the plots represent the 25% recognition rate for randomly chosen answers. The Kruskal-Wallis test was applied to the normal force identification responses and the result showed no statistical significant difference between force stimuli levels ($H(3) = 3.89$, $p = 0.27$). A one-way ANOVA was performed for slip speed responses and revealed no statistical significant difference between stimuli levels ($F(3, 36) = 1.94$, $p = 0.13$). The two analyses indicate that all four levels for each feedback modality were equally well recognized.

The average response time with force feedback was 0.92 s ($\pm$0.34 s) for all participants. A nonparametric Kruskal-Wallis test applied to response time with respect to the four normal force stimuli showed no statistical significant differences between the response time ($H(3) = 2.90$, $p = 0.40$). Similarly, a one-way ANOVA applied to the response time taken to identify the four slip speed stimuli showed no statistical significant difference between response time with respect to slip speed levels ($F(3, 36) = 0.34$, $p = 0.79$). In average, participants took 0.99 s ($\pm$0.28 s) to identify a slip speed stimulus. Correctness of force feedback answers and short response time showed a weak correlation (nonparametric Spearman correlation yielded $r = -0.32$ and $p = 0.04$). There exists no correlation between correctness of slip speed feedback answers and short response time (Pearson correlation yielded $p = 0.5$).

8.4.2 Qualitative evaluation

The ten participants completed a four-question post-experiment survey that provided a subjective evaluation of the wearable haptic device with respect to the two feedback modalities. Two questions referring to "Which feedback type felt more comfortable?" and "Which feedback type was easier to distinguish?", each with possible responses "Normal force feedback/Slip speed feedback/Both of them" received eight votes in favor for normal force feedback, one for slip speed feedback, and one for both modalities. The responses to the question "How did you evaluate the normal force?" with response choices "By amplitude/By frequency/By both of them" indicated that eight participants used frequency cues to quantify normal forces and two used both amplitude and frequency to identify normal force levels. The final question was "Which feedback modality would you select for a prosthetic hand?" with possible answers in the set "Normal force feedback/Slip speed feedback/Both of them/None of them". Three participants chose normal force feedback, one chose slip speed,

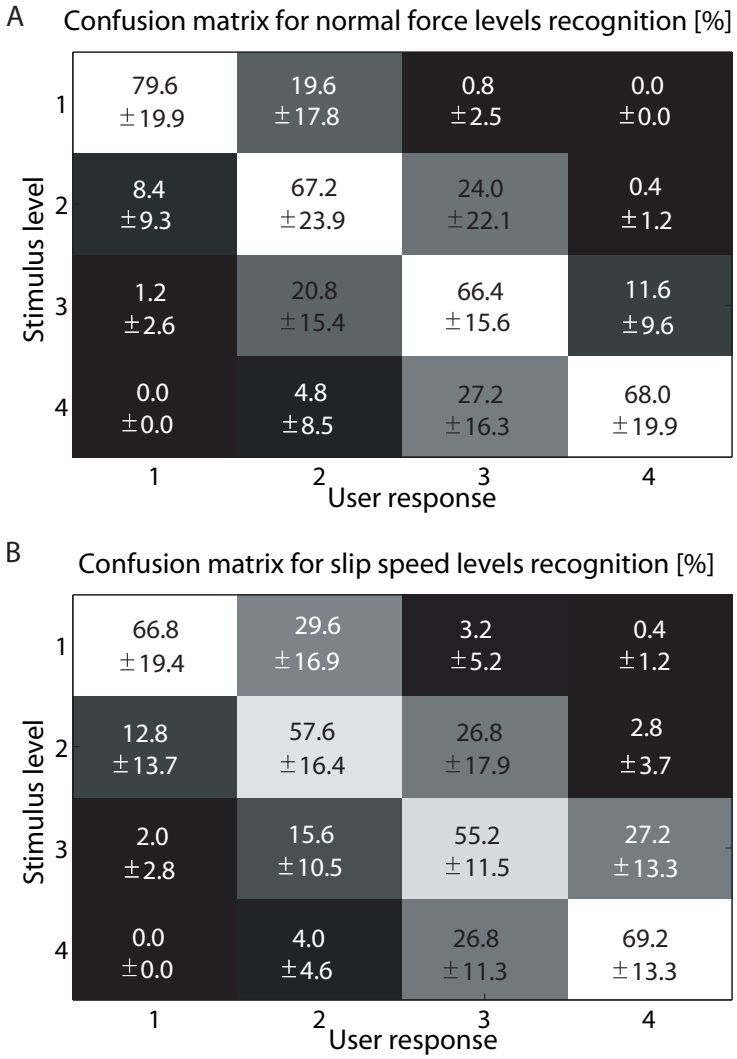

Figure 8.5: Confusion matrices showing the identification percentages obtained with the two types of feedback: normal force (A) and slip speed (B). Averages and standard deviations were computed across the responses of ten participants. Most of the identification errors involved the mismatch of the correct stimulus level by one.

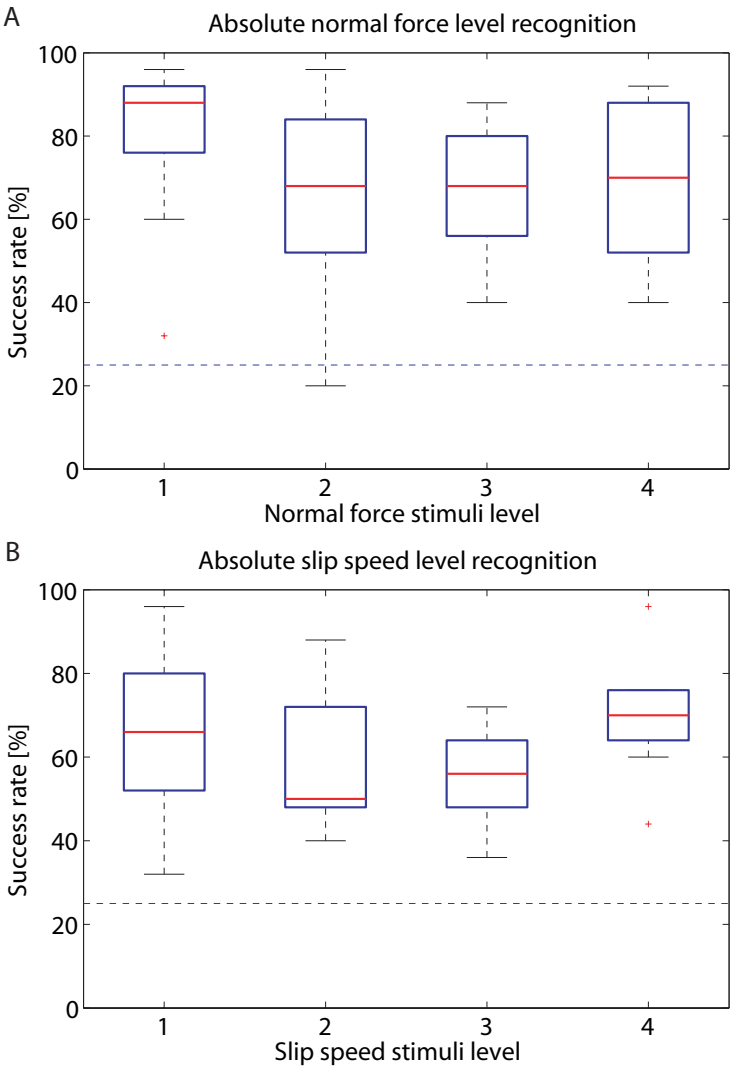

Figure 8.6: Absolute stimuli identification rate for the two feedback modalities: normal force (A) and slip speed (B). Averages and standard deviations were computed across the responses of ten participants. The horizontal lines represent the success rates for hypothetically random user responses.

five selected both force and slip speed feedback modalities, and one chose none.

8.5 Discussion

The ability of haptic devices to transmit normal forces and slip speeds holds promise in enabling grasp stability in prosthetic applications. The current study is an endeavor to design and evaluate such a haptic device. The characterization of the haptic device indicated that normal force frequency, rather than amplitude, can reliably encode grip force. Similarly, in the qualitative user study, normal force frequency rather than amplitude was used as a force evaluation cue. In manipulation tasks, grip force and slippage may quantitatively be represented by normal force frequency and slip speed, respectively, as generated by the haptic device. The underlying mechanisms for the two feedback modalities grant distinction in the tactile sensation, and consequently in the relayed information.

The qualitative results of the user study indicated that participants rated the normal force feedback better than the slip speed feedback in terms of display potential. This rating was in agreement with the results of the stimuli identification test. However, a rigorous ranking of the two feedback modalities is not possible without a common comparison unit, e.g. the JND of the display modalities. Previous studies [134] show that the sensitivity to slip speed highly depends on the surface texture. Therefore, the rates of the slip speeds identification could arguably be improved if the soft pins of the slip belt featured a surface texture. A longer training period could also enhance the user ability to identify stimuli levels for both feedback modalities. As confusion matrices indicated, although users were not perfectly accurate in identifying the stimuli levels, they were able to thoroughly estimate them with one stimulus level deviation. In manipulation tasks, users do not need to identify absolute values of stimuli, but relative values. The study suggests that one method to encode quantitative changes of either normal force or slip speed stimuli is to present pairs of stimuli between which there is a two-level or three-level difference (e.g., normal force level 1 followed by normal force level 3, slip speed level 4 followed by slip speed level 1). For these types of stimuli pairs, the identification rate was in average above 95% for both feedback modalities. Although currently force and slip are displayed in a mutually exclusive way, the functionality of the haptic device could potentially be advanced to multiplexing the force and slip stimulations for a simultaneous display of the two tactile sensations.

8.6 Conclusions and future work

We proposed the design of a wearable haptic device that displays normal forces and slip speeds. The haptic device generates normal force frequencies in the range of approximately $1.5 - 5.0$ Hz and slip speeds of $50 - 200$ mm/s. Among these values, at least four stimuli levels for each feedback modality can be identified by human users. Therefore, normal force frequency and slip speed are possible means to substitute qualitatively and quantitatively grip force and slippage, respectively, in order to endorse stable grasp in prosthetic applications. As a subsequent step, we will conduct experiments in order to assess the JND values

for the normal force frequency and the slip speed on the forearm. Furthermore, we plan to evaluate the wearable haptic device in manipulation tasks in which the two types of feedback need to be combined in order to ensure a stable grasp.

Chapter 9

Discussion

9.1 Summary of contributions

This thesis is an investigation of efficient and comprehensive haptic information for prosthetics, encompassing both tactile sensors and haptic displays. The study analyzes the requirements with regard to design and feedback interface pertaining to these two robotic components. The case application is represented by stabilizing the grasp with upper-limb prostheses, as a preliminary step towards the bodily incorporation of the prosthesis. Chapters 2 and 3 introduce our findings about grasp feedback interfaces. Within an economical approach to tactile sensing, Chapters 4 and 5 introduce the artificial ridged skins, while Chapters 6, 7 and 8 present the development of a multi-modal haptic device.

Chapter 2 reveals that stability in the interaction with the environment through a prosthesis can be characterized by a region of minimal grasp energy determined from proprioceptive (describing the self-action state, e.g., grip force) and exteroceptive (describing the environment state, e.g., object slip) stimulus mapping. In the context of upper-limb prostheses, we found that a necessary descriptor of the environment (e.g., the grasped object) includes slip occurrence and slip speed (which is a substitute for location information). Thus, conveying grip force (as a proprioceptive stimulus) and the object's slip speed information (as an exteroceptive stimulus) provided an appropriate feedback scheme for stabilizing the grasp of an object under slip perturbation. Psychophysical evaluations show that the slip speed tactile feedback boosts the agility in overcoming slip, increases the success in controlling slip with a lower effort of muscle contraction, and ensures lower variability of the muscle contraction input. Additionally, it is also shown (Chapter 3) that the slip speed tactile feedback regulates the reaction time to grip in proportion to the speed of the slipping object.

Chapters 4 and 5 present a ridged artificial skin for prosthetics. The skin is based on a single force sensor and detects the grip force in static interaction as well as the slip occurrence, speed, and position of an object subject to dynamic interaction (e.g., slip). These capabilities have been achieved by exploiting morphological cues, such as non-homogeneously distributed triangular ridges. An evolutionary algorithm generated optimal distributions of ridges in terms of the accuracy and resolution of the slip speed and position detection. Real experi-

ments with skins generated by the evolutionary algorithm show the successful detection of slip speed and position for slip speeds lower than 60 mm/s. Overall, this chapters introduce the concept of "economical tactile sensing", defined as the enhancement of tactile information using minimal resources by exploiting morphology. The concept is pertinent to prosthetics because it can enable a high ratio of information to resources, and it is promising for robust, light, and energy-efficient tactile sensing systems.

In Chapters 6, 7 and 8, the design, development and evaluation of an economical tactile feedback device are presented. Based on our previous findings from Chapter 2 according to which grasp stability is favored by both force and slip speed information, a wearable single-actuator haptic device that relays tactile feedback about the two parameters was developed. Our studies show that the materials (silicone), shape (square), and passive mechanisms contribute to the relay of realistic grasp information in an energy-efficient manner. Additional design parameters for efficient tactile displays include the exploitation of soft human skin and its friction. The wearable haptic device is able to display normal forces as a tap frequency in the range of approximately $1.5 - 5.0$ Hz and slip speed in the range of $50 - 200$ mm/s. Within these values, users with short-term training are able to identify at least four stimulation levels for each feedback modality.

9.2 Human programmability framework

Human-robot-environment and human programmability

We define human or embodied programmability as the possibility to add or alter an agent's computational resource by a sensory-motor mapping implemented through artificial tools. For example, a variety of stimulation patterns delivered by a haptic device could entail various grip forces from a prosthetic hand, through an engineered sensory-motor interface. In this example, the human learns or re-learns the sensory-motor mapping which is instantiated differently depending on the stimulus received from the haptic device. The concept of embodied programmability is different than the concept of morphological computation in that the link between the sensing and the motor units are not only physical and rigid, as in the case of morphological computation, but also logical and adaptable. Technologies for human-robot-environment interaction reside in the area of human programmability. The robotic devices can be external or internal, have various sizes, and interact with humans on various scales (cells, tissues, organs). Usually, the robotic attachment occurs when the human presents some impairment from normal functionalities (Fig. 9.1A), in which case, the robotic attachment restores the lost functionality (Fig. 9.1B). This category includes prostheses, rehabilitation machines, implants and more. A second case is represented by human function augmentation (Fig. 9.1C), in which the robotic device extends the normal functionality of the human [106]. The diagram in Fig. 9.1D shows the interconnecting paths between the environment, humans, and robots. The Table 9.1 classifies these relations in research fields at present. Although all research fields listed in Table 9.1 allow the programmability of the human user, haptics additionally provides the capability of overwriting and modifying previous computational models in the human through artificial input

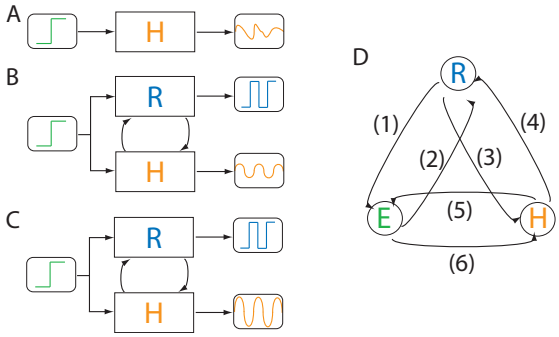

Figure 9.1: Human programmability. H is for human, R is for robot, the input represents a generic event from the environment, and the output represents a generic behavior, e.g., sine. A. Human with deficiency case (distorted sine). B. An assistive robot restores a deficiency of the human (recovered sine functionality). C. A robot augments the functionality of a human (amplified sine functionality). D. An integration of the interconnected paths between the environment, human, and robot. E is for environment. Specific paths are explained in Table 9.1.

Research field	HRE combinations	Note
Brain machine interface (BMI)	6-4-1	
Haptics	4-1-2-3	3=sensing
Rehabilitation	4-1-2-3	3=actuation
Assistive robotics	4-1-2-3	3=sensing
Robotic implants	4-3	H=E
Robotic surgery	4-1-2-3	E=patient, H=surgeon

Table 9.1: Human-robot-environment (HRE). The numbers represent a sequence of connections defined in Fig. 9.1D.

and (re)learning. This takes place in haptic applications, and assistive and rehabilitation robotics. By having control over the feedback, the end effector, and the mapping between them and the user, the human becomes a programmable living entity. Through associations, the user could learn sensory-motor routes as models in the central nervous system. For this reason, automatic prostheses do not reside in the area of human programmability because the sensing and the actuation is performed exclusively by the prosthetic device, depriving the human user of information or action involvement that contributes to the (re)learning process. The programmability concept can provide a general framework for capturing the restoration and the augmentation of human capabilities using biologic and robotic computational resources. Additionally, this framework can also be useful for devising methodologies for testing the notion of self. The research fields presented in Table 9.1 are case studies in the context of this framework.

Logic versus body programmability

The notion of human programmability is compatible with the programmability notion existent in computer science. This can be extended to robotics because it is assumed that there is an input that is fed by the human, designer, or an environment that modifies or adds or instantiates a functionality and produces a behavior (for the human and robot), e.g, grasp, or a number (for computers) through a computational process. Within this framework, education, at large, can also be viewed as human programmability meant to refine motions, social interaction, verbal utterances and more, during human lifetime. The studies of this thesis, together with the vast literature in human-robot-environment interaction, powerfully suggest that natural or artificially-induced correlations between the sensor and motor transformations drive human behavior, classifying the human as one of the most adaptable (programmable) living systems. This general statement suggests that robots, as embodied agents, could reach adaptability by careful design of the sensor and motor units and the programming of the links between these units.

9.3 Design principles for human programmability

In order to make efficient use of such a framework, design principles need to be extracted. Some of these design principles will be discussed in the following section. The design principles are based on the studies of this thesis, and therefore are valid under the assumption that vision is not provided to the user of an upper-limb prosthesis.

Exteroception and proprioception sensing for description of interaction

From our work on upper-limb prostheses, stable grasp, as a sensory-motor transformation, was achieved more quickly and adaptively when the human user was provided with two different types of feedback: exteroceptive (e.g., slip/slip speed) and proprioceptive (e.g., grip force)-in other words, information that describes the environment (e.g., the slipping object) and information that describes

the human actuation (e.g., user's force exerted on the object). The two types of information are related through a physical transformation, e.g., $\mu = \frac{F_L}{F}$ (the static friction coefficient equals the friction (load) force to grip force ratio). The presence of the two types of sensory information necessitates a sensory-motor coordination [119] [121]. The two types of feedback may thus be necessary and sufficient conditions for a fast and adaptive stable grasp. The addition of exteroceptive or proprioceptive senses is likely to provide redundancy or refinement of the sensing capability, and consequently, may contribute to the dexterity in actuation.

The flow charts and diagrams in Fig. 9.2 illustrate this design principle. Research has been centered on relaying grip force information through haptic interfaces. In this thesis, we showed that grip force feedback is not sufficient for stable grasp (Fig. 9.2A). Without any knowledge of the grasped object (exteroceptive sensing), the prosthesis wearer cannot properly influence the state of the object via the applied grip force only (proprioceptive sensing). Consequently, if the grip force F decreases significantly, the object may drop; if the grip force F increases significantly, the object may be crushed. Otherwise, the object is grasped by applying a force that is not guaranteed to be minimal (i.e., it is energy-wasteful). In this case, the prosthesis user does not know about the state of the object (Fig. 9.2A, question mark) unless it uses other exteroceptive senses such as vision. Grasp stability depends on the weight and friction coefficient of the held objects. With a prosthetic device, is is difficult to estimate these variables based on previous models in the central nervous system because of the artificial sensory-motor interface and the altered friction coefficients between the object and the artificial prosthesis. Under these conditions, grasp stability is related to overcoming perturbations such as slip; therefore, it is critical to relay information about the slipping object's position or slip speed to users. A few studies have argued that slip occurrence feedback improves grasp stability. However, the work presented in Chapter 2 showed that providing users with feedback about slip occurrence leads to poorer performance in overcoming slip relative to the case of slip speed provision. Instead, the provision of slip speed information, which is a fair substitution for location information, offers multiple benefits to grasp stability, e.g., grasp agility, regulation of the grasp time response, efficient muscle contraction. Being endowed with exteroceptive knowledge, the prosthesis user is able to evaluate whether the object is grasped or slips ($v > 0$) (see Fig. 9.2B). If the speed is positive, the user has to search within a large search space of grip force values to decrease the speed of the slipping object. Moreover, if the mapping that characterizes the sensory-motor transformation is not available to the user, this search becomes a highly non-trivial task (Δ^1 and Δ^2 express the unavailability of the mapping between the sensory-motor transformation to the user). If the user manages to stop it (check mark in the figure), the user still has no information on whether the grip force applied ensures a stable grasp (minimum force) or crushes the object. In contrast, with both exteroceptive and proprioceptive sensory information, the prosthesis user manages to guide his or her actions towards achieving a stable grasp (Fig. 9.2C).

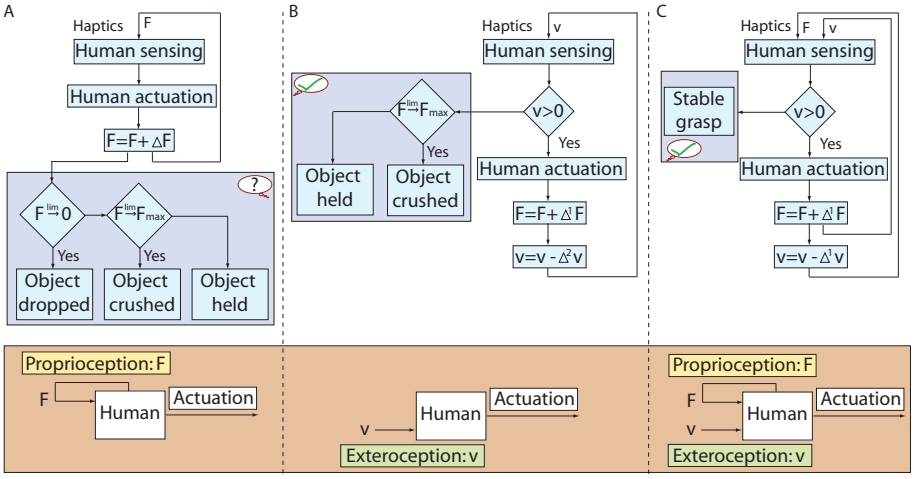

Figure 9.2: Effects of exteroceptive and proprioceptive stimuli on grasp stability. The grasp conditions are shown in the red background rectangles. The "perception" of the user is shown in speech bubbles. The state of the object is shown in the blue background rectangles. A. User is provided with proprioceptive information only (e.g., grip force). The object is subject to various final states: drop, crush, or energetically suboptimal grasp. B. User is provided with exteroceptive feedback only (e.g., slip speed). The object is subject to crush or energetically suboptimal grasp. C. User is provided with both proprioceptive and exteroceptive feedback. In this case, the user is more likely to achieve (quickly and adaptively) a stable grasp (i.e., grasp within safe margins against slip). (Δ^i and Δ^j express the unavailability ($i \neq j$) or availability ($i = j$) to the user of the mapping between the sensory-motor transformations.)

Quantified sensing for fine control

We consider the slip speed feedback to be a reverse force feedback representing "negative" forces. Therefore, relaying slip speed information is as significant as relaying quantified continuous force information. For daily activities in which users are engaged, it is imperative that the users receive not only binary event information (e.g., on-off slip detection and on-off contact with objects) about grasping events, but also continuous information about dynamical haptic events (e.g., slip speed of an object and changes of grasp force). We may argue that an appropriate scheme for overcoming the slip of an object is to always input low contraction intensity levels and gradually decrease the speed of the object until the object stops. In this case, slip occurrence feedback should be sufficient. This hypothesis was rejected based on the experimental results of this thesis, according to which, even when the speed of the slipping object was the lowest, the participants receiving slip occurrence feedback recorded the highest percentage of crushes relative to the vision and slip speed feedbacks. From the work presented in this thesis, a quantifiable slip feedback provides several advantages to the prosthesis user: (1) boosts the agility of overcoming slip; (2) increases the success in controlling slip with a lower consumption of muscle contraction intensity; (3) ensures lower variability of the muscle contraction input; and (4) controls the reaction time to grip.

Combined "human-in-the-loop" and automatic mechanisms to resolve voluntary and reflex actions

In prosthetics, the role of haptics is to provide sensory substitution for lost biological senses associated with the prosthetic device. As a consequence, it contributes to (1) regulating human behavior such that tasks are performed successfully through the prosthetic device and (2) enabling the bodily integration of the prosthetic device through brain plasticity. This "human-in-the-loop" process, however, is time-consuming due to both technological limitations of involved robotic devices (e.g., haptic device, prosthesis) and the traveling time of a signal from the afferent to the efferent nerves. The cutaneous type of feedback that has been investigated in this thesis triggers a voluntary reaction of the user, which may not be sufficiently fast for overcoming slip perturbations characterized by high speeds. For these cases, a reflex-based reaction may be more appropriate, and can be implemented via an automatic grip controller. Thus, a combination between an automatic grasp and a "human-in-the-loop" grasp control strategy may be the optimal solution for grip stabilization with prosthetic hands. Another option that could possibly be a substitute for both grasp control strategies is invasive direct nerve stimulation. However, this method requires further research and clinical testing to gain acceptance from large user communities.

Energy-efficient robotic systems

Energy is a critical feature for the development of robots that are physically (externally or internally) attached to humans and will most likely always be a catalyst for robot design selection. The significance of the economical tactile sensing systems is also apparent for prosthetics. Information availability and

gain are expected to be high, while energy consumption should be low. Prosthesis wearers need a device that is a viable replacement for the lost biological body part, has a long battery life, and is robust, light, and affordable. In this thesis, we pave the way to energy-efficient tactile sensors and haptic devices by considering shapes, space arrangement, materials, passive mechanisms and minimal electronics, and computational resources.

9.4 Monolithic sensing

Computation and information have been qualifiers for intelligence in both biological systems and robotics. A paradigm in artificial intelligence was brought up when it was argued that computation takes place not only at the level of brain synapses, but at the level of organism morphology [117] [120], as the organism interacts with the environment. Coined "morphological computation", it differs from the classical Turing computation in that the computation process occurs through the dynamics of physical forms. Thus, morphological computation may play a role in subsuming the (central) control computation. Morphological computation has been successfully exploited in the design of various artificial sensing systems. Morphology in the design of insect sensors [57] [91] [90], mammal sensors [96], human skin sensors [139]. The latter study shows that the ridges on the human fingertips may play a role in filtering in a range of stimuli frequencies that are compatible to the Pacinian mechanoreceptors and thus improve the texture recognition during tactile exploration.

Maximization of morphological computation for information gain

In our work presented in Chapters 4 and 5 we show that morphology is able to encode information. Additionally, our results demonstrate that environmental stimulation can be encoded, through morphological computation, in an integrative and unique manner into a monolithic information pathway (channel). This is due to unique properties of the morphology characterizing the artificial skin, e.g., ridges distributed non-homogeneously at a specific distance one from each other. This approach is opposite to the current sensing technologies in which sensing systems feature large arrays of sensor units. Figure 9.3 illustrates a comparative case study between distributed tactile sensing (A) and monolithic tactile sensing (B).

The former approach features an array of sensors as a physical input layer underneath a flat soft surface, whereas the latter approach features a single sensor that is placed underneath a soft surface characterized by morphological cues (e.g., ridges). Both approaches could yield the same types of information (virtual outputs, e.g., forces, slip speed, position). Nonetheless, in the latter approach, the information is obtained with minimal resources (e.g., materials, electronics, and wiring). The formulation of the monolithic information by minimizing the channels and maximizing morphology capacity allows a rough quantification of the maximum potential of morphological computation with respect to some tactile sensing system properties. We designate m as the number of sensors in the tactile system and n as the number of virtual outputs. We can therefore roughly make a comparison between some properties of the two tactile sensing approaches, as shown in Table 9.2. As an efficiency metric, we define

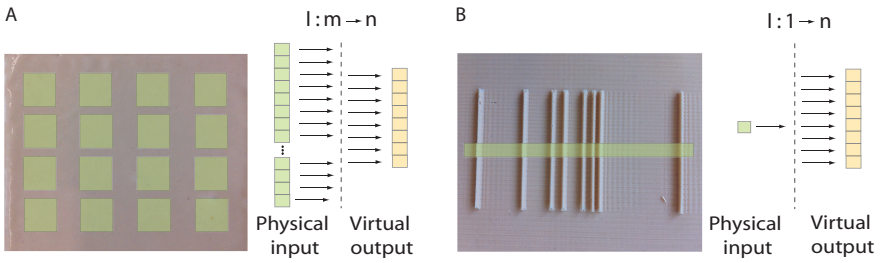

Figure 9.3: Distributed versus monolithic tactile sensing. Distributed tactile sensing example and channel representation (A). Monolithic tactile sensing example and channel representation (B). Green rectangles denote tactile sensors (inputs). Orange rectangles represent types of tactile information extracted from artificial skins (virtual outputs).

	DTS	MTS	Unit
Channel information gain	$\frac{n}{m}$	n	
Physical channels	m	1	channels
Redundancy	$\frac{m-k}{m}$	0	%

Table 9.2: Distributed (DTS) versus monolithic (MTS) tactile sensing metrics

the channel information gain as the number of information outputs to sensing elements ratio. Another indicator for the comparison of the two approaches is the physical connections, which represent the number of channels (wiring) used to transmit the stimulation input. Redundancy is a rough indicator of the information redundancy in case k sensor units are damaged. The first metric ranks the approach of monolithic information as providing a high gain of information. Monolithic sensing provides a channel information gain equal to m, while for the distributed sensing the channel information gain is 1. The former approach also offers a reduction in physical channels by $\frac{1}{m}$ relative to the second approach. The use of only one information channel entails the loss of redundancy against potential damages of the tactile sensing unit or erroneous signal transmission. While the redundancy for monolithic sensing is 0, the one for distributed sensing is $\frac{m-k}{m}$. However, this limitation of the monolithic sensing could be counteracted by using an additional similar sensor, stacked on the first sensor, to improve the information redundancy of the tactile sensing system.

Regarding the algorithmic computation, the distributed tactile sensing approach may have a higher cost than the monolithic tactile sensing approach. The former requires multiple signals' acquisition, conditioning, encoding, multiplexing, and decoding. The monolithic tactile sensing requires one signal's acquisition, conditioning, and decoding. The last operation entails matching the acquired signal with a model signal that is characteristic to the specific morphology of the artificial skin.

Space and sensing scale

The artificial ridged skin is an example of frugal information, showing the maximal potential of morphological computation for information encoding with minimal physical and computational resources. However, a combination of a tactile

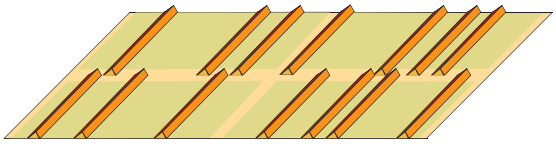

Figure 9.4: Distributed and monolithic tactile sensing. An example of artificial skin featuring four sensing elements (shown in green color), each being associated with a unique arrangement of ridges.

array and skin morphology may contribute not only to information and efficiency gain, but also to a gain in information resolution. This fusion has the potential to increase the spectral resource and enable tactile capabilities such as texture recognition. The combination of the two approaches would also improve the accuracy, redundancy, and robustness of the tactile sensing system.

Figure 9.4 illustrates the concept of a combination between distributed and monolithic tactile sensing. Each sensor is associated with a unique pattern of ridges. This way, the signal acquired by a transduction technique is able to derive more information than if no morphological patterns were present. Overall, the tactile sensing resembles the human tactile sense in that rich environmental information is integrated from a spatial region. The uniqueness of information associated with each sensor depends on the density and the arrangement of the corresponding spatial cues, thus providing a similarity with the density and spatial distribution of the mechanoreceptors in the human skin. This combined approach entails miniaturizing the current version of the artificial skin, such that spatial cues fit in regions smaller than 5 mm [141]. The current technologies, e.g., microelectrical systems (MEMS), microfabrication, etc., provide methods for achieving such artificial skins. The ridged patterns on the skin currently behave as a low-frequency filter, detecting location, slip occurrence, and speed. As the scale decreases, these patterns play the role of a high-frequency filter and could identify textures.

The artificial skin featuring ridges shows the potential of complex space geometry (shapes) to efficiently encode environmental information in dynamical events. In this respect, robot locomotion has made considerable progress in focusing attention on space distances, shapes, and stiffness for limb components [68]. Following the same principles, it would be interesting to develop mechanical brains that exploit not only time functions, which is currently performed through algorithms, but also physical space and mechanisms that mimic brain functionality. This way we could gain more insight into physical and chemical computation in the brain and their relations with sensing and actuation.

9.5 Human skin as a programming medium

The human's interaction with the environment (e.g., grasping and manipulation, walking) is facilitated by cutaneous mechanoreceptors that provide information about contact location, pressure, and events such as making and breaking contact. This intricate network of mechanoreceptors provides a rich spectrum of information to a healthy human; however, it is a significant challenge to reverse-engineer the underlying sensing mechanisms in order to create artificial, yet real-

istic tactile sensations for prosthesis wearers that have lost the biological tactile sense. Apart from the difficulty of tapping the right types of mechanoreceptors, an additional challenge in the design of haptic devices is the skin, as it is an embodied medium between the haptic device and the mechanoreceptors, with intrinsic properties.

There are numerous studies dedicated to the physiologic characterization of the skin under force or vibration stimuli. In most studies, these stimuli are applied through skin tap procedures [78]. However, real scenarios, such as grasping, manipulation, and walking, involve a far richer interaction between the skin and environment, such as for example, substantial normal and lateral (shear) motions. Our studies have indicated that a stimulus in motion on the skin may carry enhanced information. These properties should be considered and exploited in the future development of haptic devices, and are listed below.

Vibrations as force and spatial cues carriers The objective experimental characterization of the artificial skin described in [43] suggested that normal and lateral stimuli in motion may carry rich environmental information. The experimental results suggest that vibrations elicited by a moving contact point on the skin are information carriers that integrate both force and spatial cues. Analysis indicated that vibration frequency alone may enable discrimination between some speeds and between some normal forces. We found that vibration amplitude can be used to differentiate some speeds and normal forces. In addition, spatial cues resulting from a series of vibration events display accurate information about the speed of contact points.

Skin's natural frequency In our experiments, the vibration amplitude of a constant weight, moving on the skin, and plotted with respect to speed was a parabola with a global maximum at 15 mm/s. We surmise that this is a consequence of the resonant frequency of the artificial skin and may depend on various factors (e.g., material properties and thickness). The resonant frequency of natural skin has been studied physiologically in [159] and its presence could be considered in the design of haptic devices.

Skin compliance In our previous study [93], we measured the force amplitude of a soft structure tapping on a rigid flat surface as the structure was engaged in a concentric motion tangential to the flat surface. The plots showed a linear dependence between the force amplitude and the rotation speed of the soft structure. However, similar experimental procedures performed on the skin [45], instead of on a flat surface, indicated that this linear relation is no longer valid if the stimulation is transmitted to the human skin. From our experimental observations, the variation of the normal force amplitude within a session and between sessions depended on the resistive forces between the force tactor and the skin due to the initial pressure exerted by the wearable haptic device's cuff around the forearm, and on the position of the force tactor with respect to the forearm, which features varying softness of the skin. Consequently, we opted to encode grip force information in tap frequency, rather than in tap intensity. This choice was supported by a pilot user study [93], which shows that force frequency, rather than force magnitude, can be used as a force evaluation cue. The result indicates that frequency had a better tactile display reso-

lution than force magnitude. Additionally, the periodic stimulation suffers less from habituation, in contrast to static stimuli, which produce rapid adaptation of tactile sense [79].

Human skin is a medium with rich properties. Its soft material, sensitivity to pressure, motion, vibration and stretch, and natural frequency can all be exploited to input stimuli and program the consequent human behavior. Superposing these properties may provide rich sensations, though they may also give rise to stimulation effects that are difficult to predict in the design and functionality of a haptic device. It is therefore interesting to think of skin as a programming-embodied medium that transmits a large spectrum of information or sensations encoded in space, spatial density, intensity, and frequency.

9.6 Economical tactile displays

The haptic device is an extension of the prosthetic device that relays sensory feedback correlated to remote motor outputs of the prosthetic device. The haptic device represents a "programming tool" because the sensory input can drive the motor behavior of the human and can generate neurocognitive alterations such as the bodily incorporation of the prosthesis. As an attachment to the human body, the device falls into the same class of robots whose critical feature is energy efficiency. In Chapter 8, we proposed a haptic device prototype using soft tactors that features energy efficiency by relying on a single motor to provide tactile stimulation variety. Thus, the haptic device transmits grasp information to the prosthesis user (e.g., grip force, slip occurrence, and slip speed). In the following section, we provide some design guidelines, compiled from our studies, that can be considered in constructing energy-efficient tactile feedback devices.

Contact shape

In Chapter 7, we investigated means by which to relay grip force using soft tactors that transmit tapping movements on the skin as they are rotated by a DC motor. Our study considered the physical influence of the shape of the tactor's stimulus on force generation. The tactors represented nubs on a rotating belt. The four types of nubs considered- square (A), long rectangle (B), wide rectangle (C), and hemispherical (D)- generated force profiles with various properties. The belt with square nubs (A) yielded linear monotonic force magnitudes with respect to rotation speed and the highest force magnitude resolution for both average and peak force. Compared to this belt, the one with long rectangular nubs (B) reduced both average and peak force. It provided a smoother force transmission due to a low average and peak force magnitude and low magnitude resolution. The belts with wide rectangular (C) and hemispherical (D) nubs amplified the force signal relative to the type A belt. The type C belt produced a high duty rate by maintaining contact with the rigid body over a longer time. However, the force magnitude did not increase significantly as speed increased.

Soft materials

Soft materials represent a potential source for energy-efficient robots through the exploitation of elasticity and momentum. We used silicone in the construction

of the tactors of the haptic device in order to create grip force as a tactile stimulation. Square silicone nubs, equally distributed on the rotating belt, hit a rigid bar during their motion. The rigid bar, referred to as the force transmitter, had direct and perpendicular contact with the skin. Thus, as the rigid bar was periodically hit by the silicone tactor, a normal force was exerted on the human skin. The advantage of a soft material in this scenario is that it can create a realistic pressure sensation with a potentially reduced current from the motor. As the nub hits the rigid body, it gains increasing acceleration due to the friction between the nub and the rigid bar. This acceleration is transmitted to the following nub on the rotating belt, thus creating a larger force at its subsequent contact with the rigid bar. Consequently, the force exerted on the skin may potentially be amplified through the nature of the soft material. In addition, the fact that the silicone nubs become stiffer as the speed of the motor increases could also be used for the contact force amplification.

Mechanisms

It is common for current tactile displays to use a $1:1$ ratio for the used actuator versus relayed information ratio [152] [126] [11]. We approached the creation of a wearable tactile display for prosthetic grasp from an economical prospective in order to provide prosthesis wearers with an environmental tactile image using minimal resources. In the development of the haptic device presented in Chapter 8, we used motor shaft rotation as a global actuation scheme. We derived this global actuation scheme in order to realize vertical and horizontal actuation for small-area and wide-area stimulation for relaying grip force and slip speed, respectively. This was achieved using two belts featuring different lengths and tactors, rotating on the same shaft. Their mutually exclusive operation was attained using local passive actuation by means of a tooth washer to decouple the belts, and a ratchet and pawl mechanism to keep one belt fixed as the other one is operating.

Textures

Texture is an additional morphological parameter to be taken into account for tactile robots. Various textures for the tactors of the slip belt of the haptic devices have been tested in pilot experiments. Among wood, brush, and foam tactors, foam showed a better performance for creating a realistic slip sensation. Previous studies [134] also showed that the sensitivity to slip speed highly depends on the surface texture. Thus, the rates of the slip speed's identification for the haptic device presented in this thesis could arguably be improved if the soft foam tactors could further feature surface textures.

An interesting question that can be raised is whether the haptic device, as a complement of the prosthetic device, can be incorporated as a part of the body. Functionally, from the perspective of the human, the prosthetic hand enables the grasp actuation, whereas the haptic device enables the grasp sensing. To our knowledge, there have not been studies on this topic. However, it is probable that the haptic device could not be incorporated into the body schema because its motor action does not physically support grasping, which is the voluntary and expected behavioral action from the prosthesis wearer.

9.7 Conclusion

Human-robot-environment interaction has paved the way for the study of the self by offering the potential of human programmability. In contrast to other disciplines, such as genomics or regenerative medicine, robotics represents a promising tool for the systematic investigation of the paradigm of "brain, body, and self" through controlled designs or artificial interfaces and devices. This tool encompasses physical filter design (e.g., artificial skins), haptic displays, customized actuators (e.g., manipulators), and artificial sensory-motor mappings, thus making the human a highly programmable embodied agent.

The focus of this thesis has been grasp stability in upper-limb prostheses from a unified perspective of tactile sensing and display. The obtained results suggest that the sensory-motor transformations generated by grasp with prostheses may provide suitable means for inquiring the meaning of the self and the environment. In this regard, the self can be described through the interaction with the environment. A key attribute in defining the self and its interconnection to the environment is the energy efficiency. Energy efficiency can be achieved by the user if the body and the environment engaged in the interaction can be minimally but holistically described by an exteroceptive and proprioceptive sense through a sensory-motor transformation. The energy efficiency of the human-environment interaction and of prosthetic devices has been a leading factor for the acceptance of prostheses. Consequently, engineering the self may also imply building efficient robotic devices that can restore or augment human functionality with minimal resources. This thesis shows various design principles for energy-efficient human programmability in the context of sensing in upper-limb prosthetics. Morphology can be exploited for frugal information. Soft materials, shapes, and spacing configurations represent powerful computational resources for encoding information from the environment and for programming human-environment interactions in an energy-efficient manner.

The thesis deepens the understanding of sensorimotor transformations in prosthetic systems as a basis for self-restoration or self-augmentation. Additionally, it shows the capital of morphology exploitation as means for building efficient interface schemes in human-robot-environment systems.

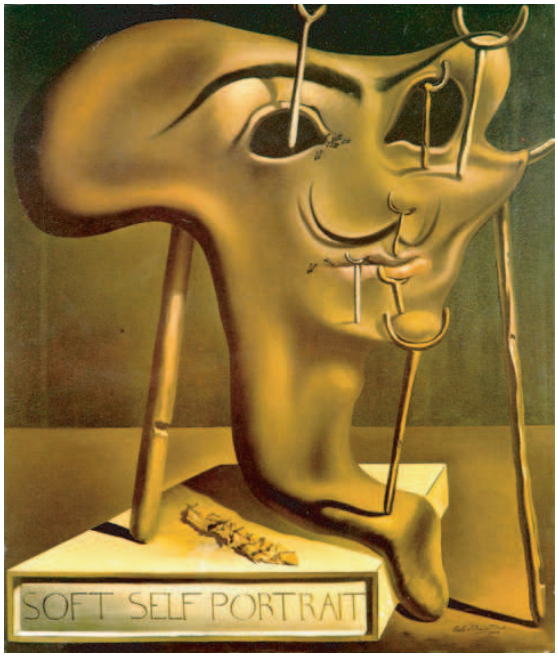

Figure 9.5: Soft Self Portrait, Salvador Dali, 1941

Bibliography

[1] J. Abbott, P. Marayong, and A. Okamura. Haptic virtual fixtures for robot-assisted manipulation. In *S. Thrun and R. Brooks and H. Durrant-Whyte, Eds., Robotics Research: Results of the 12th International Symposium ISRR*, pages 49–64. 2007.

[2] N. Adams, C. Brown, and K. Nagy. Energy expenditure of free-ranging wandering albatrosses diomedea exulans. *Physiological Zoology*, 59(6):583–591, 1986.

[3] Q. An, Y. Matsuoka, and C. Stepp. Multi-day training with vibrotactile feedback for virtual object manipulation. In *Proceedings of the IEEE International Conference on Rehabilitation Robotics*, pages 1–5, 2011.

[4] C. Antfolk, C. Balkenius, G. Lundborg, B. Rosen, and F. Sebelius. Design and technical construction of a tactile display for sensory feedback in a hand prosthesis system. *BioMedical Engineering OnLine*, 9(50), 2010.

[5] A. H. Arieta. Development of a multi-channel functional electrical stimulation system for prosthetic applications of limbs. *Doctoral Dissertation.*, 2007.

[6] A. H. Arieta, C. Dermitzakis, D. Damian, M. Lungarella, and R. Pfeifer. *Sensory-motor coupling in rehabilitation robotics.* Handbook of Service Robotics, I-Tech Education and Publishing, Vienna, Austria, 2008.

[7] A. H. Arieta, R. Kato, H. Yokoi, and W. Yu. Development of a multi-dof electromyography prosthetic system using the adaptive joint mechanism. *Applied Bionics and Biomechanics*, 3(2):101–111, 2006.

[8] A. Asbeck, S. Dastoor, A. Parness, L. Fullerton, N. Esparza, D. Soto, B. Heyneman, and M. Cutkosky. Climbing rough vertical surfaces with hierarchical directional adhesion. In *IEEE International Conference on Robotics and Automation*, pages 2675 – 2680, 2009.

[9] D. Atkins, D. Heard, and W. Donovan. Epidemiologic overview of individuals with upper-limb loss and their reported research priorities. *Journal of Prosthetics and Orthotics*, 8(2-11):718–723, 1996.

[10] A.-S. Augurelle, A. Smith, T. Lejeune, and J.-L. Thonnard. Importance of cutaneous feedback in maintaining a secure grip during manipulation of hand-held objects. *J. of Neurophysiology*, 89:665–671, 2003.

[11] R. Baavour, M. Fuchs, and U. Ben-Hanan. Grip-slip: A slip/shear tactile display master unit for grip tasks. In *IEEE Proceedings of the Mediterranean Conference on Control and Automation*, pages 1 – 6, 2007.

[12] P. BachyRita. Sensory plasticity. applications to a vision substitution system. *Acta Neurol Scand.*, 43(4):417–426, 1967.

[13] L. Bahrick and J. Watson. Detection of intermodal proprioceptive-visual contingency as a basis of self perception in infancy. *Developmental Psychology*, 21:963–973, 1985.

[14] B.B.Edin, R. Howe, G. Westling, and M. Cutkosky. A physiological method for relaying frictional information to a human operator. *IEEE Transactions on Systems, Man, and Cybernetics*, 23(2):427–432, 1993.

[15] L. Beccai, S. Roccella, L. Ascari, P. Valdastri, A. Sieber, M. Carrozza, and P. Dario. Development and experimental analysis of a soft compliant tactile microsensor for anthropomorphic artificial hand. *IEEE/ASME Transactions on Mechatronics,*, 13(2):158–168, 2008.

[16] B. Bethea, A. Okamura, M. Kitagawa, T. Fitton, S. Cattaneo, V. Gott, W. Baumgartner, and D. Yuh. Application of haptic feedback to robotic surgery. *J Laparoendosc Adv Surg Tech A*, page 191195, 2004.

[17] A. Bicchi and V. Kumar. Robotic grasping and contact: a review. In *IEEE Proceedings of International Conference on Robotics and Automation*, pages 348 – 353, 2000.

[18] A. Bicchi, J. Salisbury, and P. Dario. Augmentation of grasp robustness using intrinsic tactile sensing. In *IEEE Proceedings of International Conference on Robotics and Automation*, pages 302 – 307, 1989.

[19] E. Biddiss and T. Chau. Upper limb prosthesis use and abandonment: a survey of the last 25 years. *Prosthet Orthot Int*, 31(3):236–257, 2007.

[20] A. Blank, A. Okamura, and K. Kuchenbecker. Identifying the role of proprioception in upper-limb prosthesis control: Studies on targeted motion. *ACM Transactions on Applied Perception*, 7(3), 2010.

[21] D. Bloor, K. Donnelly, P. J. Hands, P. Laughlin, and D. Lussey. A metalpolymer composite with unusal properties. *J. Phys. D: Appl. Phys.*, 38(6):2851–2860, 2005.

[22] M. Botvinick and J. Cohen. Rubber hands "feel" touch that eyes see. *Nature*, 391:756, 1998.

[23] D. Brown and W. Christian. Simulating what you see. In *Proceedings of MPTL 16 and HSCI*, 2011.

[24] E. Brown, N. Rodenberg, J. Amend, A. Mozeika, E. Steltz, M. Zakin, H. Lipson, and H. Jaeger. Universal robotic gripper based on the jamming of granular material. *Proceedings of the National Academy of Sciences (PNAS)*, 107(44):18809–18814, 2010.

[25] L. Cardinali, F. Frassinetti, C. Brozzoli, C. Urquizar, A. Roy, and A. Farne. Tool-use induces morphological updating of the body schema. *Current Biology*, 19(12):R478–R479, 2009.

[26] J. Carpaneto, S. Micera, F. Zaccone, F. Vecchi, and P. Dario. A sensorized thumb for force closed-loop control of hand neuroprostheses. *IEEE Transactions on Neural Systems and Rehabilitation Engineering*, 11(4):346 – 353, 2003.

[27] M. Carrozza, B. Massa, S. Micera, R. Lazzarini, M. Zecca, and P. Dario. The development of a novel prosthetic hand-ongoing research and preliminary results. *IEEE/ASME Transactions on Mechatronics*, 7(2):108 – 114, 2002.

[28] M. C. Carrozza, G. Cappiello, S. Micera, B. B. Edin, L. Beccai, and C. Cipriani. Design of a cybernetic hand for perception and action. *Biol Cybern*, 95:629–644, 2006.

[29] M. Cartmill. The volar skin of primates: its frictional characteristics and their functional significance. *American Journal of Physical Anthropology*, 50:497–510, 1979.

[30] A. Chatterjee, V. Aggarwal, A. Ramos, S. Acharya, and N. Thakor. A brain-computer interface with vibrotactile biofeedback for haptic information. *Journal of Neuroengineeting and Rehabilitation*, 4(40), 2007.

[31] A. Chatterjee, P. Chaubey, J. Martin, and N. Thakor. Quantifying prosthesis control improvements using a vibrotactile representation of grip force. In *IEEE Region 5 Conference*, pages 1–5, 2008.

[32] M.-Y. Cheng, C.-L. Lin, Y.-T. Lai, and Y.-J. Yang. A polymer-based capacitive sensing array for normal and shear force measurement. *Sensors*, 10(11):10211–10225, 2010.

[33] D. Childress. Expert analysis of the tirr national upper-limb amputee database. In *Archived at The Institute for Rehabilitation and Research in Houston*, 1994.

[34] M. Ciocarlie and P. Allen. Hand posture subspaces for dexterous robotic grasping. *International Journal of Robotics Research*, 28(7):851–867, 2009.

[35] C. Cipriani, F. Zaccone, S. Micera, and M. Carrozza. On the shared control of an emg controlled prosthetic hand: analysis of user-prosthesis interaction. *IEEE Transactions on Robotics*, 24(1):170–184, 2008.

[36] F. Clark and K. Horch. *Kinesthesia. In K. B. Boff, L. Kaufman and J. P. Thomas (Eds.), Handbook of Human Perception and Performance: Sensory Processes and Perception.* John Wiley and Sons, Inc, New York, USA, 1986.

[37] S. Collins, A. Ruina, R. Tedrake, and M. Wisse. Efficient bipedal robots based on passive-dynamic walkers. *Science*, 307(5712):1082–1085, 2005.

[38] D. P. J. Cotton, A. Cranny, N. M. White, and P. H. Chappell. A thick-film piezoelectric slip sensor for a prosthetic hand. *IEEE Sensors Journal*, 7(5):752–761, 2007.

[39] M. Cutkosky. On grasp choice, grasp models, and the design of hands for manufacturing tasks. *IEEE Transactions on Robotics and Automation*, 5(3):269 – 279, 1989.

[40] M. R. Cutkosky, R. D. Howe, and W. Provancher. *Force and tactile sensors, Springer Handbook of Robotics, B. Siciliano and O. Khatib,*. Springer-Verlag, Berlin/Heidelberg, Germany, 2008.

[41] R. Dahiya, G. Metta, M. Valle, and G. Sandini. Tactile sensing from humans to humanoids. *IEEE Trans. on Robotics*, 26(1):1–20, 2010.

[42] D. Damian, A. Arieta, H. Martinez, and R. Pfeifer. Slip speed sensory feedback for prosthetic applications. *IEEE Transactions on Biomedical Engineering*, 2012. accepted.

[43] D. Damian, A. H. Arieta, and A. Okamura. Design and evaluation of a multi-modal haptic skin stimulation apparatus. In *Proceedings of the International Conference of the IEEE Engineering in Medicine and Biology Society*, pages 3455–3458, 2011.

[44] D. Damian, M. Fischer, K. Dermitzakis, A. Hernandez-Arieta, and R. Pfeifer. Force and slip feedback guidance role in grasp intensity and time response. *ACM Transactions on Applied Perception*, 2012. to be submmited.

[45] D. Damian, M. Ludersdorfer, Y. Kim, A. H. Arieta, R. Pfeifer, and A. Okamura. Wearable haptic device for cutaneous force and slip feedback. In *Proc. of the IEEE International Conference on Robotics and Automation (ICRA)*, page in press, 2012.

[46] D. Damian, H. M. Salazar, K. Dermitzakis, A. H. Arieta, and R. Pfeifer. Artificial ridged skin for slippage speed detection in prosthetic hand applications. In *Proc. of the 2010 IEEE/RSJ International Conference on Intelligent Robots and Systems (IROS)*, pages 904–909, 2010.

[47] D. D. Damian, T. Newton, R. Pfeifer, and A. Okamura. Intrinsic slip and location detection with a non-uniformly ridged artificial skin. *International Journal of Robotics Research*, 2012. to be submmited.

[48] D. Dennett. *The Intentional Stance*. MIT Press, Cambridge, USA, 1989.

[49] K. Dermitzakis, M. Morales, and A. Schweizer. Frictional interaction in the tendon-sheath system of the human finger and its use in robotics. In *International Conference on Morphological Computation*, 2011.

[50] A. Dollar and R. Howe. The highly adaptive sdm hand: Design and performance evaluation. *International Journal of Robotics Research*, 29(5):585597, 2010.

[51] S. Dorgan and R. Reilly. A model for human skin impedance during surface functional neuromuscular stimulation. *IEEE Transactions on Rehabilitation Engineering*, 7(3), 1999.

[52] S. Douady and Y. Couder. Phyllotaxis as a physical self-organized growth process. *Physical Review Letters*, 68(13):2098 – 2101, 1992.

[53] J. Duque, D. Masset, and J. Malchaire. Evaluation of handgrip force from emg measurements. *Applied Ergonomics*, 26(1):61–66, 1995.

[54] B. Edin, L. Ascari, L. Beccai, S. Roccella, J.-J. Cabibihan, and M. Carrozza. Bio-inspired sensorization of a biomechatronic robot hand for the grasp-and-lift task. *Brain Research Bulletin*, 75(6):785–795, 2008.

[55] F. Faul, E. Erdfelder, A.-G. Lang, and A. Buchner. G*power 3: A flexible statistical power analysis program for the social, behavioral, and biomedical sciences. *Behavior Research Methods*, 39(2):175–191, 2007.

[56] R. Fearing and J. M. Hollerbach. Basic solid mechanics for tactile sensing. *The International Journal of Robotics Research*, 4(3):40–54, 1985.

[57] N. Franceschini, J. M. Pichon, and C. Blanes. From insect vision to robot vision. *Philosophical Transactions: Biological Sciences*, 337(1281):283–294, 1992.

[58] M. Gabiccini and A. Bicchi. On the role of hand synergies in the optimal choice of grasping forces. *Autonomous Robots*, 31(2):235–252, 2011.

[59] F. Geldard. Some neglected possibilities of communication. *Science*, 131(3413):1583–1588, 1960.

[60] V. Gilja, C. Chestek, I. Diester, J. Henderson, K. Deisseroth, and K. Shenoy. Myoelectric forearm prostheses: State of the art from a user-centered perspective. *IEEE Transactions on Biomedical Engineering*, 58(7):1891 1899, 2011.

[61] B. Gleeson, S. Horschel, and W. Provancher. Perception of direction for applied tangential skin displacement: Effects of speed, displacement and repetition. *IEEE Transactions on Haptics- World Haptics Spotlight*, 3(3):177–188, 2010.

[62] B. Gray and R. Fearing. A surface micromachined microtactile sensor array. In *Proceedings of the IEEE International Conference on Robotics and Automation*, pages 1 – 6, 1996.

[63] C. Haeger-Ross, K. Cole, and R. Johansson. Grip-force responses to unanticipated object loading: load direction reveals body- and gravity-referenced intrinsic task variables. *Experimental Brain Research*, 110(1):142–150, 1996.

[64] B. Hannaford and A. Okamura. Chapter 30: Haptics. In *In B. Siciliano and O. Khatib, Eds., Handbook of Robotics*. Springer, 2008.

[65] O. B. Healthcare. *URL:http://www.ottobockus.com/*, 2008.

[66] W. Howard and V. Kumar. On the stability of grasped objects. *IEEE Transactions on Robotics and Automation*, 12(6):904 – 917, 1996.

[67] J. Hunter, J. Katz, and K. Davis. The effect of tactile and visual sensory inputs on phantom limb awareness. *Brain*, 126(3):579–589, 2003.

[68] F. Iida and R. Pfeifer. Cheap rapid locomotion of a quadruped robot: Self-stabilization of bounding gait. In *Proceedings of the 8th International Conference on Intelligent Autonomous Systems (IAS-8)*, pages 642–649, 2004.

[69] I. Inc. *http://www.interlinkelec.com/catalog/Force-Sensors*, Camarillo, CA.

[70] A. Inmann and M. Haugland. Functional evaluation of natural sensory feedback incorporated in a hand grasp neuroprosthesis. *Medical Engineering and Physics*, 26(6):439–447, 2003.

[71] P. Jenmalm, A. Goodwin, and R. Johansson. Control of grasp stability when humans lift objects with different surface curvatures. *J Neurophysiol*, 79:1643–1652, 1998.

[72] R. Johansson and K. Cole. Grasp stability during manipulative actions. *Canadian Journal of Physiology and Pharmacology*, 72(5):511–524, 1994.

[73] R. Johansson and K. Cole. Grasp stability during manipulative actions. *Can J Physiol Pharmacol*, 72(5):511–524, 1994.

[74] R. Johansson and A. Valbo. Tactile sensory coding in the glabrous skin of the human hand. *Trends in Neuroscience*, 6:27–32, 1983.

[75] R. Johansson and G. Westling. Roles of glabrous skin receptors and sensorimotor memory in automatic control of precision grip when lifting rougher or more slippery objects. *Experimental Brain Research*, 56(3):550–564, 1984.

[76] R. Johansson and G. Westling. Roles of glabrous skin receptors and sensorimotor memory in automatic control of precision grip when lifting rougher or more slippery objects. *Experimental Brain Research*, 56:550–564, 1984.

[77] R. Johansson and G. Westling. Signals in tactile afferents from the fingers eliciting adaptive motor responses during precision grip. *Experimental Brain Research*, 66(141–154), 1987.

[78] L. Jones and S. Lederman. *Human Hand Function*. Oxford University Press, New York, USA, 2006.

[79] K. A. Kaczmarek, J. G. Webster, P. B. y Rita, and W. J. Tompkins. Electrotactile and vibrotactile displays for sensory substitution systems. *IEEE Trans. on Biomedical Engineering*, 38:1–16, 1991.

[80] E. Kandel, J. Schwartz, and T. Jessell. *Principles of Neural Science, 4th edn.* McGraw-Hill, New York,USA, 2000.

[81] D.-H. Kim, J.-H. Ahn, W. Choi, H.-S. Kim, T.-H. Kim, J. Song, Y. Huang, Z. Liu, C. Lu, and J. Rogers. Stretchable and foldable silicon integrated circuits. *Science*, 320(5875):507–511, 2008.

[82] K.Kim, J. Colgate, J. Santos-Munne, A. Makhlin, and M. Peshkin. On the design of miniature haptic devices for upper extremity prosthetics. *IEEE/ASME Transactions on Mechatronics*, 15(1):27–39, 2010.

[83] A. Kron and G. Schmidt. Multi-fingered tactile feedback from virtual and remote environments. In *Proceedings of the 11th Symposium on Haptic Interfaces for Virtual Environment and Teleoperator Systems*, 2003.

[84] K. J. Kuchenbecker, J. Gewirtz, W. McMahan, D. Standish, P. Martin, J. Bohren, P. J. Mendoza, and D. I. Lee. Verrotouch: High-frequency acceleration feedback for telerobotic surgery. In *Proceedings of the 8th international conference on Haptics*, 2010.

[85] P. Kyberd, M. Evans, and S. te Winkel. An intelligent anthropomorphic hand, with automatic grasp. *Robotica*, 16:531–536, 1998.

[86] P. J. Kyberd, D. Gow, H. Scott, M. Griffiths, L. Sperling, L. Sandsjo, C. Almstrom, C. Wartenberg, and S. Jonsson. A comparison of upper limb prostheses users in europe. In *Myoelectr. Controls Symp. Fredericton*, 1999.

[87] S. Lederman, R. Klatzky, C. Tong, and C. Hamilton. The perceived roughness of resistive virtual textures: Ii. effects of varying viscosity with a force-feedback device. *ACM Trans. on Applied Perception*, 3(1):15–30, 2006.

[88] H.-K. Lee, J. Chung, S.-I. Chang, and E. Yoon. Real-time measurement of the three-axis contact force distribution using a flexible capacitive polymer tactile sensor. *Journal of Micromechanics and Microengineering*, 21(3):035010, 2011.

[89] J. Li, M. Cutkosky, J. Ruutiainen, and R. Raisamo. Using haptic feedback to improve grasp force control in multiple sclerosis patients. *IEEE Transactions on Robotics*, 25(3):593–601, 2009.

[90] L. Lichtensteiger and R. Pfeifer. An optimal sensor morphology improves adaptability of neural network controllers. *Proceeding ICANN '02 Proceedings of the International Conference on Artificial Neural Networks*, 337(1281):283–294, 1992.

[91] L. Lichtensteiger and R. Pfeifer. An optimal sensor morphology improves adaptability of neural network controllers. In *Proceeding ICANN '02 Proceedings of the International Conference on Artificial Neural Networks*, pages 850 – 855, 2002.

[92] D. Lipomi, M. Vosgueritchian, B.-K. Tee, S. Hellstrom, J. Lee, C. Fox, and Z. Bao. Skin-like pressure and strain sensors based on transparent elastic films of carbon nanotubes. *Nature Nanotechnology*, 6:788792, 2011.

[93] M. Ludersdorfer, D. Damian, A. H. Arieta, R. Pfeifer, and A. Okamura. Cutaneous force display via shaped contacts. In *Proceedings of the International Conference on Morphological Computation*, pages 127–129, 2011.

[94] V. J. Lumelsky, M. S. Shur, and S. Wagner. Sensitive skin. *IEEE Sensors Journal*, 1(1):41–51, 2001.

[95] G. Lundborg and B. Rosén. Sensory substitution in prosthetics. *Hand Clin.*, 3:481–488, 2001.

[96] M. Lungarella, V. Hafner, R. Pfeifer, and H. Yokoi. An artificial whisker sensors in robotics. In *Proceedings of the IEEE/RSJ International Conference on Intelligent Robots and Systems*, pages 2931–2936, 2002.

[97] M. MacIver, N. Patankar, and A. Shirgaonkar. Energy-information tradeoffs between movement and sensing. *PLoS Comput Biol*, 6(5):e1000769, 2010.

[98] K. MacLean. Designing with haptic feedback. In *Proceedings of IEEE Robotics and Automation*, 2000.

[99] D. A. Mahns, N. M. Perkins, V. Sahai, L. Robinson, and M. J. Rowe. Vibrotactile frequency discrimination in human hairy skin. *Journal of Neurophysiology*, 95(3):1442–1540, 2005.

[100] R. Maldonado-Lopez, F. Vidal-Verdu, G. Linan, E. Roca, and A. Rodriguez-Vazquez. Early slip detection with a tactile sensor based on retina. *Analog Integr Circ Sig Process*, 53:97–108, 2007.

[101] P. Marasco, K. Kim, J. Colgate, M. Peshkin, and T. Kuiken. Robotic touch shifts perception of embodiment to a prosthesis in targeted reinnervation amputees. *Brain*, 134(3):747–758, 2011.

[102] S. Meek, S. Jacobsen, and P. Goulding. Extended physiologic taction: design and evaluation of a proportional force feedback system. *Journal of Rehabilitation Resource and Development*, 26(3):53–62, 1989.

[103] A. Mingrino, A. Bucci, R. Magni, and P. Dario. Slippage control in hand prostheses by sensing grasping forces and sliding motion. In *Proceedings of the IEEE/RSJ/GI International Conference on Intelligent Robots and Systems*, pages 1803 – 1809, 1994.

[104] S. Miyashita. *Effect of Morphology on Scalable Self-Assembling Robots - in Pursuit of Living Artificial Systems*. PhD Thesis, University of Zurich, 2010.

[105] D. Morris, H. Tan, F. Barbagli, T. Chang, and K. Salisbury. Haptic feedback enhances force skill learning. In *Symposium on Haptic Interfaces for Virtual Environment and Teleoperator Systems, World Haptics*, 2007.

[106] A. Moseman. Are a sprinterś prosthetic legs an unfair advantage. *Scientist Smackdown*, 2009.

[107] H. Muhammada, C. Recchiuto, C. Oddo, L. Beccai, C. Anthony, M. Adams, M. Carrozza, and M. Ward. A capacitive tactile sensor array for surface texture discrimination. *Microelectronic Engineering*, 88:18111813, 2011.

[108] L. M.-L. no, D. Vinkovi, E. D. Mas, G. Corcobado, and E. Moreno. Morphological evolution of spiders predicted by pendulum mechanics. *PLoS One*, 3(3):e1841, 2008.

[109] D. Nowak, S. Glasauer, and J. Hermsdorfer. How predictive is grip force control in the complete absence of somatosensory feedback? *Brain*, 127:182192, 2003.

[110] C. Oddo, L. Beccai, M. Felder, F. Giovacchini, and M. Carrozza. Artificial roughness encoding with a bio-inspired mems based tactile sensor array. *Sensors*, 9:3161–3183, 2009.

[111] J. ODoherty, M. Lebedev, P. Ifft, K. Zhuang, S. Shokur, H. Bleuler, and M. Nicolelis. Active tactile exploration using a brainmachinebrain interface. *Nature*, 479:228231, 2011.

[112] M. Ohka, Y. Mitsuya, I. Higashioka, and H. Kabeshita. An experimental optical three-axis tactile sensor for micro-robots. *Robotica*, 23(4):457–465, 2005.

[113] A. Okamura, M. Cutkosky, and J. T. Dennerlein. Reality-based models for vibration feedback in virtual environments. *IEEE/ASME Trans. on Mechatronics*, 6(9):245 – 252, 2001.

[114] A. Panarese, B. Edin, F. Vecchi, M. Carrozza, and R. Johansson. Humans can integrate force feedback to toes in their sensorimotor control of a robotic hand. *IEEE Transactions on Neural Systems and Rehabilitation Engineering*, 17(6), 2009.

[115] J. Pasquero, V. Levesque, V. Hayward, and M. Legault. Display of virtual braille dots by lateral skin deformation: Feasibility study. *ACM Transactions on Applied Perception*, 2(2):132–149, 2005.

[116] P. Patterson and J. Katz. Design and evaluation of a sensory feedback system that provides grasping pressure in a myoelectric hand. *Journal of Rehabilitation Resource and Development*, 29(1):1–8, 1992.

[117] C. Paul. Morphological computation: A basis for the analysis of morphology and control requirements. *Robotics and Autonomous Systems*, 54(8):619–630, 2006.

[118] B. Peerdeman, D. Boere, H. Witteveen, R. H. in t̀ Veld, H. Hermens, S. Stramigioli, H. Rietman, P. Veltink, and S. Misra. Myoelectric forearm prostheses: State of the art from a user-centered perspective. *Journal of Rehabilitation Research and Development*, 48(6):719 738, 2011.

[119] R. Pfeifer and J. Bongard. *How the Body Shapes the Way We Think:A New View of Intelligence*. MIT Press, Cambridge, USA, 2006.

[120] R. Pfeifer, F. Iida, and G. Gomez. Morphological computation for adaptive behavior and cognition. *International Congress Series*, 1291:22–29, 2006.

[121] R. Pfeifer and C. Scheier. Sensory-motor coordination: The metaphor and beyond. *Robotics and Autonomous Systems*, 20:157–178, 1997.

[122] R. Pfeifer and C. Scheier. *Understanding Intelligence*. MIT Press, Cambridge, MA, USA, 1999.

[123] R. Pfeifer and C. Scheier. *Understanding Intelligence*. MIT Press, Cambridge, MA, 1999.

[124] D. Philipona, J. O'Regan, and J.-P. Nadal. Is there something out there? infering space from sensorimotor dependencies. *Neural Computation*, 15, 2002.

[125] H. Pongrac. Vibrotactile perception: examining the coding of vibrations and the just noticeable difference under various conditions. *Multimedia Systems*, 13:297–307, 2008.

[126] C. Pylatiuk, A. Kargov, and S. Schulz. Design and evaluation of a low-cost force feedback system for myoelectric prosthetic hands. *Journal of Prosthetics and Orthotics*, 18(2):57–61, 2006.

[127] P. Richard, G. Burdea, and P. Coiffet. Human performance in tasks involving virtual objects with force feedback. In *Proceedings of Interface Real and Virtual Worlds Conference*, pages 229 – 238, 1993.

[128] P. Richard and P. Coiffet. Human perceptual issues in virtual environments: sensory substitution and information redundancy. In *IEEE Int Workshop Robot Hum Commun*, pages 301 – 306, 1995.

[129] R. Riso. Strategies for providing upper extremity amputees with tactile and hand position feedback moving closer to the bionic arm. *Technology and health care: official journal of the European Society for Engineering and Medicine*, 7(6):401–409, 1999.

[130] R.M.Suryan, D. Anderson, S. Shaffer, D. Roby, Y. Tremblay, D. Costa, P. Sievert, F. Sato, K. Ozaki, G. Balogh, and N. Nakamura. Wind, waves, and wing loading: Morphological specialization may limit range expansion of endangered albatrosses. *PLoS ONE*, 12(3):e4016, 2008.

[131] F. Robineau, F. Boy, J.-P. Orliaguet, J. Demongeot, and Y. Payan. Guiding the surgical gesture using an electro-tactile stimulus array on the tongue: A feasibility study. *IEEE Transactions on Biomedical Engineering*, 54(4):711 – 717, 2007.

[132] G. Robles-De-La-Torre. The importance of the sense of touch in virtual and real environments. *IEEE Multimedia, Special issue on Haptic User Interfaces for Multimedia Systems*, 13(3):24–30, 2006.

[133] M. Rothenberg, R. Verrillo, S. Zahorian, M. Brachman, and S. B. Jr. Vibrotactile frequency for encoding a speech parameter. *Journal of the Acoustical Society of America*, 62(4):1003–1012, 1977.

[134] M. Salada, P. Vishton, J. Colgate, and E. Frankel. Two experiments on the perception of slip at the fingertip. In *IEEE Proceedings of the International Symposium on Haptic Interfaces for Virtual Environment and Teleoperator Systems*, pages 146–153, 2004.

[135] L. Salisbury and A. Colman. A mechanical hand with automatic proportional control of prehension. *Medical and Biological Engineering and Computing*, 5(5):505–511, 1967.

[136] M. Santello, M. Flanders, and J. Soechting. Postural hand synergies for tool use. *Journal of Neuroscience*, 18(23):10105–10115, 1998.

[137] L. Santos-Carreras, R. Beira, A. Sengul, R. Gassert, and H. Bleuler. Influence of force and torque feedback on operator performance in a vr-based suturing task. *Applied Bionics and Biomechanics*, 7(3):217–230, 2010.

[138] I. Saunders and S. Vijayakumar. The role of feed-forward and feedback processes for closed-loop prosthesis control. *Journal of NeuroEngineering and Rehabilitation*, 8(60), 2011.

[139] J. Scheibert, S. Leurent, A. Prevost, and G. Debregeas. The role of fingerprints in the coding of tactile information probed with a biomimetic sensor. *Science*, 13(323(5920)):1503–1506, 2009.

[140] P. Schmidt, E. Mal, and R. Wrtz. A sensor for dynamic tactile information with applications in humanrobot interaction and object exploration. *Robotics and Autonomous Systems*, 54(12):1005–1014, 2006.

[141] A. Schmitz, P. Maiolino, M.Maggiali, L. Natale, G. Cannata, and G. Metta. Methods and technologies for the implementation of large-scale robot tactile sensors. *IEEE Trans. on Robotics*, 27(3):389–400, 2011.

[142] M. Seps. *Non-Invasive Feedback System for Smart Prosthetic Devices. Master Thesis.* University of Zurich, Zurich, Switzerland, 2010.

[143] M. Seps, K. Dermitzakis, and A. Hernandez-Arieta. Study on lower back electrotactile stimulation characteristics for prosthetic sensory feedback. In *IEEE Proc. Int. Conf .on Intelligent Robots and Systems*, pages 3454–3459, 2011.

[144] R. Shepherd, F. Ilievski, W. Choi, S. Morin, A. Stokes, A. Mazzeo, X. Chen, M. Wang, and G. Whitesides. Multi-gait soft robot. *Proceedings of the National Academy of Sciences (PNAS)*, 2011.

[145] C. Sherrick and R. Cholewiak. *Cutaneous Sensitivity, In K. Boff, L. Kaufman and J.L. Thomas (Eds.), Handbook of perception and human performance.* Wiley, New York, USA, 1986.

[146] D. I. Silcox, M. Rooks, R. Vogel, and L. Fleming. Myoelectric prostheses. a long-term follow-up and a study of the use of alternate prostheses. *J Bone Joint Surg Am.*, 75(12):1781–1789, 1993.

[147] D. Simpson. *The Choice of Control System for multimovement prostheses: Extended Physiological Proprioception (EPP), in: The Control of Upper-Extremity Prostheses and Orthoses.* Charles Thomas, Springfield, 1974.

[148] R. Spencer, T. Verstynen, M. Brett, and R. Ivry. Cerebellar activation during discrete and not continuous timed movements: An fmri study. *NeuroImage*, 36(2):378–387, 2007.

[149] R. Steeper. *URL:http://rslsteeper.com/*, 2010.

[150] S. Takamuku, G. Gomez, K. Hosoda, and R. Pfeifer. Haptic discrimination of material properties by a robotic hand. In *Proceedings of the 6th IEEE International Conference on Development and Learning*, 2007.

[151] M. Tremblay and M. Cutkosky. Estimating friction using incipient slip sensing during a manipulation task,. In *IEEE Proc. Int.Conf .on Robotics and Automation*, volume 1, pages 429–434, 1993.

[152] N. Tsagarakis, T.Horne, and D.G.Caldwell. Slip aestheasis: A portable 2d slip/skin stretch display for the fingertip. In *IEEE Proceedings of the Joint Eurohaptics Conference and Symposium on Haptic Interfaces for Virtual Environment and Teleoperator Systems*, pages 214 – 219, 2005.

[153] M. Tsakiris, L. Carpenter, D. James, and A. Fotopoulou. Hands only illusion: multisensory integration elicits sense of ownership for body parts but not for non-corporeal objects. *Experimental Brain Research*, 204(3):343352, 2009.

[154] R. Velazquez, E. Pissaloux, M. Hafez, and J. Szewczyk. A low-cost highly-portable tactile display based on shape memory alloy micro-actuators. In *IEEE International Conference on Virtual Environments, Human-Computer Interfaces, and Measurement Systems*, pages 121 – 126, 2005.

[155] M. Velliste, S. Perel, M. Spalding, A. Whitford, and A. Schwartz. Cortical control of a prosthetic arm for self-feeding. *Nature*, 453:1098–1101, 2008.

[156] M. Venkadesan and F. Valero-Cuevas. Neural control of motion-to-force transitions with the fingertip. *Journal of Neuroscience*, 28(6):13661373, 2008.

[157] J. Vincent, O. A. Bogatyreva, N. R. Bogatyrev, A. Bowyer, and A.-K. Pahl. Biomimetics: its practice and theory. *Journal of the Royal Society*, 3:471–482, 2006.

[158] C. Wagner, S. Lederman, and R. Howe. A tactile shape display using rc servomotors. In *Symposium on Haptic Interfaces for Virtual Environment and Teleoperator Systems*, 2002.

[159] J. Wakeling, B. Nigg, and A. Rozitis. Muscle activity damps the soft tissue resonance that occurs in response to pulsed and continuous vibrations. *Journal of Applied Physiology*, 93(3):1093–1103, 2002.

[160] R. J. WebsterIII, T. E.Murphy, L. N. Verner, and A. M.Okamura. A novel two-dimensional tactile slip display: design, kinematics and perceptual experiment. *ACM Trans. Appl. Percept.*, 2(2):150–165, 2005.

[161] R. Weir and J. Sensinger. *The Design of artificial arms and hands for prosthetic application. Handbook of Biomedical Design*. McGraw-Hill, New York, 2003.

[162] N. Wettels, A. Parnandi, J.-H. Moon, G. Loeb, and G. Sukhatme. Grip control using biomimetic tactile sensing systems. *IEEE/ASME Transactions on Mechatronics*, 14(6):718–723, 2009.

[163] N. Wettels, D. Popovic, V. Santos, R. Johansson, and G. Loeb. Biomimetic tactile sensor array. *Advanced Robotics*, 22(8):829–849, 2008.

[164] H. Wheat, L. Salo, and A. Goodwin. Human ability to scale and discriminate forces typical of those occurring during grasp and manipulation. *Journal of Neuroscience*, 24(13):3394 – 3401, 2004.

[165] J. Wheeler, K. Bark, J. Savall, and M. Cutkosky. Investigation of rotational skin stretch for proprioceptive feedback with application to myoelectric systems. *IEEE Trans Neural Syst Rehabil Eng*, 18(1):58–66, 2010.

[166] P. B. y Rita, K. A. Kaczmarek, M. E. Tyler, and J. Garcia-Lara. Form perception with a 49-point electrotactile stimulus array on the tongue: A technical note. *Journal of Rehabilitation Research and Development*, 35(4):427–430, 1998.

[167] D. Yamada, T. Maeno, and Y. Yamada. Artificial finger skin having ridges and distributed tactile sensors used for grasp force control. *Journal of Robotics and Mechatronics*, 14(2):140–146, 2002.